Aspects of Design and Analysis of Cognitive Radios and Networks

Muhammad Fainan Hanif

A thesis submitted in fulfillment
of the requirements for the degree of

Doctor of Philosophy

in

Electrical and Electronic Engineering

University of Canterbury
Christchurch, New Zealand

September 2010

Abstract

Recent survey campaigns have shown a tremendous under utilization of the bandwidth allocated to various wireless services. Motivated by this and the ever increasing demand for wireless applications, the concept of cognitive radio (CR) systems has rendered hope to end the so called spectrum scarcity. This thesis presents various different facets related to the design and analysis of CR systems in a unified way. We begin the thesis by presenting an information theoretic study of cognitive systems working in the so called low interference regime of the overlay mode. We show that as long as the coverage area of a CR is less than that of a primary user (PU) device, the probability of the cognitive terminal inflicting small interference at the PU is overwhelmingly high. We have also analyzed the effect of a key parameter governing the amount of power allocated to relaying the PU message in the overlay mode of operation in realistic environments by presenting a simple and accurate approximation. Then, we explore the possibilities of statistical modeling of the cumulative interference due to multiple interfering CRs. We show that although it is possible to obtain a closed form expression for such an interference due a single CR, the problem is particularly difficult when it comes to the total CR interference in lognormally faded environments. In particular, we have demonstrated that fitting a two or three parameter lognormal is not a feasible option for all scenarios. We also explore the second-order characteristics of the cumulative interference by evaluating its level crossing rate (LCR) and average exceedance duration (AED) in Rayleigh and Rician channel conditions. We show that the LCRs in both these cases can be evaluated by modeling the interference process with gamma and noncentral χ^2 processes, respectively. By exploiting radio environment map (REM) information,

we have presented two CR scheduling schemes and compared their performance with the naive primary exclusion zone (PEZ) technique. The results demonstrate the significance of using an intelligent allocation method to reap the benefits of the tremendous information available to exploit in the REM based methods. At this juncture, we divert our attention to multiple-input multiple-output (MIMO) CR systems operating in the underlay mode. Using an antenna selection philosophy, we solve a convex optimization problem accomplishing the task and show via analysis and simulations that antenna selection can be a viable option for CRs operating in relatively sparse PU environments. Finally, we study the impact of imperfect channel state information (CSI) on the downlink of an underlay multiple antenna CR network designed to achieve signal-to-interference-plus-noise ratio (SINR) fairness among the CR terminals. By employing a newly developed convex iteration technique, we solve the relevant optimization problem exactly without performing any relaxation on the variables involved.

Acknowledgements

Well, let me begin with the bottom line. In plain words, this thesis would not have been possible without the superb supervision, brilliant patience and intelligent tolerance of Prof. Peter J. Smith, my principal supervisor. In addition to learning 'tricks of the trade', I have tremendously benefitted from him in terms of acquiring essential skills for my professional life. No doubt, the years I spent as a PhD student will go a long way in my life and the memories of this tenure, both pleasant and bitter ones, will remain ever green in my mind.

I will also like to take this opportunity to extend my thanks to my co-supervisors, Prof. Desmond P. Taylor and Dr. Philippa A. Martin. Lively discussions with both of them have been a great source of enthusiasm and learning. Especially, Friday afternoon tea/coffee meetings with Prof. Taylor have both been fun and a source of scholarship.

My gratitude also goes to the generous financial support provided by Telecom New Zealand and National ICT Innovation Institute (NZi3) for my graduate studies. I am thankful to them for putting their faith in my capabilities and I hope I have delivered.

I should also express my gratitude to all those who have remained with me in E338b during these years. Certainly, Abdulla, Tim, Vijay and Krishna top this list of people. The technical and computer staff, the cleaning staff and all those who have helped make my stay a pleasant experience deserve both appreciation and thanks on my part.

Last but by no means least, I would like to dedicate this thesis to the astronomical patience and forbearance of my family towards me during all these years.

Contents

List of Figures

List of Tables

Chapter 1

Introduction

1.1 Overview of Cognitive Radio Systems

It is no exaggeration that wireless communication has completely revolutionized our lives. The ever increasing efforts to introduce new wireless devices capable of delivering high data rates over the unfriendly wireless channel seem insatiable. The existence of mobile communication, being one of the most successful wireless services, is totally reliant on certain small usable chunks (normally below 3.5 GHz) of very expensive radio-frequency (RF) spectrum. With the immense proliferation of mobile telephony services (applications) that has already taken place, it appears natural to consider the possibility that we will eventually run out of the bandwidth required to accommodate emerging wireless products.

Motivated by this spectrum shortage perception, recent spectrum occupancy measurement campaigns [1, 2], conducted under the authorization of various government bodies, reported a startling fact. The spectrum is poorly utilized. In fact, it has been clearly stated in [1], that "... spectrum access is a more significant problem than physical scarcity of spectrum, in large part due to legacy command-and-control regulation that limits the ability of potential spectrum users to obtain such access". This inflexible frequency allocation procedure adopted worldwide by government agencies has resulted in vacant bands of frequencies at a particular time

or geographic location, also described as *spectrum holes* or *white spaces*. Cognitive radios (CRs) have been suggested as a solution to this so-called spectrum scarcity.

CRs are being considered to work in *spectrum agile* mode where they adapt their transmission parameters (center frequency, bandwidth etc.) according to their environment [3]. *Fully cognitive* devices completely following the full extent of Mitola's ideas [4] are still a distant reality. In addition to this, a *hierarchical spectrum access model* is being envisaged for successful operation of CRs [3]. In such a spectrum access model the primary (licensed) users (PUs) are given priority. CRs are allowed to co-exist with the primary devices subject to the condition that, ideally, they do not interfere with their operation. There is a wide choice of RF bands that are potential candidates for CR deployment. For example, all bands below 3.5 GHz are candidates for such installations, especially on account of their low propagation losses [3]. *UHF* bands used by broadcast television are being considered by the Federal Communications Commission (FCC) in the United States to allow dynamic spectrum access to CR devices [5]. Similarly, *cellular bands* (800/900 MHz, 1.8/1.9 GHz, 2.1 GHz, 2.3 GHz, and 2.5 GHz) and *fixed wireless access bands* (centered near 2.5 and 3.5 GHz) provide a plausible option for the deployment of spectrum agile cognitive devices. We note that the term "secondary user" is typically used when the primary users are termed "licensed devices". In a similar way, cognitive models can be extended to include the more general notions of "public park" (for example, devices capable of unlicensed spectrum usage) and dynamic spectrum leasing discussed below.

Successful deployment of CR devices for dynamic spectrum access purposes will rely on the type, quantity and quality of the side information available at their disposal. In the words of [6], a CR device can be defined as: "a wireless communication system that intelligently utilizes any available side information about the a) activity, b) channel conditions, c) codebooks, or d) messages of other nodes with which it shares the spectrum." Based on the categorization provided in this definition, cognitive wireless communications can be broadly classified into *underlay*, *overlay* and *interweave* paradigms [3, 6, 7]. We briefly describe these cognitive spectrum

access techniques below.

In underlay CR networks, the cognitive devices maintain their interference to the licensed PU system below an acceptable threshold. By doing so they are able to simultaneously transmit with the legacy licensed users, thereby minimizing the tedious task of finding white spaces. However, in order to satisfy this interference constraint, the CR(s) need to know the channel gains to the licensed system(s) as side information. Based on this knowledge, the CRs can use smart power allocation algorithms or use multiple antenna techniques to steer their signals in such a way that the licensed users remain as oblivious as possible of their presence. Because of the simplicity of the approach, underlaying CR signals appears the most promising technique from the point of view of the inception of cognitive devices in the near future. For example, spreading a CR signal below the noise floor, a technique commonly used in ultra wide band (UWB) systems, and then nullifying the spreading effect at the cognitive receiver can form one such option [6]. However, the underlay access technique comes with its own unique challenges. For example, acquiring perfect channel state information from CR transmitters to primary receivers is a daunting task that involves substantial, complex and tedious signal processing. Similarly, the constraint of maintaining an interference level at the licensed users below an acceptable threshold may only leave the cognitive device(s) with enough power to communicate over short range distances [6].

In overlay CR approaches, the CR devices can also transmit, together with the PUs, in the same time/frequency/space slot. However, in this technique the CRs, in addition to knowing the exact channel strengths to all nodes, also need to be equipped with the message sets of the licensed users [6]. Clearly this is a big requirement. Using sophisticated encoding techniques like dirty paper coding (DPC), the CR can nullify the effect of interference at its own receiver (RX) due to PU transmission. Similarly, by relaying the noncognitive user's message to its RX, the CR device is able to mitigate the effect of its own interference. For details on how these methods work, please see [6, 7, 3] and the references therein. It is clear that, unlike the underlay paradigm, the CRs can transmit at any power as long

as they are able to dedicate some portion of their energy resources to relaying the licensed user's message.

The last technique, commonly referred to as the interweave model, relies on the CR knowing the exact location of white spaces in time frequency and space coordinates. This capability of the cognitive user depends on its spectrum sensing signal processing module. Spectrum sensing has been an area of rigorous research over the last decade. For an overview of the myriad techniques proposed, the reader is referred to [8]. Clearly, in this case the accuracy of detecting white spaces will determine the performance of a CR device in terms of protecting the legacy users from harmful interference. From this overview, it is relatively easy to categorize the interweave model as an example of a spectrum agile or *opportunistic spectrum access* philosophy. In contrast, the remaining two techniques can be considered as examples of a *spectrum sharing* model.

1.2 Thesis Contributions

From the overview presented in the previous section, it is clear that at present all CR spectrum access paradigms are accompanied by their associated advantages and disadvantages. In addition to this, there are still many unknown questions and gaps in our knowledge concerning the performance of CR systems in the vicinity of noncognitive users. Furthermore, multiple-input multiple-output (MIMO) wireless technology is a very promising candidate for integration with CR networks. Reliability and higher throughput are known benefits of MIMO techniques. The extra degrees of freedom provided by the multiple antennas on both sides of the communication link can also be used for interference protection purposes in the spatial domain. Thus, MIMO can serve the cause of CR networks.

Whenever a new communication technology (like CRs in our case) is introduced, the question of determining the fundamental limits of data rates forms the backbone of the rest of the remaining research activity. Likewise, this question has been tackled from several different perspectives in the CR domain. In particular, the question

of determining the maximum data rates of a CR network operating in overlay mode has been answered in the so called "low interference regime"[1]. However, the known results only account for additive white Gaussian noise (AWGN) channels. Motivated by this, we have analytically characterized this capacity in the presence of more realistic environments involving the phenomenon of path loss, fast fading and shadowing. In addition, we also determine the probability of occurrence of such a regime in real world scenarios.

The statistical characteristics of interfering signals from the CR devices will play an important role in the design of CR networks. However, once the cumulative effect of interfering signal strengths is considered, the problem of evaluating an exact expression for the distribution of such a sum can become a tedious task. This is especially true in the case of lognormal fading environments. In particular, the distribution of aggregate lognormal interference is a long standing problem. In the thesis, we show that, although the distribution of interference due a single CR device can be analytically characterized, the cumulative CR interference in lognormal environments does not admit any closed form solution. We also show that the traditional methods of approximating this interference with another lognormal are not applicable any more.

One of the important performance parameters that has been largely ignored in the current literature is that of the level crossing rate (LCR) of interference in CR networks. In traditional radio designs this metric has been used to gauge the fluctuations of the received signal strength for radio design purposes. In the context of cognitive devices operating in the presence of licensed users, this rate can be employed to design, for example, CR access techniques, resource allocation at cognitive devices etc. We have evaluated the LCR of cumulative CR interference in Rayleigh and Rician environments by judiciously approximating the distribution functions with a gamma distribution and a scaled non-central χ^2 distribution with fractional degrees of freedom, respectively. Then, by appropriately adapting the

[1]When the strength of the channel between the CR and licensed user RX is small relative to that of the direct channel between the CR transmitter (TX) and its RX.

known results related to the LCR of these cases, we analytically characterize the LCR of CR devices in these two environments.

The future of CRs is critically dependent on the techniques they will employ to access the RF spectrum. As discussed previously, all known techniques in this regard are limited in some way or other. Motivated by this and the fact that successful CR operation will heavily rely on the type and amount of side information available at its disposal, we have proposed and evaluated CR access schemes using the so called radio environment map (REM) information. Just as an ordinary map on a GPS device can be helpful to a person aiming to find the least congested and quickest way to his destination, a REM is suppose to drive CR operation by helping it communicate in a less crowded spectrum while simultaneously enabling it to achieve higher throughput. We have also assessed the performance of CR allocation schemes in the presence of imperfect or coarse REM information. Overall, our explorations suggest an appreciable improvement of our schemes over the straightforward method of allowing CRs to only operate in certain geographical zones.

As mentioned previously, MIMO systems show great promise as a method to help CRs use spectrum even more efficiently. However, it is well known that reaping the traditional benefit of higher spectral efficiency comes with a greater hardware cost. Antenna selection provides an elegant solution to this problem. Motivated by this, we study the design and analysis of MIMO CR systems employing antenna selection and working in the underlay mode of operation. In addition to formulating this as a convex optimization problem, we also propose a low complexity norm based solution to this problem. Furthermore, we provide some preliminary investigations of the performance analysis of such a system fulfilling interference constraints at the PU RXs.

Finally, it is well known that the traditional way of scheduling multiple users being served by a single base station is to dedicate more resources to those with better channel conditions than the ones with inferior signal-to-interference-plus-noise ratio (SINR) values at their RXs. Clearly, this approach can be harmful to those users that are supposed to deliver performance under strict delay constraints. This

motivates the need for the so called fairness based scheduling schemes. Max-min fairness method form one such possibility. Motivated by this, we study the design of beamforming in the downlink of such systems working in CR underlay mode. Plagued by imperfect channel knowledge, our algorithm caters for such deficiencies by solving convex optimization problems thereby yielding robust beamformers under such hostile conditions.

1.3 Thesis Outline

The rest of the thesis is organized as follows:

In Chapter 2 we discuss the fundamentals of wireless communications theory while simultaneously providing a bird's eye view of significant concepts relevant to convex optimization modeling. Starting with a discussion of wireless propagation, we provide an overview of MIMO systems. Afterwards we describe common metrics used to gauge the performance of wireless systems. The remaining half of the chapter deals with the basics and the classification of convex optimization problems.

Chapter 3 studies the fundamental capacity limits of CR systems operating in overlay mode. The chapter begins with determining the occurrence of the probability of the low interference regime in different combinations of fading channels. In the later half of the chapter, we provide an approximation to a key factor determining the power allocation at the CR node. Finally, simulation results are conducted validating the accuracy of the analyses.

Chapter 4 focuses on the study of statistical interference characterization and the LCR of aggregate interference at the PU RXs. Beginning with an analytical expression for the interference due to a single CR, we prove that approximating the cumulative interference with a lognormal (either with two or three parameters) is not a viable option and that more complex models are needed. The second half of the chapter explores LCRs of the total CR interference in Rayleigh and Rician fading conditions. By appropriately approximating the distribution of such random variables, we analytically characterize interference fluctuation rates and exceedance

durations in such environments.

Chapter 5 is the study of different CR allocation techniques. Due to the difficulty of analysis based on novel REM allocation methods, the chapter provides a simulation study conducting a comparison between the geographical separation and REM based methods. It has been shown in the results section that exploiting REM information is in general superior to relying solely on position information. However, the CRs need to be allocated judiciously.

Chapter 6 presents the novel idea of incorporating antenna selection to fulfill the task of interference management while simultaneously maximizing the rates of such a MIMO CR system. After an analytical formulation of the problem, we present three methods in order of decreasing complexity. The second half of the chapter deals with the performance evaluation of antenna selection systems in simple fading environments. In the last section, we show that antenna selection based CR systems can be a feasible option especially in sparse PU environments.

In Chapter 7 we deal with the issue of max-min SINR balancing in the downlink of a CR channel with imperfect channel information available at the base-station. After formulating the problem, we present a novel algorithm that accomplishes this task. The results presented show that the proposed technique outperforms the known solution to the current problem.

Finally in Chapter 8 we conclude the thesis while also pointing to some future research directions.

1.4 List of Publications

Many of the results presented in the thesis are based on the following papers in various journals and conferences.

Journal Papers

- **M. F. Hanif** and P. J. Smith, "On the Statistics of Cognitive Radio Capacity in Shadowing and Fast Fading Environments," *IEEE Transactions on Wireless*

Communications, vol. 9, no. 2, pp. 844-852, February 2010.

- **M. F. Hanif** and P. J. Smith, "Level Crossing Rates of Interference in Cognitive Radio Systems," *IEEE Transactions on Wireless Communications*, vol. 9, no. 4, pp. 1283-1287, April, 2010.

- **M. F. Hanif**, P. J. Smith and M.-S. Alouini, "On Optimal SINR Balancing in the Downlink of Cognitive Radio Networks with Imperfect Channel State Information," submitted to the *IEEE Transactions on Communications*.

- **M. F. Hanif**, P. J. Smith, D. P. Taylor and P. A. Martin, "MIMO Cognitive Radios with Antenna Selection," submitted to the *IEEE Transactions on Wireless Communications* (received minor revisions).

- **M. F. Hanif**, P. J. Smith and P. A. Dmochowski, "On Interference and Deployment Issues for Cognitive Radio Systems in Shadow Fading Environments," submitted to the *IET Communications*.

Conference Papers

- **M. F. Hanif**, P. J. Smith and M. Shafi, "Performance of Cognitive Radio Systems with Imperfect Radio Environment Map Information," in *Proc. IEEE Australian Communication Theory Workshop (AusCTW 2009)*, Sydney, Australia, Feb. 2009, pp. 61-66.

- **M. F. Hanif**, M. Shafi, P. J. Smith and P. A. Dmochowski, "Interference and Deployment Issues for Cognitive Radio Systems in Shadowing Environments," in *Proc. IEEE International Conference on Communications (ICC 2009)*, Dresden, Germany, June 2009, pp. 1-6.

- **M. F. Hanif**, P. J. Smith and M. Shafi, "On the Statistics of Cognitive Radio Capacity in Shadowing and Fast Fading Environments," in *Proc. IEEE International Conference on Cognitive Radio Oriented Wireless Networks and Communications (CrownCom 2009)*, Hannover, Germany, June 2009, pp. 1-6.

- **M. F. Hanif** and P. J. Smith, "On MIMO Cognitive Radios with Antenna Selection," in *Proc. IEEE Wireless Communications and Networking Conference (WCNC 2010)*, Sydney, Australia, April 2010, pp. 1-6.

- **M. F. Hanif**, P. J. Smith and M.-S. Alouini, "SINR Balancing in the Downlink of Cognitive Radio Networks with Imperfect Channel Knowledge," in *IEEE International Conference on Cognitive Radio Oriented Wireless Networks and Communications (CrownCom 2009)*, Cannes, France, June, 2010. (**Won Best Student Paper Award**)

Chapter 2

Fundamentals of Wireless Communications and Convex Optimization Theory

In this chapter we will provide a review of the concepts and techniques used throughout the thesis. Beginning with a brief overview of propagation through a wireless medium, we will explore the statistical characterization of various parameters of fading signals in such environments. After this brief introduction to the point to point wireless propagation phenomenon, we will shift our focus to the recently introduced MIMO systems. We will provide a brief review of the gains and the conditions under which such gains can be achieved for MIMO systems. In addition to this, we will also describe various performance metrics used for the purpose of analysis and design of wireless communications systems. Finally, we will introduce the fundamentals of convex optimization theory. Without going into great depth, we emphasize the significance of these techniques from an algorithmic point of view.

2.1 Fading in Wireless Channels

Wireless propagation of electromagnetic (EM) waves is a complex phenomenon. Unlike wired media, wireless propagation is a complex phenomenon. In this thesis we

will only focus on the special case of narrowband channel models. In particular, our channel is assumed to follow a *time varying, frequency flat (non frequency selective) narrowband* model. We will clarify these terms as we proceed forward. Such a channel model for a SISO scenario leads to the input-output relationship

$$y(t) = h(t)x(t) + n(t), \tag{2.1}$$

where $y(t)$, $h(t)$, $x(t)$ and $n(t)$ represent the received signal, channel impulse response, transmitted signal and receiver side additive (Gaussian) noise, respectively. The index t represents the time, t. If we assume $x(t)$ is a bandpass signal with carrier frequency f_c, then with $\tilde{x}(t)$ as its *complex lowpass equivalent signal* (also known as the *complex envelope*), we can write

$$x(t) = \mathcal{R}[\tilde{x}(t)e^{j2\pi f_c t}], \tag{2.2}$$

where $\mathcal{R}[.]$ gives the real part of a complex number. Before we consider the scenario of multiple waves arriving at the receiver (RX), let us assume that the RX is in relative motion with respect to the transmitter (TX) with a constant velocity v. Further, if the arriving EM signal makes an angle of θ relative to the direction of motion, then due to the *Doppler effect*, the frequency of the received signal shifts (*Doppler shift*) by an amount f_D, given by

$$f_D = f_c \frac{v}{c}\cos(\theta) = \frac{v}{\lambda}\cos(\theta), \tag{2.3}$$

where $\lambda = c/f_c$ and $c \approx 3 \times 10^8$ m/s, the speed of light. Note that f_D can be either positive or negative depending on whether the TX is moving towards or away from the RX.

Now we assume that there are N paths of arrival available to the transmitted signal. If A_i, θ_i (corresponding to the Doppler frequency $f_{D,i}$), τ_i represent the amplitude, angle of arrival and time delay of the ith multipath component, the received bandpass signal *without noise* is given by

$$y(t) = \mathcal{R}\bigg[\sum_{i=1}^{N} A_i e^{j2\pi[f_c + f_{D,i}](t-\tau_i)}\tilde{x}(t-\tau_i)\bigg]. \tag{2.4}$$

As in (2.2), the received bandpass signal can be written as

$$y(t) = \mathcal{R}[\tilde{y}(t)e^{j2\pi f_c t}], \tag{2.5}$$

where $\tilde{y}(t)$ is the complex envelope and with the substitution $\phi_i(t) = 2\pi[(f_c + f_{D,i})\tau_i - f_{D,i}t]$ as the phase of the ith multipath component, it can be rewritten as [9, 10]

$$\tilde{y}(t) = \sum_{i=1}^{N} A_i e^{-j\phi_i(t)} \tilde{x}(t - \tau_i). \tag{2.6}$$

It is clear from (2.6) that the time varying channel impulse response is

$$h(t, \tau) = \sum_{i=1}^{N} A_i e^{-j\phi_i(t)} \delta(t - \tau_i), \tag{2.7}$$

where $\delta(.)$ is the Dirac delta function.

Before proceeding further we consider the physical scenario in a bit more depth. Assuming that for the ith multipath component $\theta_i = 0$, it is easy to observe that the rate at which phase changes in different multiple paths is much higher than the corresponding change in the attenuations of those paths. Following [11], we note that when the delay of ith path, τ_i, changes by $1/f_c$ the corresponding phase, $2\pi f_c(t - \tau_i)$, changes by 2π. Now if the relative motion between this path and the RX occurs with constant velocity v_i, the time rate of change of the phase of this EM ray is $c/f_c v_i$ i.e., the inverse of Doppler shift. Hence, proportional to the inverse of the maximum Doppler shift (called *Doppler spread*), B_D, among the various paths, there is a *coherence time*, T_c, beyond which changes in the channel become significant. For example, if T_x denotes the symbol period of a transmitted signal with $T_x >> T_c$, the signal will be received in a distorted form. Thus the coherence time of a fading channel corresponds to its time rate of change. It is convenient to define the coherence time as

$$T_c \approx \frac{1}{B_D}. \tag{2.8}$$

The dual of the above quantity in the frequency domain, called the *coherence bandwidth*, can be similarly articulated [11]. If we denote the time delay associated with the ith and the jth multipath components as τ_i and τ_j, respectively, then the

phase difference between these components ($2\pi f(\tau_i - \tau_j)$) is most significant when f changes by an amount proportional to the inverse of the difference $\tau_i - \tau_j$. Now for $T_D = \max|\tau_i - \tau_j|, \forall i, j$, called the *delay spread* (or *multipath spread*), if the bandwidth B_x of a signal is greater than the inverse of T_D, the frequency distortion of the transmitted signal becomes significant. The quantity representing this inverse is termed as the *coherence bandwidth*, B_c, i.e.,

$$B_c \approx \frac{1}{T_D}. \tag{2.9}$$

Coherence bandwidth is related to the phenomenon of the multipath components being resolvable or not. Any two multipath components become resolvable if the inverse of their maximum delay difference is greater than the coherence bandwidth. This can also be viewed as the frequency separation beyond which the two frequency components are highly uncorrelated and suffer from independent attenuations. Hence, the term, *frequency selective* channel. If $B_x << B_c$, the channel is described as *narrowband* and *flat* in frequency, i.e., all frequency components in the transmitted signal undergo the same random attenuation and phase shift. It is easy to observe that under flat fading conditions, we have

$$h(t, \tau) = \sum_{i=1}^{N} A_i e^{-j\phi_i(t)} \delta(t - \bar{\tau}) \triangleq h(t)\delta(t - \bar{\tau}), \tag{2.10}$$

where $\bar{\tau}$ shows that under narrowband conditions all path delays are small compared to the symbol duration and can be considered as having the same value of $\bar{\tau}$.

2.1.1 Correlation Properties of the Received Signal

Under narrowband channel conditions, the received signal can be characterized by assuming transmission of an unmodulated carrier, i.e., $\tilde{x}(t) = 1$. With this supposition we note from (2.6) and (2.10) that $h(t) = \tilde{y}(t)$. We also note that under this condition (2.5) reduces to

$$y(t) = h_I(t) \cos 2\pi f_c t - h_Q(t) \sin 2\pi f_c t, \tag{2.11}$$

where

$$h_I(t) = \sum_{i=1}^{N} A_i \cos \phi_i(t), \tag{2.12}$$

$$h_Q(t) = \sum_{i=1}^{N} A_i \sin \phi_i(t). \tag{2.13}$$

In order to evaluate the autocorrelation and cross correlations of the inphase and quadrature components given above, we briefly describe the well known *uniform scattering environment* based on Clarke's model [12] (later upgraded by Jakes [13]). This isotropic scattering model assumes densely packed reflecting entities which are uniformly distributed in azimuth angle. With N different multipaths assumed above, the angle of arrival of the ith component is $\theta_i = i2\pi/N$. Furthermore, each multipath beam is assumed to possess the same received power. In addition to this, we also assume that the phases, delays and amplitudes of the various multipath components do not change in the relevant time interval. With these assumptions, the following properties can be derived

$$\mathbb{E}[h_I(t)] = \mathbb{E}[h_Q(t)] = \mathbb{E}[y(t)] = \mathbb{E}[h_I(t)h_Q(t)] = 0, \tag{2.14}$$

$$A_{h_I}(t,\tau) \triangleq \mathbb{E}[h_I(t)h_I(t+\tau)] = \frac{P_y}{2} J_0(2\pi f_D \tau), \tag{2.15}$$

$$A_{h_Q}(t,\tau) \triangleq \mathbb{E}[h_Q(t)h_Q(t+\tau)] = \frac{P_y}{2} J_0(2\pi f_D \tau), \tag{2.16}$$

$$A_{h_I,h_Q}(t,\tau) \triangleq \mathbb{E}[h_I(t)h_Q(t+\tau)] = 0, \tag{2.17}$$

$$\mathbb{E}[y(t)y(t+\tau)] = A_{h_I}(t,\tau)\cos(2\pi f_c \tau) - A_{h_I,h_Q}(t,\tau)\sin(2\pi f_c \tau) = \frac{P_y}{2} J_0(2\pi f_D \tau), \tag{2.18}$$

where $\mathbb{E}[.]$ denotes the statistical expectation operator. The derivation details of these equations can be found in [13, 10, 9]. Equation (2.14) states that the received signal is a zero mean Gaussian process. Equations (2.15) and (2.16) give the autocorrelation of the in phase and quadrature components of the received signal as the product of the received bandpass signal power $P_y/2 = (\mathbb{E}[h_I(t)^2] + \mathbb{E}[h_Q(t)^2])/2 = (\sum_{i=1}^{N} A_i^2)/2$ and the zeroth-order Bessel function of the first kind $J_0(x) = \frac{1}{\pi}\int_0^{\pi} e^{-jx\cos\theta} d\theta$. With the cross correlation between the inphase and quadrature components as 0 in (2.17), (2.18) shows that the autocorrelation of the total

received signal is equal to that in (2.15) and (2.16). We stress that the formulas given in the analysis above do not incorporate a line-of-sight (LOS) component. Further analytical developments pertaining to this and other issues (like power spectral density etc.) are available in [9, 10].

2.1.2 Statistical Models For Fading Channel/Received Envelope

To overcome the issue of the large number of random parameters involved in characterizing the received signal, using the central limit theorem it is reasonable to assume that for sufficiently large N, under narrowband conditions the received signal envelope $\tilde{y}(t) = h(t)$[1] follows a Gaussian distribution. Since (2.14) shows the inphase and quadrature components of the channel as zero mean processes, with a variance of $\sigma_p^2 = P_y/2$ in each of these components, the envelope amplitude

$$r(t) \triangleq |h(t)| = \sqrt{h_I(t)^2 + h_Q(t)^2}, \tag{2.19}$$

follows a Rayleigh distribution using standard transformation theory [14]. That is, the probability density function (PDF) of $R = r(t)$, $f_R(r)$, is

$$f_R(r) = \frac{r}{\sigma_p^2} e^{-r^2/2\sigma_p^2}, \quad r \geq 0. \tag{2.20}$$

The average power of the received signal envelope is given by

$$\mathbb{E}[R^2] = 2\sigma_p^2. \tag{2.21}$$

Normally, the PDF of the Rayleigh faded channel is normalized to have unit average received power, i.e., $\mathbb{E}[R^2] = 2\sigma_p^2 = 1$ is enforced. With this substitution, $f_R(r) = 2re^{-r^2}$. The distribution of the channel gain is characterized by an exponential distribution with a PDF

$$f_{R^2}(z) = \frac{1}{2\sigma_p^2} e^{-z/2\sigma_p^2} = e^{-z}, \tag{2.22}$$

[1] On the basis of this relation between the complex envelope and the channel impulse response, we will use these terms alternatively in Sec. 2.1.2.

where the second equality follows from the normalized channel assumption.

On the other hand, if the channel possesses a LOS (specular) component, its in-phase and quadrature components do not remain zero mean any more. In such cases the distribution of envelope amplitude follows the well known *Rician* PDF given by [10]

$$f_R(r) = \frac{r}{\sigma_p^2} \exp\left(- \frac{r^2 + v^2}{2\sigma_p^2} \right) I_0\left(\frac{rv}{\sigma^2} \right), \tag{2.23}$$

where $2\sigma_p^2$ is the power in the scattered components, v^2 the power of the LOS (specular) ray and $I_0(.)$ denotes the zeroth-order modified Bessel function of the first kind. The average channel gain in this case is $\mathbb{E}[R^2] = v^2 + 2\sigma_p^2$. Furthermore, it is common to introduce the so-called *Rice factor*, K, given as the ratio of the LOS to the scattered power, i.e.,

$$K = \frac{v^2}{2\sigma_p^2}. \tag{2.24}$$

The normalized Rician fading channel PDF is obtained by assuming $v^2 + 2\sigma_p^2 = 1$. Combining this with (2.24), we have

$$f_R(r) = 2r(1+K)\exp(-(1+K)r^2 - K) I_0(2r\sqrt{K(1+K)}), \quad r \geq 0. \tag{2.25}$$

It is easy to observe that for $K = 0$, the channel behaves as a Rayleigh channel and for $K \to \infty$, the channel tends to act as a LOS channel only. For a detailed and in depth exploration of various statistical characterizations of the phenomenon of channel fading, the reader is referred to [15].

2.1.3 Path Loss and Shadow Fading

In addition to the fast multipath fading taking place on a very small distance scale, the transmitted signal also undergoes distance dependent attenuation. Various techniques like ray tracing methods, empirical path loss modeling of the channel etc. are used to characterize this phenomenon. Details can be seen in [10] and the references therein. However, in order to analyze many practical systems, the following generic path loss model is sufficient. In this model the ratio of the received to the

transmitted power, $P_{y_{PL}}$, is given by

$$P_{y_{PL}} = A\left(\frac{d_0}{d}\right)^{\gamma}, \tag{2.26}$$

where d is the distance between the TX and the RX, d_0 is the reference distance (usually taken as 100 m), A is a dimensionless constant depending upon the physical characteristics of the antenna and the channel attenuation (we will fully characterize A below when we define the complete channel model) and γ is the path loss exponent (usually in the range 2 to 4).

The features of the received signal are also critically dependent upon the terrain where the communication between two entities is taking place. However, physical structures like mountains, buildings etc. may vary from one place to another. Naturally, owing to these random obstructions between the TX and the RX, the signal is *shadowed* (attenuated). It is conventional to model this random large scale attenuation in the transmitted signal as a *lognormal* random variable. Hence, the name *lognormal shadow fading*. When the received signal undergoes lognormal fading, the natural logarithm of its channel gain, Y, i.e., $X = \ln Y$ is a Gaussian random variable. Hence, the PDF of Y is given as

$$f_Y(y) = \begin{cases} \frac{1}{\sqrt{2\pi}\sigma_{sf} y} \exp\left(\frac{-(\ln y - m_X)^2}{2\sigma_{sf}^2}\right), & y > 0, \\ 0 & y \leq 0, \end{cases} \tag{2.27}$$

where σ_{sf} and m_X denote the mean and standard deviation of X. However, in wireless communications, it is common to represent the signal power in dB units. With this requirement, we wish to relate a random variable $V = 10\log_{10} Y$ with X. To do so, we observe that

$$e^X = 10^{(V/10)} \Rightarrow X = \lambda V, \tag{2.28}$$

where $\lambda = \ln 10/10$. If σ and m_V represent the *shadow fading standard deviation* (normally from 6 to 12 dB) and the mean of V in dB units, we have $m_X = \lambda m_V, \sigma_{sf} = \lambda\sigma_V$. Furthermore, in this case the PDF of Y is

$$f_Y(y) = \begin{cases} \frac{1}{\sqrt{2\pi}\lambda\sigma y} \exp\left(\frac{-(10\log_{10} y - m_V)^2}{2\sigma^2}\right), & y > 0, \\ 0 & y \leq 0. \end{cases} \tag{2.29}$$

The above transformations are helpful when the lognormal random variable is expressed using the natural logarithm definition. This is because the use of the natural logarithm is much simpler for mathematical analysis than, say, $\log_{10}(.)$.

After extensive field measurements, [16] arrived at a widely accepted lognormal correlation model. Assuming two points separated by a distance d_{sep}, the correlation between the signal strengths received at these two points, $R(d_{sep})$, is given by

$$R(d_{sep}) = \sigma^2 \rho^{d_{sep}/\Omega}, \tag{2.30}$$

where ρ gives the correlation at some fixed distance Ω. This quantity depends upon the carrier frequency f_c and the type of environment. For example, in suburban macrocells with $f_c = 900$ MHz, $\rho = 0.82$ for $\Omega = 100$ m and with $f_c = 1700$ MHz, $\rho = 0.3$ for $\Omega = 10$ m in urban cellular environments [10, 16]. To remove this empirical dependence, it is common to assume $\rho = e^{-1}$ at a distance X_c (called the *decorrelation distance*) where the autocorrelation of the received signal becomes e^{-1} of its maximum value. Thus, we have

$$R(d_{sep}) = \sigma^2 e^{-d_{sep}/X_c}. \tag{2.31}$$

It is worth emphasizing here that Gudmundson's model is valid only if the pair of links being investigated have a common end point [17].

With this description, we are now in a position to completely describe the instantaneous path gain between a SISO TX-RX pair. We have

$$h = \sqrt{ALr^{-\gamma}}h_m \triangleq \sqrt{AL\left(\frac{d_0}{d}\right)^{\gamma}}h_m, \tag{2.32}$$

where L represents large scale shadow fading with its dB value giving a zero mean Gaussian random variable with a standard deviation of σ. The variable $h_m \sim \mathcal{CN}(0,1)$ represents small scale fading due to the multipath phenomenon with $\mathcal{CN}(0,1)$ depicting a complex normal random variable with zero mean and unit variance. The term $r^{-\gamma}$ corresponds to the path loss between a TX and a RX separated by a distance r. It is noteworthy that we use the normalized distance $r \triangleq \frac{d_0}{d}$ in (2.32). In the thesis, unless otherwise mentioned, we determine A to ensure that the signal-to-noise ratio (SNR) remains greater than a specific threshold at least 95% of the

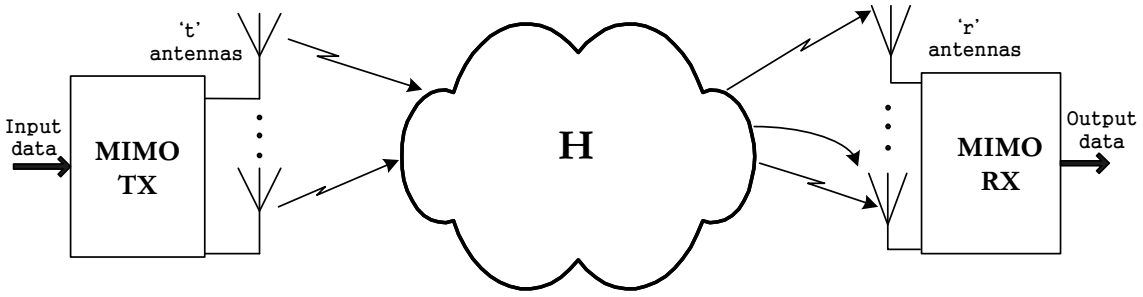

Figure 2.1: A schematic diagram of a generic MIMO system.

time. This corresponds to ensuring that a threshold SNR is being met throughout the coverage area at least 95% of the time.

2.2 MIMO Communications

With a brief overview of SISO fading point-to-point wireless channels, we provide an introduction to MIMO communication systems, a recent breakthrough in wireless communications. It is largely due to the seminal works of [18, 19], that a proper utilization of the extra dimension of space culminated in the so called MIMO techniques. In our discussion, we will mainly limit ourselves to the fundamentals of these techniques. For an excellent elaboration, the reader is referred to [20].

Let us focus on the narrowband, frequency flat, point-to-point MIMO channel. Assume that the TX is equipped with t and the RX with r antennas as shown in Fig. 2.1. The output at the RX is given by

$$\mathbf{y} = \mathbf{H}\mathbf{x} + \mathbf{n}, \tag{2.33}$$

where $y \in \mathbb{C}^t$, $x \in \mathbb{C}^r$, $\mathbf{H}$ lies in the space of $r \times t$ matrices having complex and possibly random entries i.e., $\mathbf{H} \in \mathbb{C}^{r \times t}$ with h_{ij} denoting the channel between jth TX and ith RX and $\mathbf{n}$ is a zero mean circularly symmetric complex Gaussian (ZMCSCG) noise vector with independent and identically distributed (i.i.d.) entries. We mention that for notational clarity we exclude the time index t from (2.33). If we assume a noise variance of σ_n^2 at each receive antenna, we have

$$\mathbb{E}[\mathbf{n}\mathbf{n}^\dagger] = \sigma_n^2 \mathbf{I}_r, \tag{2.34}$$

where $(.)^\dagger$ denotes Hermitian transpose and $\mathbf{I}_r$ represents an $r \times r$ identity matrix, i.e., $\mathbf{n} \sim \mathcal{CN}(0, \sigma_n^2 \mathbf{I}_r)$. In addition to this, we also suppose that $\mathbb{E}[|h_{ij}|^2] = 1, \forall i, j$. With these assumptions we impose a constraint that the total transmit power is $\mathbb{E}[\mathbf{x}^\dagger \mathbf{x}] = P$. This can be equivalently rewritten as $\mathrm{Tr}(\mathbb{E}[\mathbf{x}\mathbf{x}^\dagger]) \triangleq \mathrm{Tr}(\mathbf{Q}) = P$ where $\mathrm{Tr}(.)$ denotes the trace operation. The SNR at the ith RX branch is

$$\frac{\mathbb{E}_{\mathbf{H},\mathbf{x}}[|\mathbf{H}_{(i,:)}\mathbf{x}|^2]}{\sigma_n^2} = \frac{\mathbb{E}_{\mathbf{H},\mathbf{x}}[\mathbf{x}^\dagger \mathbf{H}_{(i,:)}^\dagger \mathbf{H}_{(i,:)}\mathbf{x}]}{\sigma_n^2} = \frac{\mathbb{E}_{\mathbf{x}}[\mathbf{x}^\dagger \mathbf{I}_t \mathbf{x}]}{\sigma_n^2} = \frac{P}{\sigma_n^2}, \tag{2.35}$$

where $\mathbb{E}_{\mathbf{H},\mathbf{x}}$ performs the joint expectation operation over the channel and the transmitted symbols, $\mathbf{H}_{(i,:)}$ denotes the ith row of $\mathbf{H}$ and in the second to last inequality we use the fact that $\mathbf{H}_{(i,:)}$ and $\mathbf{x}$ are statistically independent and that we have an uncorrelated channel, i.e., $\mathbb{E}_{\mathbf{H}}[\mathbf{H}_{(i,:)}^\dagger \mathbf{H}_{(i,:)}] = \mathbf{I}_t$.

2.2.1 MIMO Capacity with Deterministic and Perfect Channel State Information

Before providing an explicit expression for the capacity of MIMO systems, let us first perform a singular value decomposition (SVD) of the MIMO channel. It is assumed that channel state information (CSI) $\mathbf{H}$ is perfectly available at both the TX and the RX. With this information, $\mathbf{H}$ can be decomposed using its SVD as

$$\mathbf{H} = \mathbf{U} \begin{pmatrix} \mathbf{\Sigma}_{R_H} & \mathbf{0} \\ \mathbf{0} & \mathbf{0} \end{pmatrix} \mathbf{V}, \tag{2.36}$$

where R_H denotes the rank of $\mathbf{H}$ and $R_H \leq \min(r, t)$, $\mathbf{\Sigma}_{R_H}$ is an $R_H \times R_H$ diagonal matrix with ith diagonal entry (*singular value*) σ_i and $\mathbf{U}$ and $\mathbf{V}$ are unitary matrices, i.e., $\mathbf{U}\mathbf{U}^\dagger = \mathbf{I}_r, \mathbf{V}\mathbf{V}^\dagger = \mathbf{I}_t$. $\mathbf{V}$ and $\mathbf{U}$ are also known as *transmit precoding* and *receiver shaping* matrices, respectively [10]. This means that for an input stream of data, $\tilde{\mathbf{x}}$, $\mathbf{x} = \mathbf{V}^\dagger \tilde{\mathbf{x}}$ is the precoded signal which is transmitted and $\tilde{\mathbf{y}} \triangleq \mathbf{U}^\dagger \mathbf{y}$ is the received signal, $\mathbf{y}$, shaped by the matrix $\mathbf{U}$. With this symbolic notation, it is easy to verify that,

$$\tilde{\mathbf{y}} = \mathbf{U}^\dagger(\mathbf{H}\mathbf{x} + \mathbf{n}) = \mathbf{\Sigma}_{R_H}\tilde{\mathbf{x}} + \tilde{\mathbf{n}} = \mathrm{diag}(\mathbf{\Sigma}_{R_H}) \odot \tilde{\mathbf{x}} + \tilde{\mathbf{n}}, \tag{2.37}$$

where $\tilde{\mathbf{n}} = \mathbf{U}^{\dagger}\mathbf{n}$, i.e., the statistical properties of $\tilde{\mathbf{n}}$ are same as those of $\mathbf{n}$, diag(.) produces the diagonal entries of a matrix as a column vector and $\odot$ denotes the Schur product of two matrices. It is easy to infer from this development that an appropriate decomposition of the MIMO channel can result in a non-interfering set of parallel channels. The number of such channels depends on R_H, which in turn relies on the nature of the scattering environment. Thus, the greater the number of independent multipath channels, the greater the rank of $\mathbf{H}$ and the greater the total number of orthogonal parallel channels. We note that $\sigma_i = \sqrt{\lambda_i}$, where λ_i is the ith eigenvalue of the matrix $\mathbf{H}\mathbf{H}^{\dagger}$.

Equipped with this information, we present formulae for the capacity of MIMO static channels. We start of with [21],

$$\max_{p(\mathbf{x})} I(\mathbf{x};\mathbf{y}) \triangleq \max_{p(\mathbf{x})} [H(\mathbf{y}) - H(\mathbf{y}|\mathbf{x})], \tag{2.38}$$

where $p(\mathbf{x})$ denotes the distribution of the input symbols, $I(\mathbf{x};\mathbf{y})$ represents mutual information between the output and the input, $H(\mathbf{y}) \triangleq \mathbb{E}_{\mathbf{y}}[\ln \frac{1}{f_{\mathbf{y}}(y)}]$ and $H(\mathbf{y}|\mathbf{x}) \triangleq \mathbb{E}_{\mathbf{y}|\mathbf{x}}[\ln \frac{1}{f_{\mathbf{y}|\mathbf{x}}(y|x)}]$ are the entropies of the random variables $\mathbf{y}$ and $\mathbf{y}|\mathbf{x}$ with PDFs $f_{\mathbf{x}}(x)$ and $f_{\mathbf{y}|\mathbf{x}}(y|x)$, respectively. It is easy to verify that $H(\mathbf{y}|\mathbf{x}) = H(\mathbf{n})$ [21]. Furthermore, for a random variable in $\mathbb{C}^n$ such that $\mathbf{g} \sim \mathcal{CN}(0, \mathbf{R}_g)$, we have

$$\begin{aligned}
H(\mathbf{g}) &= \mathbb{E}_{\mathbf{g}}[\ln \det(\pi \mathbf{R}_g) + \mathbf{g}^{\dagger}(\mathbf{R}_g)^{-1}\mathbf{g} \ln e] \\
&= \ln \det(\pi \mathbf{R}_g) + \mathbb{E}_{\mathbf{g}}[\mathbf{g}^{\dagger}\mathbf{R}_g^{-1}\mathbf{g}] \ln e \\
&= \ln \det(\pi \mathbf{R}_g) + \mathrm{Tr}(\mathbf{R}_g^{-1}\mathbb{E}_{\mathbf{g}}[\mathbf{g}\mathbf{g}^{\dagger}]) \ln e \\
&= \ln \det(\pi \mathbf{R}_g) + \mathrm{Tr}(\mathbf{I}) \ln e \\
&= \ln \det(\pi \mathbf{R}_g) + \ln e^n \\
&= \ln \det(\pi \mathbf{R}_g) e^n \\
&= \ln \det(\pi e \mathbf{R}_g),
\end{aligned} \tag{2.39}$$

where in the last step above we have used the property that for a constant c, $\det(c\mathbf{A}) = c^n \det(\mathbf{A})$. From (2.39) we observe that $H(\mathbf{y}|\mathbf{x})$ is independent of $p(\mathbf{x})$ so that in order to maximize (2.38), we need to find the distribution that maximizes

$H(\mathbf{y})$. It is also well known that $H(\mathbf{y}) \leq \ln \det(\pi e \mathbf{R}_y)$ with equality iff (if and only if) $\mathbf{y} \sim \mathcal{CN}(0, \mathbf{R}_y)$, where $\mathbf{R}_y = \mathbf{HQH}^\dagger + \mathbf{I}_r$. Similarly, we can calculate the entropy of $\mathbf{n}$ using (2.39). Thus the final expression of the maximum mutual information becomes,

$$\max_{p(\mathbf{x})} I(\mathbf{x}; \mathbf{y}) = \log_2 \det(\mathbf{I}_r + \mathbf{HQH}^\dagger). \tag{2.40}$$

Hence, the capacity (in bps/Hz) can be obtained by maximizing this mutual information expression over the transmit covariance matrix subject to a total power constraint, i.e.,

$$C \triangleq \max_{\mathbf{Q}:\mathrm{Tr}(\mathbf{Q}) \leq P, \mathbf{Q} \succeq \mathbf{0}} \log_2 \det(\mathbf{I}_r + \mathbf{HQH}^\dagger), \tag{2.41}$$

where $\mathbf{Q} \succeq \mathbf{0}$ shows that $\mathbf{Q}$ is a positive semidefinite (PSD) matrix. This capacity expression can be easily evaluated. With perfect CSI available at the TX, the SVD can be used to decompose the MIMO channel into a set of independent parallel channels. Hence, (2.40) amounts to evaluating the capacity of such channels with a total power constraint. The solution is the well known *water filling* [21] algorithm, i.e.,

$$C = \sum_{i=1}^{R_H} \log_2(\lambda_i \mu)^+, \tag{2.42}$$

where $\sum_i (\mu - \frac{1}{\lambda_i})^+ = \frac{P}{\sigma_n^2}$ and $(.)^+ \triangleq \max(0, .)$ maps its input to the non-negative reals. The water filling algorithm can be interpreted as an approach which gives more resources (i.e., power) to the stronger *eigenmodes* (i.e., the members of the set of independent and orthogonal channels obtained by applying the SVD) and gives fewer resources to the weaker ones while simultaneously maintaining the total power constraint.

2.2.2 MIMO Capacity Under Fading Channel Conditions

With Perfect CSI

When the channel is known at both the TX and the RX, then for each channel realization the optimum input covariance matrix follows the water filling allocation policy. The total capacity is just the average of capacities obtained in each of these

realizations, also known as ergodic capacity (more on this in Sec. 2.3). For more details, please refer to [10, Sec. 10.3.2].

With Perfect CSI at the RX Only

Once the CSI is available at the RX only, it was shown in [19] that the optimal strategy for a Gaussian codebook and i.i.d. Gaussian channel conditions involves distributing the power uniformly across all TX antennas, i.e.,

$$\mathbf{Q} = \frac{P}{t}\mathbf{I}_t. \tag{2.43}$$

An important measure of interest in such a regime is that of *ergodic (mean)* capacity when the channel is changing at a sufficiently high speed (we explain this more later). Hence, the ergodic capacity can be calculated as,

$$\begin{aligned} C &= \mathbb{E}\left[\log_2 \det\left(\mathbf{I}_r + \frac{P}{t}\mathbf{H}\mathbf{H}^\dagger\right)\right] \\ &= \mathbb{E}\log_2 \prod_{i=1}^{m}\left(1 + \frac{P}{t}\lambda_i\right) \\ &= \mathbb{E}\sum_{i=1}^{m}\log_2\left(1 + \frac{P}{t}\lambda_i\right) \\ &= \sum_{i=1}^{m}\mathbb{E}\log_2\left(1 + \frac{P}{t}\lambda_i\right) \\ &= m\mathbb{E}\log_2\left(1 + \frac{P}{t}\lambda_1\right), \end{aligned} \tag{2.44}$$

where the expectation is over the channel, $m \triangleq \min(r, t)$ and we have used the facts that the determinant of a matrix is equal to the product of its eigenvalues and that all unordered eigenvalues of $\mathbf{H}\mathbf{H}^\dagger$ are i.i.d. The exact expression for (2.44) is involved, well known and available in [19]. However, to provide an insight, we will concentrate on asymptotic cases. First, consider the situation where the number of RX antennas $r > 1$ and $t \to \infty$. Using the strong law of large numbers, we have

$$\frac{1}{t}\mathbf{H}\mathbf{H}^\dagger \to \mathbf{I}_r \quad \text{as} \quad t \to \infty. \tag{2.45}$$

Hence the ergodic capacity becomes

$$C = \log_2 \det(\mathbf{I}_r + P\mathbf{I}_r) = \log_2(1+P)^r = r\log_2(1+P). \tag{2.46}$$

Thus we see an r-fold increase in the capacity as $t \to \infty$. This shows the benefit of MIMO systems in rich scattering environments. However, this approximation to the ergodic capacity is very crude. Thus we resort to an approximation [11], when both t and r grow to infinity while their ratio remains constant. In this case the ergodic capacity in (2.44) is shown to be

$$\frac{C}{m} = \mathbb{E}\left[\log\left(1 + P\frac{m}{t}\nu\right)\right], \tag{2.47}$$

where $\nu \triangleq \lambda_1/m$. Using the representation in (2.47), the mean value has been reported as obeying the following limit [11]

$$\frac{C}{m} \to (\log_2(w+P) + (1-\zeta)\log_2(1-\omega_-) - (\omega_-\zeta)\log_2 e).\max(1, 1/\zeta) \tag{2.48}$$

where $\omega_\pm \triangleq (\omega \pm \sqrt{\omega^2 - 4/\zeta})$ $\omega \triangleq 1 + 1/\zeta + 1/P$ and $\zeta = t/r$. Remarkably, this asymptotic mean calculation provides an excellent agreement with the ergodic capacity values obtained for small r and t. A similar asymptotic analysis was carried out in [22].

The final case of no CSI available at both the TX and the RX is heavily dependent on the type of channel model being utilized. The straightforward interpretation of linear growth of capacity with TX and RX antennas does not remain valid anymore. For a comprehensive note on this scenario, please refer to [10, Chapter 10] and the references therein.

Effect of Channel Correlation on Capacity and Beamforming Techniques

As is evident from the previous discussion, the ergodic capacity tends to be maximum when the MIMO system operates in a rich scattering environment and increases linearly with the number of antennas being used. In our discussion we concentrate on Rayleigh channel conditions only. However, on account of the finite space available to pack antennas on either side of the link, the signals tend to become correlated. One of the popular analytical channel models used to characterize this is the *Kronecker model*. When there is no LOS path, the entries of the channel matrix are complex normal with zero mean under the Rayleigh fading assumption.

The channel covariance matrix is given by

$$\mathbf{R}_H = \mathbb{E}[\text{vec}(\mathbf{H})\text{vec}(\mathbf{H})^\dagger] = \mathbf{R}_t \otimes \mathbf{R}_r, \tag{2.49}$$

where vec(.) denotes the vector operation, $\otimes$ denotes the Kronecker product and

$$\mathbf{R}_t = \mathbb{E}[\mathbf{H}_{(i,:)}^\dagger \mathbf{H}_{(i,:)}], \quad i = 1, 2, \ldots, r, \tag{2.50}$$

$$\mathbf{R}_r = \mathbb{E}[\mathbf{H}_{(:,j)} \mathbf{H}_{(:,j)}^\dagger], \quad j = 1, 2, \ldots, t, \tag{2.51}$$

where $\mathbf{H}_{(i,:)}$ and $\mathbf{H}_{(:,j)}$ represent the ith row and the jth column of $\mathbf{H}$. Now if $\mathbf{h} = \text{vec}(\mathbf{H})$, then $\mathbf{h} \sim \mathcal{CN}(0, \mathbf{R}_H)$ can be expressed as

$$\mathbf{h} = \mathbf{R}_H^{1/2} \mathbf{h}_w, \tag{2.52}$$

where $\mathbf{h}_w$ is a $rt \times 1$ vector with zero mean unit variance complex Gaussian entries. Substituting (2.49) in (2.52) we get,

$$\mathbf{h} = (\mathbf{R}_t \otimes \mathbf{R}_r)^{1/2} \mathbf{h}_w \iff \mathbf{H} = \mathbf{R}_r^{1/2} \mathbf{H}_w \mathbf{R}_t^{1/2} \tag{2.53}$$

where we have used the property that $\text{vec}(\mathbf{ABC}) = (\mathbf{C}^T \otimes \mathbf{A})\text{vec}(\mathbf{B})$, $\mathbf{H}_w \in \mathbb{C}^{r \times t}$ is a matrix with i.i.d. zero mean unit variance complex Gaussian variable entries and $(.)^T$ denotes transpose operation. For a detailed review of MIMO channel models, the reader is referred to [23, 24, 25].

With this information, the ergodic capacity under the assumption that the TX correlation is unknown can be written as

$$C = \mathbb{E}\left[\log_2 \det \left(\mathbf{I}_r + \frac{P}{t} \mathbf{H}_w \mathbf{R}_t \mathbf{H}_w^\dagger \mathbf{R}_r \right) \right]. \tag{2.54}$$

The exact expression for this mean is complex and for the special case of semicorrelated (when correlation exists either at the TX or the RX) channels is available in [26, 27]. Intuitively, such a correlation model will result in a decrease in the mean capacity under ergodic channel assumptions. To provide a more concrete perspective, asymptotic results have been presented in [11, Sec. 10.5].

As a final point, we will end our discussion on MIMO techniques by briefly explaining the concept of *beamforming* in MIMO systems. Multiple antenna systems

have long been used to perform unidirectional transmission of data [28]. The eigenvalues and eigenvectors of the input covariance matrix of such a system determines the power and the direction of transmission, respectively. The case of a unit rank transmit covariance matrix is commonly referred to as beamforming. In particular, for a serial to parallel data conversion rate of k, beamforming involves weighting a transmit data vector $\mathbf{d} \in \mathbb{C}^k$, whose covariance matrix is the identity matrix, with $\sqrt{\mathbf{p}} = [\sqrt{p_1}, \ldots, \sqrt{p_k}]$ and then multiplying by the beamforming vectors $\mathbf{w}_1, \ldots, \mathbf{w}_k$ with each being $\mathbb{C}^t$. Thus the signal to be transmitted becomes,

$$\mathbf{x} = \sum_{i=1}^{k} \sqrt{p_i} d_i \mathbf{w}_i = \mathbf{W}\mathbf{s}, \tag{2.55}$$

where $\mathbf{W} \in \mathbb{C}^{t \times k}$ has $\mathbf{w}_i$ as its ith column and $\mathbf{s} \triangleq [\sqrt{p_1} d_1, \ldots, \sqrt{p_k} d_k]^T$. The signal $\mathbf{x}$ is then launched into space. In the case of multiple-input single-output (MISO) systems, beamforming has been shown to be capacity optimal under perfect channel conditions, see [29, 30] and references therein. Specifically, for the MISO case, beamforming refers to finding the only non-zero eigenmode (since the channel is of rank-1) of the channel and transmitting along that mode. On the other hand, if the CSI is not perfectly known at the TX, then with only its statistical information, it is not possible to find the nonzero eigen channel. Thus as shown by [19, 18], the best strategy is to uniformly allocate powers across all eigenmodes. In the case of MIMO systems, the story is not that different. [29] was the first to prove that for the Kronecker product channel model, the eigenvectors of the TX covariance matrix should be matched with those of the TX correlation matrix, thus, determining the optimal direction of launch for the signal. The exact conditions of optimality of beamforming and the powers allocated to different eigenmodes are complex and can be obtained from [29].

For a detailed discussion about information theoretic limits of multiuser MIMO systems, the interested reader is referred to [31]. In addition to this, various other concepts like topics concerned with space-time codes, MIMO transceiver design, diversity multiplexing trade off, the effect of channel uncertainties on various metrics etc. can be seen in [11, 20, 32] and the references therein.

2.3 Performance Metrics

With a brief overview of modern wireless communication systems, we present an introduction to various metrics commonly used to gauge the performance of communication systems. Our discussion will include brief details of performance metrics such as ergodic capacity, outage capacity, signal-to-interference-plus-noise ratio (SINR) outage and level crossing rates.

2.3.1 Ergodic Capacity

We have seen that propagation through a wireless medium is a random process. This gives rise to two important aspects of capacity depending on whether the channel is ergodic. In particular, if the symbol transmitted is long enough to experience all states of the channel, the capacity can be considered as an ensemble average if the channel is ergodic. In symbols, if T_x is the symbol time and $T_x >> T_c$, the *coherence time*, then the channel is ergodic and the capacity of a SISO system is given by

$$C_{erg} = \mathbb{E}_h \left[\log_2 \left(1 + \frac{P_s |h|^2}{\sigma_n^2} \right) \right], \tag{2.56}$$

where h is the channel between the TX and the RX, P_s is the transmitted power and σ_n^2 is the noise variance at the RX. Under similar conditions we have already seen expressions for the ergodic capacity of MIMO channels in (2.44) and (2.54).

2.3.2 Outage Capacity

If the channel is not ergodic, then the above definition of capacity in (2.56) does not remain valid anymore. This can be clarified by considering that the transmitted symbol does not undergo all states of the channel i.e., the equivalence of time average with ensemble average does not remain valid anymore. In this situation, clearly, capacity would be limited by the maximum bit carrying capability of the worst channel realization. From the perspective of capacity being a random variable, its instantaneous value is $C(h) \triangleq \log_2(1 + |h|^2 \text{SNR})$. Now if the transmission rate

r exceeds this variable we say that outage has occurred. Thus the probability of outage is

$$P_{out} = P[C(h) \leq r] = 1 - \exp\left(-\frac{2^r - 1}{\text{SNR}}\right), \tag{2.57}$$

where the second equality follows since $|h|$ is Rayleigh distributed. Hence, we define an ε *outage capacity* as the maximum rate r that can ensure an outage probability of $P_{out} \leq \varepsilon$ [11, 20].

With this definition, we are now in a position to characterize outage capacity of a MIMO channel in nonergodic Rayleigh fading environment. Assuming CSI availability at the RX only, the instantaneous capacity is given by

$$C(\mathbf{H}) = \log_2 \det\left(\mathbf{I}_r + \frac{P}{t}\mathbf{H}\mathbf{Q}\mathbf{H}^\dagger\right). \tag{2.58}$$

Thus the outage capacity becomes,

$$P_{out} = P(C(\mathbf{H}) < r). \tag{2.59}$$

Astonishingly, this probability has been shown to be well approximated by a Gaussian random variable even for small numbers of TX and RX antennas [33, 11]. An explicit and simplified expression is available in [11, Sec. 10.6]. Thus we conclude that the mean of the variable in (2.58) is the actual capacity of the MIMO system if the channel fulfills the conditions of ergodicity, else we deal with the notion of outage capacity.

Before closing this section, we mention that from a system design point of view it is common to consider a probability, known as *outage probability*, which describes the probability of the signal SNR (or SINR) being less than a certain threshold. This probability arises due to various impairments (such as multipath fading, lognormal shadowing, path loss effects etc.) to propagation in the wireless medium. Such probabilities can help calculate system design parameters such as cell coverage areas, outage probability of the cell etc. For details, please refer to [10] and the references therein.

2.3.3 Level Crossing Rate

From our previous discussion it is evident that the amplitude of the received signal cannot be characterized deterministically. Thus, in addition to the significance of a statistical characterization of various parameters, it is also necessary to study the temporal behavior of a received signal. This can be done using the notion of *level crossing rate* (LCR) and *average fade duration* (AFD) of the faded signal.

Since the received signal can be undergo huge fluctuations in its amplitude, it becomes necessary to characterize its rate of crossing a particular threshold, T. LCR determines how often the signal crosses T in the downward (or upward) direction per unit time. The LCR of a random process $\Theta(t)$ across T is known to be [13, 34, 9, 10],

$$\mathrm{LCR}_{\Theta}(T) = \int_0^{\infty} \dot{x} f_{\Theta\dot{\Theta}}(T, \dot{x}) d\dot{x}, \tag{2.60}$$

where $\dot{x}$ denotes the time derivative of x and $f_{\Theta\dot{\Theta}}(T, \dot{x})$ is the joint PDF of the process $\Theta(t)$ and its time derivative at the same instant. For the simplest case of a Rayleigh faded signal, the LCR can be expressed in closed form and is given by [34],

$$\mathrm{LCR}_{Ray}(T) = \sqrt{\frac{\beta}{2\pi}} \frac{T}{\sigma_p^2} e^{-\frac{T^2}{2\sigma^2}}, \tag{2.61}$$

where $\sigma_p^2 = \rho_{Ray}(0)$ denotes the value of the autocorrelation function of a Rayleigh process at time $t = 0$ i.e., the mean power of the underlying Gaussian process. The parameter β represents the negative curvature of the autocorrelation function, i.e.,

$$\beta = -\ddot{\rho}_{Ray}(0). \tag{2.62}$$

A similar expression for the LCR of a Rician process is available in [34].

Related to the concept of LCR is that of the AFD. The AFD describes the duration for which the received faded signal remains below a threshold. For a random process, $\Theta(t)$, it is defined as

$$\mathrm{AFD}_{\Theta}(T) = \frac{P(\Theta(t) \leq T)}{\mathrm{LCR}_{\Theta}(T)}. \tag{2.63}$$

For the case of a Rayleigh fading process, the AFD admits the following expression [34]

$$\mathrm{AFD}_{Ray} = \sqrt{\frac{2\pi}{\beta}}\frac{\sigma_p^2}{T}\left(e^{-\frac{T^2}{2\sigma_p^2}} - 1\right). \tag{2.64}$$

The AFD expression for a Rician process can be seen from [34].

2.4 An Overview of Convex Optimization

After presenting a bird's eye view of wireless communications theory, we move towards the next part of the chapter that deals with the basics of convex optimization. Convex optimization is the only class of optimization theory that permeates all branches of optimization, namely, discrete, continuous, dynamic, integer, etc. Most importantly, it forms the only class of optimization problems that possesses globally converging and polynomial time algorithms. In addition to this, a large number of problems can either be directly written or approximated (*relaxed*) to some type of convex optimization problem. However, the process of exposing the hidden convexity of a problem is not at all trivial. Our discussion will include a brief overview of the fundamentals of convex optimization theory that will introduce various types of convex optimization problems. We will not resort to an in depth study of convex analysis and duality theory. The reader is referred to the excellent texts [35, 36, 37] and the references therein.

Generally speaking a convex optimization problem can be written as

$$\begin{aligned} \underset{\mathbf{x}}{\text{minimize}} \quad & f_0(\mathbf{x}) \\ \text{subject to} \quad & \mathbf{x} \in \mathcal{S}, \end{aligned} \tag{2.65}$$

where $f_0 : \mathbb{R}^n \to \mathbb{R}$ is the convex *cost* or *objective* function and the variable of optimization $\mathbf{x}$ is assumed be constrained to lie in a convex set $\mathcal{S} \subseteq \mathbb{R}^n$. Unless otherwise specified, for the purpose of exposition we will limit our variables to lie in a space of n-tuples, i.e., $\mathbb{R}^n$. For a description of vector (general) and multiple objective optimization problems, the reader is referred to [36, Sec. 4.6-4.7].

Let us first define the notion of a convex set. A set $\mathcal{C}$ is said to be convex if, for $\mathbf{x}, \mathbf{y} \in \mathcal{C}$, all *convex combinations*, $\lambda\mathbf{x} + (1-\lambda)\mathbf{y} \in \mathcal{C}$, where $\lambda \in \mathbb{R}$, the set of real

numbers, and $0 \leq \lambda \leq 1$. In words, a set is said to be convex if for any two elements inside the set, the line segment joining them is also included in the set. Roughly speaking, in two dimensions, this would correspond to sets without indentations. Non empty *polyhedral* sets of the form $\{\mathbf{x}|\mathbf{a}_j^T\mathbf{x} \leq b_j, j = 1 \ldots r\}$ and *convex cones* $\{\mathbf{x}_1, \mathbf{x}_2|\zeta_1, \zeta_2 \geq 0, \zeta_1\mathbf{x}_1 \in C, \zeta_2\mathbf{x}_2 \in C \Rightarrow \zeta_1\mathbf{x}_1 + \zeta_2\mathbf{x}_2 \in C\}$ are a couple of examples of convex sets. It is relatively easy to observe that the intersection of convex sets is also convex. To understand this suppose we take a convex combination of two elements that belongs to one of the sets of the intersecting convex sets. The same convex combination will also belong to the intersection of all those sets, thus proving the property. For a detailed account of convex sets, the reader is referred to [35, 36, 37].

Now we define the notion of a convex function. A function $f : \mathcal{C} \rightarrow \mathbb{R}$ where $\mathcal{C} \subseteq \mathbb{R}^n$ is said to be convex if for all $\alpha \in [0, 1]$

$$f(\alpha\mathbf{x} + (1 - \alpha)\mathbf{y}) \leq \alpha f(\mathbf{x}) + (1 - \alpha)f(\mathbf{y}), \quad \forall \mathbf{x}, \mathbf{y} \in \mathcal{C}. \tag{2.66}$$

Thus, a convex function can be visualized as a bowl shaped function with a chord joining two of its points lying above it. If the above inequality holds strictly, we call f *strictly* convex over $\mathcal{C}$. Furthermore, the *level set* $\mathcal{L} = \{\mathbf{x} \in \mathcal{C}|f(\mathbf{x}) \leq t\}$ where t is a scalar, of a convex function is always convex. To see this let us suppose that $\mathbf{x}$ and $\mathbf{y}$ are any two points in $\mathcal{L}$. Then their convex combination $\mathbf{z} = \lambda\mathbf{x} + (1 - \lambda)\mathbf{y}$ for $\lambda \in [0, 1]$ also belongs to $\mathcal{L}$ i.e.,

$$\begin{aligned} f(\mathbf{z}) = f(\lambda\mathbf{x} + (1 - \lambda)\mathbf{y}) &\leq \lambda f(\mathbf{x}) + (1 - \lambda)f(\mathbf{y}) \\ &\leq \lambda t + (1 - \lambda)t \leq t. \end{aligned} \tag{2.67}$$

However, we note that the converse does not hold [36]. A function f is said to be *concave* iff $-f$ is convex. The maximization of a concave function subject to convex constraints can be solved by performing the minimization of the negative of the concave function subject to the same convex constraints. Thus it is conventional to consider convex minimization problems as shown in (2.65).

An important fact related to convex optimization problems is that a local optimizer is also a global optimizer. Before proving this fact, we proceed to define a

few standard definitions. A point $\mathbf{x}$ that satisfies the constraints in (2.65) is said to be *feasible*. The set of all such points that satisfy the constraints is called a *feasible set* or *region*. A member of this feasible set, $\mathbf{x}^\star$, is said to be the *global optimizer* (*minimizer*) of (2.65) if

$$f(\mathbf{x}^\star) \leq f(\mathbf{x}), \quad \forall \mathbf{x} \in \mathcal{S}. \tag{2.68}$$

If the above inequality is satisfied strictly, $\mathbf{x}^\star$ is also described as a *strict global optimizer*. Similarly, if the point $\mathbf{x}^\star$ is the *best* amongst all feasible points in an ϵ-neighborhood of f, we call it a *local* minimizer, i.e.,

$$f(\mathbf{x}^\star) \leq f(\mathbf{x}), \quad \forall \mathbf{x} \in \mathcal{S} \text{ such that } \parallel \mathbf{x} - \mathbf{x}^\star \parallel \leq \epsilon, \tag{2.69}$$

where $\epsilon > 0$. Now we proceed with the proof of global optimality of a local minimizer of a convex optimization problem. Assume that $\mathbf{x}^\star$ is a local optimum with respect to the ϵ-neighborhood inside the convex set $\mathcal{S} \subseteq \mathbb{R}^n$ for any $\epsilon > 0$. Let $\mathbf{y}$ be any feasible point, *not* necessarily inside the ϵ-neighborhood. Assume $\mathbf{z} = \lambda \mathbf{x}^\star + (1-\lambda)\mathbf{y}, \lambda \in [0,1]$, is the convex combination of these two points. Now let us assume λ to be sufficiently small so that the point $\mathbf{z}$ lies within the ϵ-neighborhood of $\mathbf{x}^\star$. Owing to the convexity of f we have

$$f(\mathbf{z}) = f(\lambda \mathbf{x}^\star + (1-\lambda)\mathbf{y}) \leq \lambda f(\mathbf{x}^\star) + (1-\lambda) f(\mathbf{y}). \tag{2.70}$$

Rearranging, we obtain

$$f(\mathbf{y}) \geq \frac{f(\mathbf{z}) - \lambda f(\mathbf{x}^\star)}{1-\lambda}. \tag{2.71}$$

Since we have assumed that $\mathbf{z}$ lies inside the ϵ-neighborhood, we have $f(\mathbf{z}) \geq f(\mathbf{x}^\star)$. Thus we have

$$f(\mathbf{y}) \geq \frac{f(\mathbf{x}^\star) - \lambda f(\mathbf{x}^\star)}{1-\lambda} = f(\mathbf{x}^\star), \tag{2.72}$$

Hence for any feasible point, $\mathbf{y}$, $f(\mathbf{y}) \geq f(\mathbf{x}^\star)$ and so $\mathbf{x}^\star$ which was a local optimum must also be the global optimum. Note that while deriving this result we have have not constrained f to be differentiable.

We should also mention another consequence of convexity in an optimization problem. If the objective function, f, of a convex optimization problem is strictly

convex, then the global optimizer is unique. To prove this fact we follow a similar path as above. Suppose, for the sake of argument, that $\mathbf{x}^\star$ and $\mathbf{x}^{\star\star}$ are both global optimizers of a convex problem, i.e., $f(\mathbf{x}^\star) = f(\mathbf{x}^{\star\star}) \leq f(\mathbf{x}), \forall \mathbf{x} \in \mathcal{S}$, such that $\mathbf{x}^\star \neq \mathbf{x}^{\star\star}$. Let $\mathbf{z} = \lambda \mathbf{x}^\star + (1-\lambda)\mathbf{x}^{\star\star}$ be a convex combination of these two points. Thus, from the strict convexity of f, we have,

$$f(\mathbf{x}^{\star\star}) > \frac{f(\mathbf{z}) - \lambda f(\mathbf{x}^\star)}{(1-\lambda)}. \tag{2.73}$$

Using the fact that $f(\mathbf{z}) \geq f(\mathbf{x}^{\star\star})$ we end up obtaining

$$f(\mathbf{x}^{\star\star}) < f(\mathbf{x}^\star), \tag{2.74}$$

which is a contradiction to the fact that $\mathbf{x}^\star$ and $\mathbf{x}^{\star\star}$ are globally optimal. Again observe that (2.73) can be rewritten as

$$f(\mathbf{x}^\star) > \frac{f(\mathbf{z}) - (1-\lambda) f(\mathbf{x}^{\star\star})}{\lambda}. \tag{2.75}$$

Since $f(\mathbf{z}) \geq f(\mathbf{x}^\star)$, we end up obtaining $f(\mathbf{x}^\star) < f(\mathbf{x}^{\star\star})$, which is again a contradiction to the optimality of $\mathbf{x}^\star$ and $\mathbf{x}^{\star\star}$. Thus we arrive at the conclusion that $\mathbf{x}^\star \neq \mathbf{x}^{\star\star}$ is not possible. After having discussed an introduction to convex optimization problems, we provide a brief overview of different classes of convex optimization problems.

2.5 Broad Classification of Convex Optimization Problems

Surprisingly, many optimization problems are, either directly or after some manipulations (approximations or relaxations), transformable to one or other type of convex problem. In this section we provide a brief overview of these different classes.

2.5.1 Linear Programs

Probably one of the most widely used class of convex optimization problems has been that of linear programs (LPs). Generally, an LP can be written as

$$\begin{aligned} \underset{\mathbf{x}}{\text{minimize}} \quad & \mathbf{c}^T\mathbf{x} + \mathbf{d} \\ \text{subject to} \quad & \mathbf{A}\mathbf{x} = \mathbf{b} \\ & \mathbf{G}\mathbf{x} \preceq \mathbf{h}, \end{aligned} \tag{2.76}$$

where $\mathbf{A}, \mathbf{G}, \mathbf{c}, \mathbf{d}, \mathbf{b}, \mathbf{h}$ are known matrices and vectors of appropriate dimensions and $\preceq$ denotes componentwise inequality. It is easy to see that the above LP can be equivalently rewritten as

$$\begin{aligned} \underset{\mathbf{x}}{\text{minimize}} \quad & \mathbf{c}^T\mathbf{x} + \mathbf{d} \\ \text{subject to} \quad & \mathbf{A}\mathbf{x} = \mathbf{b} \\ & \mathbf{G}\mathbf{x} + \mathbf{s} = \mathbf{h} \\ & \mathbf{s} \succeq 0, \end{aligned} \tag{2.77}$$

where $\mathbf{s}$ is a vector of slack variables. Huge interest was spurred in the use of LPs to solve various optimization problems after the discovery of the *simplex* method [38]. For a detailed account of LPs the reader is referred to [38, 39, 36].

2.5.2 Conic Programming

We will provide a glimpse of optimization problems in which the set over which optimization is performed is either a *second order cone (Lorentz cone)* or a *cone of semidefinite* matrices. Such problems can be generally written as,

$$\begin{aligned} \underset{\mathbf{x}}{\text{minimize}} \quad & \mathbf{c}^T\mathbf{x} \\ \text{subject to} \quad & \mathbf{F}\mathbf{x} + \mathbf{g} \preceq_K 0 \\ & \mathbf{A}\mathbf{x} = \mathbf{b}, \end{aligned} \tag{2.78}$$

where K is a convex cone and $\preceq_K$ represents a *generalized* inequality constraint (for precise properties of the cone and the generalized inequalities, the reader is referred to [37]).

Second Order Cone Programs

A second order cone program (SOCP) can be written as

$$\begin{aligned} \underset{\mathbf{x}}{\text{minimize}} \quad & \mathbf{c}^T\mathbf{x} \\ \text{subject to} \quad & (\mathbf{A}_i\mathbf{x}+\mathbf{b}_i, \mathbf{c}_i^T\mathbf{x}+\mathbf{d}_i) \in \mathbf{L}^{m_i}, \quad i=1,\ldots,m \\ & \mathbf{F}\mathbf{x}=\mathbf{b}, \end{aligned} \tag{2.79}$$

where $\mathbf{L}^{m_i} = \{(y,t) \in \mathbb{R}^{n+1} | \parallel y \parallel_2 \leq t\}$ is an m-dimensional second-order (ice cream or Lorentz) cone. Thus, in this case, the cone K in (2.78) corresponds to $\mathbf{L}^{m_i}$. It is easy to observe that if $\mathbf{c}_i = 0$, squaring both sides of the inequality constraints reduces (2.79) to a quadratically constrained linear program (we can also obtain a convex quadratically constrained quadratic program (QCQP) provided the objective is a convex quadratic function). Similarly, if $\mathbf{A}_i = 0$, (2.79) boils down to an LP. Thus SOCPs form a more general class than both convex QCQPs and LPs. A large variety of optimization problems can be written as SOCPs. For a comprehensive description of these categories, please see [40].

Semidefinite Programs

If we optimize (2.78) over a cone of PSD matrices i.e., $K = \mathbb{S}_+^k$, we end up solving a semidefinite program (SDP). A general SDP can be written as [36]

$$\begin{aligned} \underset{\mathbf{x}}{\text{minimize}} \quad & \mathbf{c}^T\mathbf{x} \\ \text{subject to} \quad & \mathbf{F}(\mathbf{x}) = \textstyle\sum_{i=1}^n \mathbf{x}_i\mathbf{F}_i + \mathbf{G} \preceq 0 \\ & \mathbf{A}\mathbf{x}=\mathbf{b}, \end{aligned} \tag{2.80}$$

where $\mathbf{G}, \mathbf{F}_i, \forall i$ are PSD matrices and $\mathbf{A}$ is the data matrix of appropriate dimension. The inequality constraint of (2.80) is described as a *linear matrix inequality* (LMI). For an excellent exposition on LMIs, the reader is referred to [41]. The case of multiple LMIs can easily be handled by using a block-diagonal LMI from individual LMIs [36, 41]. We note that when $\mathbf{G}, \mathbf{F}_i, \forall i$ are diagonal, the SDP in (2.80) becomes an LP [36]. Similarly an SOCP can be cast as an SDP. To see this, we first state

the Schur complement lemma [42]. Consider a block diagonal matrix $\mathbf{X}$ given by,

$$\mathbf{X} = \begin{pmatrix} \mathbf{A} & \mathbf{B} \\ \mathbf{B}^T & \mathbf{C} \end{pmatrix}. \tag{2.81}$$

The Schur complement of $\mathbf{A}$ in $\mathbf{X}$ (provided $\det(\mathbf{A}) \neq 0$) is $\mathbf{S} = \mathbf{C} - \mathbf{B}^T\mathbf{A}^{-1}\mathbf{B}$. Now if $\mathbf{A} \succ 0$ (positive definite), then $\mathbf{X} \succeq 0$ iff $\mathbf{S} \succeq 0$. Using this property, we see that the second-order cone constraint of (2.79) can be written as the following LMI:

$$\begin{pmatrix} (\mathbf{c}^T\mathbf{x} + \mathbf{d})\mathbf{I} & \mathbf{A}\mathbf{x} + \mathbf{b} \\ (\mathbf{A}\mathbf{x} + \mathbf{b})^T & \mathbf{c}^T\mathbf{x} + \mathbf{d} \end{pmatrix} \succeq 0. \tag{2.82}$$

Thus we notice that SDPs form the most general class of optimization problems in terms of its modeling capabilities. However, an SDP is also the most computationally burdensome among all classes of convex problems [40]. For a comprehensive overview of SDPs, the reader is referred to [43].

2.5.3 Geometric Programs

An optimization problem with the structure

$$\begin{aligned} \underset{\mathbf{x}}{\text{minimize}} \quad & f_0(\mathbf{x}) \\ \text{subject to} \quad & f_i(\mathbf{x}) \leq 1, \quad i = 1, \ldots, m \\ & h_i(\mathbf{x}) = 1, \quad i = 1, 2, \ldots, p, \end{aligned} \tag{2.83}$$

where $f_0(\mathbf{x}) \ldots f_m(\mathbf{x})$ are of the form $\sum_{k=1}^{K} c_k x_1^{a_{1k}} x_2^{a_{2k}} \ldots x_n^{a_{nk}}$ and $h_i(x)$ are of the form $c_0 x_1^{a_1} x_2^{a_2} \ldots x_n^{a_n}$ is known as a geometric program (GP). The functions $f_i(\mathbf{x}), i = 1, 2, \ldots, m$ are known as *posynomials* and the functions $h_i(\mathbf{x})$ are called *monomials* [36]. These functions are constrained to have $c_k > 0$ and $a_{ik} \in \mathbb{R}, \forall i, k$. However, (2.83) is a nonconvex optimization problem.

To convert (2.83) into a convex program, if we substitute $y_i = \ln x_i, b_k = \ln c_k$ and notice the fact that a log-sum-exponential is a convex function, a few manipulations lead to the following program [36]

$$\begin{aligned} \underset{\mathbf{y}}{\text{minimize}} \quad & \ln\left(\textstyle\sum_{k=1}^{K_0} e^{\mathbf{a}_{0k}^T\mathbf{y} + \mathbf{b}_{0k}}\right) \\ \text{subject to} \quad & \ln\left(\textstyle\sum_{k=1}^{K_i} e^{\mathbf{a}_{ik}^T\mathbf{y} + \mathbf{b}_{ik}}\right) \leq 0, \quad i = 1, \ldots, m \\ & \mathbf{g}_i^T\mathbf{y} + h_i = 0, \quad i = 1, 2, \ldots, p, \end{aligned} \tag{2.84}$$

where $\mathbf{g}_i \in \mathbb{R}^n$ contains exponents i.e., the a_i terms and $h_i = \ln c_0$ represents logarithm of the constant term in the monomial constraints of (2.83). Now (2.84) is a convex optimization problem.

GPs have been extensively used for designing power control algorithms in mobile communication systems. See for example, [44]. Similarly, a broad perspective on GPs can be seen in the tutorial [45].

Before concluding this chapter, we mention that convex programs can be solved using polynomial time interior-point algorithms. Various software packages are available, either in the freeware or payware category, that contain efficient and robust implementations of these algorithms. See for example, [46]. Based on interior-point methods, the worst case complexity (i.e., the number of iterations) of a generic convex optimization problem to reach a ϕ accurate solution [2] is roughly $\mathcal{O}(\sqrt{\eta} \ln \phi^{-1})$, where η represents a measure of the problem size depending on the number of variables and constraints and $\mathcal{O}(.)$ represents the worst case order of growth of the complexity of the problem with respect to its size [47]. The worst case complexity for specific classes such as SOCPs and SDPs can be seen in [40]. Finally, we mention that detailed accounts of duality theory, convex analysis and applications of convex programming are available in excellent texts, such as [37, 35, 36].

[2] When we solve an optimization problem, the algorithm used to accomplish this task produces a sequence of variables to be optimized. If the difference between the optimum variable and the kth member of the sequence is less than, say, ϕ according to some metric (that could be absolute difference, relative difference between them etc.), we say we have obtained a ϕ accurate solution.

Chapter 3

Fundamental Capacity Limits of Cognitive Radio Systems

Until recently, the frequency bands below 3.5 GHz were thought to be severely congested. Due to the superior propagation conditions in the lower frequencies there is a desire for all services to find a place in this sought after "real estate". However, spectrum occupancy measurements performed in the United States [2] show that spectrum scarcity cannot be confirmed by the measurements. Instead, the apparent congestion is due to the way in which spectrum is allocated into specific bands for specific services (i.e., fixed, mobile and broadcasting) and then by the national regulatory authorities who license the band/service combinations to private owners. Therefore even when the licensed owner is not using their spectrum, there is no access to other users, hence the apparent congestion. In order to improve spectrum occupancy and utilization, various regulatory bodies worldwide are considering the benefits offered by CR [1]. The key idea behind the deployment of CR is that greater utilization of spectrum can be achieved if they are allowed to co-exist with the incumbent licensed PUs provided that they cause minimal interference. The CRs must therefore learn from the radio environment and adapt their parameters so that they can co-exist with the primary systems. The CR field has proven to be a rich source of challenging problems. A large number of papers have appeared

on various aspects of CR, namely spectrum sensing (see [48, 49] and the references therein), fundamental limits of spectrum sharing [50], information theoretic capacity limits [51, 52, 53, 54, 55] etc.

The 2 user cognitive channel [51, 52, 53, 54, 55] consists of a primary and a secondary user. It is very closely related to the classic 2 user interference channel, see [56] and references therein. The formulation of the CR channel is due to Devroye *et al.* [51]. In this channel, the CR has a non-causal knowledge of the intended message of the primary and by employing dirty paper coding [57] at the CR transmitter it is able to circumvent the PU's interference to its receiver. However, the interference from the CR to the primary receiver remains and has the potential to cause a rate loss to the primary.

In recent work, Jovicic and Viswanath [53] have studied the fundamental limits of the capacity of the CR channel. They show that if the CR is able to devote a part of its power to relaying the primary message, it is possible to compensate for the rate loss to the primary via this additional relay. They have provided exact expressions for the PU and CR capacity of a 2 user CR channel when the CR transmitter sustains a power loss by devoting a fraction, α, of its transmit power to relay the PU message. Furthermore, they have provided an exact expression for α such that the PU rate remains the same as if there was no CR interference. It should be stressed here that their system model is such that at the expense of CR transmit power, the PU device is always able to maintain a constant data rate. Hence, we focus on CR rate, α and their statistics. They also assume that the PU receiver uses a single user decoder. Their result holds for the so called low interference regime when the interference-to-noise ratio (INR) at the PU receiver is less than the SNR at the CR receiver. The authors in [55] also arrived at the same results in their parallel but independent work. Note that the capacity of the 2 user CR channel has only recently been studied. Multi-user extensions are not currently available although some related work is now appearing [6]. Hence, in this chapter we restrict our attention to the 2 user scenario.

The Jovicic and Viswanath study is for a static channel, i.e., the direct and cross

link gains are constants. In a system study, these gains will be random and subject to distance dependent path loss and shadow fading. Furthermore, the channel gains also experience fast fading. As the channel gains are random variables, the power loss parameter, α, is also random.

In this chapter we focus on the power loss, α, the capacity of the CR channel and the probability that the "low interference regime" holds. The motivation for this work arises from the fact that maximum rate schemes for the CR in the low interference regime [53, 55] and the achievable rate schemes for the high interference regime [52, 54] are very different. Hence, it is of interest to identify which scenario is the most important. To attack this question we propose a simple, physically based geometric model for the CR, PU layout and compute the probability of the low interference regime. Results are obviously limited to this particular model but provide some insight into reasonable deployment scenarios. Since the results show the low interference regime can be dominant, it is also of interest to characterize CR performance via the α parameter. In this area we make the following contributions:

- Assuming lognormal shadowing, Rayleigh fading and path loss effects we derive the probability that the "low interference regime" holds. We also extend the results to Rician fading channels.

- In both Rayleigh and Rician fading environments we derive an approximation for α and its statistics. This extremely accurate approximation leads to simple interpretations of the effect of system parameters on the capacity.

- Using the statistics of α we investigate the mean rate loss of the CR and the CDF of the CR rates. For both the above we show their dependence on the propagation parameters.

- We also show how the mean value of α varies with the CR transmit power and therefore the CR coverage area.

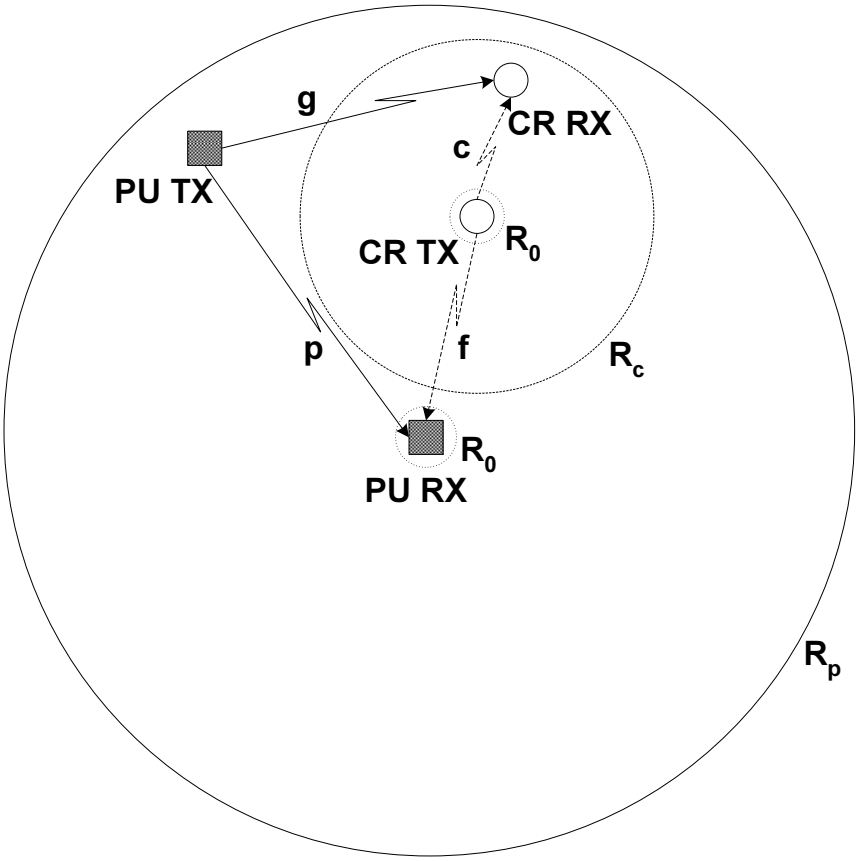

Figure 3.1: System model.

3.1 System Model

Consider a PU receiver in the center of a circular region of radius R_p. The PU transmitter is located uniformly in an annulus of outer radius R_p and inner radius R_0 centered on the PU receiver. It is to be noted that we place the PU receiver at the center only for the sake of mathematical convenience (see Fig. 3.1). The use of the annulus restricts the length of the PU link from becoming too small. This matches physical reality and also avoids problems with the classical inverse power law relationship between signal strength and distance [58]. In particular, having a minimum distance, R_0, prevents the signal strength from becoming infinite as the transmitter approaches the receiver. Similarly, we assume that a CR transmitter is uniformly located in the same annulus. Finally, a CR receiver is uniformly located in an annulus centered on the CR transmitter. The dimensions of this annulus are

defined by an inner radius, R_0, and an outer radius, R_c. This choice of system layout is asymmetric in the sense that the PU receiver is at the center of its circular region whereas the CR transmitter is at the center of its smaller region. This layout is chosen for mathematical simplicity since the lengths of the CR-PU and CR-CR links have a common simple distribution which leads to the closed form analysis in Sec. 3.2. Following the work of Jovicic and Viswanath [53], the four channel gains which define the system are denoted p, g, f, c. In this paper, these complex channel gains include shadow fading, path-loss and Rayleigh and Rician fast fading effects. To introduce the required notation we consider the link from the CR transmitter to the PU receiver, the CP link. For this link we have

$$|f|^2 = \Gamma_{cp}|\tilde{f}|^2, \tag{3.1}$$

where $|\tilde{f}|^2$ is an exponential random variable with unit mean for Rayleigh channels or a noncentral χ^2 variable for Rician fading and Γ_{cp} is the link gain[1]. The link gain comprises shadow fading and distance dependent path loss effects so that,

$$\Gamma_{cp} = A_c L_{cp} r_{cp}^{-\gamma}, \tag{3.2}$$

where A_c is a constant that depends on physical deployment parameters such as antenna height, antenna gain, cable loss etc. Following our discussion in Chapter 2, in (3.2) the variable $L_{cp} = 10^{\tilde{X}_{cp}/10}$ is lognormal, $\tilde{X}_{cp}$ is zero mean Gaussian and r_{cp} is the link distance. The standard deviation which defines the lognormal is σ (dB) and γ is the path loss exponent. For convenience, we also write $L_{cp} = e^{X_{cp}}$ so that $X_{cp} = \beta\tilde{X}_{cp}$, $\beta = \ln(10)/10$ and σ_{sf}^2 is the variance of X_{cp}. Hence, for the CP link we have

$$|f|^2 = A_c e^{X_{cp}} r_{cp}^{-\gamma}|\tilde{f}|^2. \tag{3.3}$$

The other three links are defined similarly where $\tilde{p}, \tilde{g}, \tilde{c}$ are standard exponentials for Rayleigh fading and represent noncentral χ^2 random variables for Rician fading, X_{pp}, X_{pc}, X_{cc}, are Gaussians with the same parameters as X_{cp} and r_{pp}, r_{pc}, r_{cc} are link

[1]Link gains Γ_{cc}, Γ_{pc} and Γ_{pp} are defined similarly. However, the parameters of Γ_{pc} and Γ_{pp} are modified appropriately.

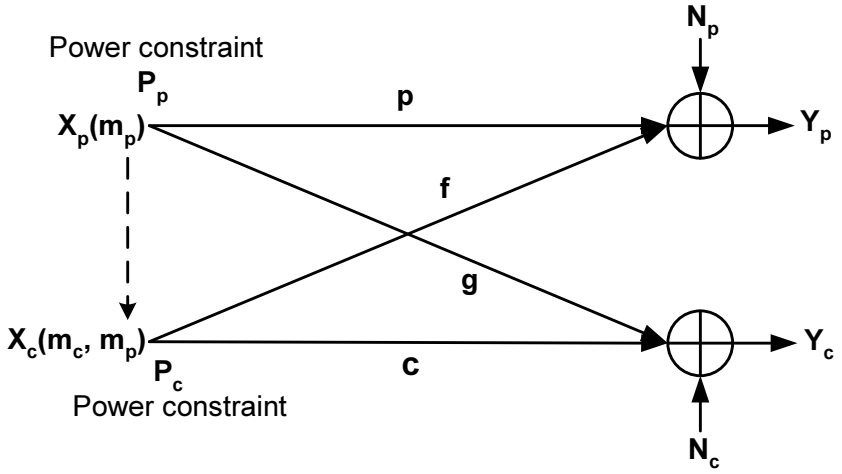

Figure 3.2: Information theoretic model (taken from [53]).

distances. However, for the links involving the PU transmitter we assume a different constant A_p in the model of link gains. The parameters A_p and A_c are constants and all links are assumed independent. The remaining parameters required are the transmit powers of the PU and CR devices, given by P_p and P_c respectively, and the noise powers at the PU and CR receivers, given by N_p and N_c respectively.

The physical model described above corresponds to the information theoretic model shown in Fig. 3.2. For fixed channel coefficients, p, g, f and c, Jovicic and Viswanath [53] compute the highest rate that the CR can achieve subject to certain constraints using the model in Fig. 3.2. In this figure the arrow on the transmitter side indicates the noncausal availability of the PU's message to the cognitive device for dirty paper coding (DPC) purposes [57]. A key constraint is that the PU must not suffer any rate degradation due to the CR and this is achieved by the CR dedicating a portion, α, of its transmit power to relaying the PU message. The parameter, α, is therefore central to determining the CR rate. Furthermore, the results in [53] are valid in the "low interference regime" defined by $a < 1$ where

$$a = \frac{\sqrt{N_c}\sqrt{\Gamma_{cp}}|\tilde{f}|}{\sqrt{N_p}\sqrt{\Gamma_{cc}}|\tilde{c}|} = \frac{\sqrt{N_c}e^{X_{cp}/2}r_{cp}^{-\gamma/2}|\tilde{f}|}{\sqrt{N_p}e^{X_{cc}/2}r_{cc}^{-\gamma/2}|\tilde{c}|}. \tag{3.4}$$

We note that a can be considered as the ratio of link strengths of the CR-PU to

CR-CR channels. In this regime, the highest CR rate is given by

$$R_{CR} = \log_2\left(1 + \frac{|c|^2(1-\alpha)P_c}{N_c}\right), \tag{3.5}$$

with the power loss parameter, α, defined by

$$\alpha = \frac{|s|^2}{|t|^2}\left[\frac{\sqrt{1+|t|^2(1+|s|^2)}-1}{1+|s|^2}\right]^2, \tag{3.6}$$

where $|s| = \sqrt{P_p}\sqrt{\Gamma_{pp}}|\tilde{p}|N_p^{-1/2}$ and $|t| = \sqrt{P_c}\sqrt{\Gamma_{cp}}|\tilde{f}|N_p^{-1/2}$. We call α the power loss parameter since it accounts for the portion of CR's power dedicated towards relaying PU's message. Note that the definitions of α and R_c are conditional on $a < 1$. Since a is a function of $\tilde{f}$ and $\tilde{c}$ we see that both $\tilde{f}$ and $\tilde{c}$ are conditional random variables.

Note that all results are built on the assumptions that the CR has access to the PU message and has perfect knowledge of all 4 channels in Figs. 3.1 and 3.2, namely p, f, g and c. These assumptions are built into the fundamental work on the 2 user CR channel model in [53]. This approach is typical of research in this area where the initial results are developed for the ideal case and later work attempts to relax these assumptions. Hence, the resulting capacity is an upper bound on any realistic system where the key practical concerns include CSI availability at the CR transmitter and access of the CR transmitter to the PU message.

3.2 The Low Interference Regime

Note that the 4 paths which characterize the channels in Figs. 3.1 and 3.2 can all be Rayleigh or Rician. This leads to 16 possible combinations of Rayleigh or Rician channels. To make the study more concise we assume that the PP and PC paths are Rayleigh and vary the CC and CP paths. Hence, we consider the 4 combinations where $\tilde{c}$ (CC) and $\tilde{f}$ (CP) can be Rician or Rayleigh. This is sensible since $\tilde{c}$, $\tilde{f}$ affect both the low interference regime (3.4) and the cognitive rate (R_{CR} in (3.5)), whereas the PP, PC links only affect R_{CR}. The notation Ray/Rice etc. denotes the nature of the $\tilde{f}/\tilde{c}$ variables or the CP/CC paths.

3.2.1 Rayleigh/Rayleigh Scenario

The low interference regime is defined by $a < 1$, where a is defined in (3.4). The probability, $P(a < 1)$, depends on the distribution of r_{cc}/r_{cp}. Using standard transformation theory [14], some simple but lengthy calculations show that the CDF of r_{cc}/r_{cp} is given by (3.7). A sketch proof is given in Appendix A.

$$P\left(\frac{r_{cc}}{r_{cp}} < x\right) = \begin{cases} 0 & x \le \frac{R_0}{R_p} \\ \frac{0.5x^2(R_p^4 - R_0^4x^{-4}) - R_0^2(R_p^2 - R_0^2x^{-2})}{(R_c^2 - R_0^2)(R_p^2 - R_0^2)} & \frac{R_0}{R_p} < x \le \frac{R_c}{R_p} \\ \frac{0.5(R_c^4 - R_0^4) - R_0^2(R_c^2 - R_0^2) + (x^2R_p^2 - R_c^2)(R_c^2 - R_0^2)}{x^2(R_c^2 - R_0^2)(R_p^2 - R_0^2)} & \frac{R_c}{R_p} < x \le 1 \\ 1 - \frac{0.5R_c^4x^{-2} + 0.5R_0^4x^2 - R_0^2R_c^2}{(R_c^2 - R_0^2)(R_p^2 - R_0^2)} & 1 < x \le \frac{R_c}{R_0} \\ 1 & x > \frac{R_c}{R_0} \end{cases} \tag{3.7}$$

The CDF in (3.7) can be written as

$$P\left(\frac{r_{cc}}{r_{cp}} < x\right) = c_{i0}x^{-2} + c_{i1} + c_{i2}x^2, \quad x \in S_i,\ i = 1, 2, 3, 4, 5, \tag{3.8}$$

where $i = 1, 2, 3, 4, 5$ refers to the 5 equations in (3.7) running from the top ($i = 1$) to the bottom ($i = 5$) and S_1, S_2, S_3, S_4, S_5 refers to the five sets of x values in (3.7) so that $S_1 = \{x | x \le R_0/R_p\}$ etc. Using the notation $\Delta = (R_c^2 - R_0^2)(R_p^2 - R_0^2)$, the constants in (3.8) are defined by $c_{10} = 0$, $c_{11} = 0$, $c_{12} = 0$, $c_{20} = 0.5R_0^4/\Delta$, $c_{21} = -R_0^2R_p^2/\Delta$, $c_{22} = 0.5R_p^4/\Delta$, $c_{30} = 0.5(R_0^4 - R_c^4)/\Delta$, $c_{31} = R_p^2(R_c^2 - R_0^2)/\Delta$, $c_{32} = 0$, $c_{40} = -0.5R_c^4/\Delta$, $c_{41} = 1 + R_0^2R_c^2/\Delta$, $c_{42} = -0.5R_0^4/\Delta$, $c_{50} = 0$, $c_{51} = 1$ and $c_{52} = 0$. Note that the result in (3.7) assumes $R_p > R_c$ but the corresponding result for $R_c > R_p$ is also given in Appendix A.

Now $P(a < 1) = P(a^2 < 1)$ can be written as $P(Y < Ke^XZ^{-\gamma})$ where $Y = |\tilde{f}|^2/|\tilde{c}|^2$, $K = N_p/N_c$, $X = X_{cc} - X_{cp}$ and $Z = r_{cc}/r_{cp}$. Thus the required probability

is

$$\begin{aligned} P(Y < Ke^X Z^{-\gamma}) &= P(Z < K^{1/\gamma} e^{X/\gamma} Y^{-1/\gamma}) \\ &= \mathbb{E}[P(Z < W|W)] \\ &= \int_0^\infty P(Z < w) f_W(w) dw, \end{aligned} \tag{3.9}$$

where $W = K^{1/\gamma} e^{X/\gamma} Y^{-1/\gamma}$, $f_W(.)$ is the PDF of W and we use the independence of Z and W to arrive at the last line. Note that $P(Z < w)$, given in (3.8), only contains constants and terms involving $w^{\pm 2}$. Hence, we need

$$\int_\theta^\kappa w^{2m} f_W(w) dw = \iint (Ke^x y^{-1})^{2m/\gamma} f_{X,Y}(x,y) dx dy, \tag{3.10}$$

where $m = -1, 0, 1$ and $f_{X,Y}(.)$ is the joint PDF of X, Y. Now, since $W = K^{1/\gamma} e^{X/\gamma} Y^{-1/\gamma}$, the limits $\theta \leq w \leq \kappa$ in (3.10) imply the following limits for x:

$$\ln(\theta^\gamma K^{-1} y) \leq x \leq \ln(\kappa^\gamma K^{-1} y).$$

Let $\ln(\theta^\gamma K^{-1} y) = A$ and $\ln(\kappa^\gamma K^{-1} y) = B$, then noting that $f_{X,Y}(x,y) = f_X(x) f_Y(y)$, the integral in (3.10) becomes

$$\int_\theta^\kappa w^{2m} f_W(w) dw = \int_0^\infty K^{2m/\gamma} y^{-2m/\gamma} f_Y(y) \int_A^B e^{2mx/\gamma} f_X(x) dx dy. \tag{3.11}$$

Since $X \sim \mathcal{N}(0, 2\sigma_{sf}^2)$, the inner integral in (3.11) becomes

$$\int_A^B e^{2mx/\gamma} f_X(x) dx = \exp\left(\frac{4m^2\sigma_{sf}^2}{\gamma^2}\right) \left[\Phi\left(\frac{B - \frac{4m\sigma_{sf}^2}{\gamma}}{\sqrt{2}\sigma_{sf}}\right) - \Phi\left(\frac{A - \frac{4m\sigma_{sf}^2}{\gamma}}{\sqrt{2}\sigma_{sf}}\right)\right], \tag{3.12}$$

where Φ is the CDF of a standard Gaussian. Since $f_Y(y)$ is the density function of the ratio of two standard exponentials, it is given by [50]

$$f_Y(y) = \frac{1}{(1+y)^2}, \qquad y \geq 0. \tag{3.13}$$

Using (3.12) and (3.13), the total general integral in (3.10) reduces to

$$\begin{aligned} \int_\theta^\kappa w^{2m} f_W(w) dw &= \int_0^\infty K^{2m/\gamma} y^{-2m/\gamma} (1+y)^{-2} \exp\left(\frac{4m^2\sigma_{sf}^2}{\gamma^2}\right) \\ &\quad \times \left[\Phi\left(\frac{B - \frac{4m\sigma_{sf}^2}{\gamma}}{\sqrt{2}\sigma_{sf}}\right) - \Phi\left(\frac{A - \frac{4m\sigma_{sf}^2}{\gamma}}{\sqrt{2}\sigma_{sf}}\right)\right] dy \\ &\triangleq I(m, \theta, \kappa). \end{aligned} \tag{3.14}$$

Substituting (3.8) and (3.14) in (3.9) gives $P(a<1)$ as

$$\begin{aligned} P(a<1) &= P(Y < Ke^X Z^{-\gamma}) \\ &= \sum_{i=2}^{5} c_{i0} I(-1,\theta_i,\kappa_i) + c_{i1} I(0,\theta_i,\kappa_i) + c_{i2} I(1,\theta_i,\kappa_i) \\ &= \sum_{i=2}^{5}\sum_{j=0}^{2} c_{ij} I(j-1,\theta_i,\kappa_i). \end{aligned} \tag{3.15}$$

Finally, it can be seen from the limits given in (3.7) that $\kappa_i = \theta_{i+1}$. Hence, the final expression for the probability of occurrence of the low interference regime is

$$P(a<1) = \sum_{i=2}^{5}\sum_{j=0}^{2} c_{ij} I(j-1,\theta_i,\theta_{i+1}), \tag{3.16}$$

where the c_{ij} were defined after (3.8), $I(j-1,\theta_i,\theta_{i+1})$ is given in (3.14), $\theta_2 = R_0/R_p$, $\theta_3 = R_c/R_p$, $\theta_4 = 1$, $\theta_5 = R_c/R_0$ and $\theta_6 = \infty$. Therefore, $P(a<1)$ can be derived in terms of a single numerical integral. For numerical convenience, (3.14) is rewritten using the substitution $v = y(y+1)^{-1}$ so that a finite range integral over $0 < v < 1$ is used for numerical results, i.e.,

$$\begin{aligned} \int_{\theta}^{\kappa} w^{2m} f_W(w)dw &= \int_0^1 K^{2m/\gamma}\Big(\frac{v}{1-v}\Big)^{-2m/\gamma} \exp\left(\frac{4m^2\sigma_{sf}^2}{\gamma^2}\right) \\ &\quad \times \left[\Phi\left(\frac{B-\frac{4m\sigma_{sf}^2}{\gamma}}{\sqrt{2}\sigma_{sf}}\right) - \Phi\left(\frac{A-\frac{4m\sigma_{sf}^2}{\gamma}}{\sqrt{2}\sigma_{sf}}\right)\right] dv \\ &\triangleq \quad I(m,\theta,\kappa), \end{aligned} \tag{3.17}$$

where $\ln(\theta^\gamma K^{-1}\frac{v}{1-v}) = A$ and $\ln(\kappa^\gamma K^{-1}\frac{v}{1-v}) = B$. Further simplification of (3.14) appears difficult but the result in (3.17) is stable and rapid to compute.

It can be easily inferred from the above discussion that the probability of the low interference regime in (3.16) depends on the ratio (3.13) of random variables representing fast fading in the interfering and direct links from the point of view of the cognitive device. Hence, we focus on the following three cases of interest as well.

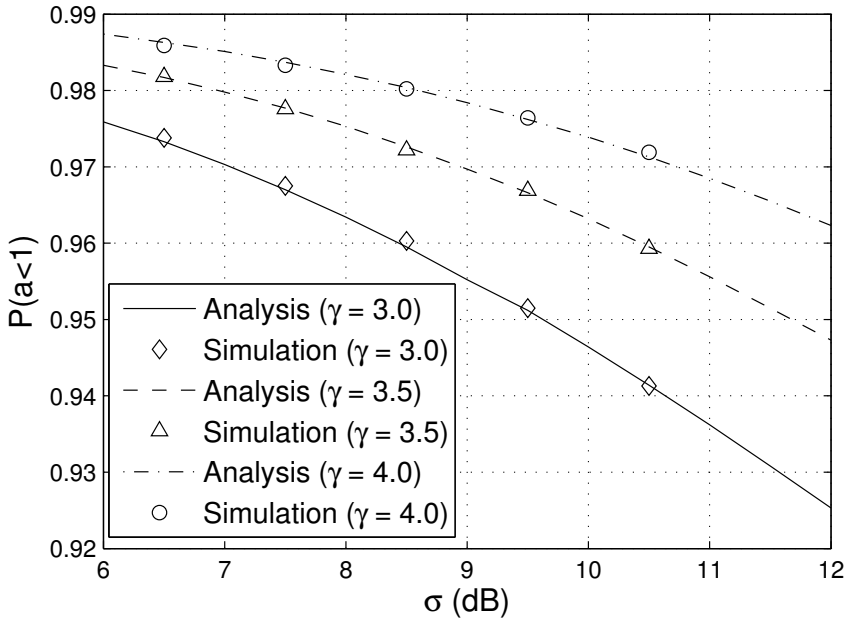

Figure 3.3: Probability of occurrence of the low interference regime as a function of shadow fading standard deviation, σ (dB) for Ray/Ray scenario.

3.2.2 Rayleigh/Rician Scenario

In this case the probability density function (PDF) of the ratio $Y = |\tilde{f}|^2/|\tilde{c}|^2$ is given by [59]

$$f_Y(y) = (K_r + 1)\frac{y + (K_r + 1)^2}{(y + K_r + 1)^3} e^{-K_r + \frac{K_r^2 + K_r}{y + K_r + 1}}, \tag{3.18}$$

where K_r is the Rician K_r factor defined as the ratio of signal power in the dominant component to the scattered power and $f_Y(y)$ represents the PDF of the ratio of a standard exponential to a noncentral χ^2 random variable. Now $P(a < 1)$ can easily be calculated by substituting (3.18) in (3.11) and evaluating (3.16). However, as mentioned above the substitution $v = y(y + 1)^{-1}$ is again used to obtain the numerical results.

3.2.3 Rician/Rayleigh Scenario

When the interfering signal is a Rician variable and the direct signal follows Rayleigh distribution, the PDF of Y, after correcting the expression in [59], is

$$f_Y(y) = \frac{K_r(1+K_r)}{(y+K_r y+1)^2} e^{-\frac{K_r}{y+K_r y+1}} + \frac{1-K_r^2+y(1+2K_r+K_r^2)}{(y+K_r y+1)^3} e^{-K_r+\frac{K_r y+K_r^2 y}{y+K_r y+1}}, \tag{3.19}$$

where K_r is the Rician K factor defined as above.

3.2.4 Rician/Rician Scenario

In this final case, the PDF $f_Y(y)$ represents the ratio of two noncentral χ^2 variables. It is known that [60] this ratio characterizes the *doubly noncentral F-distribution*. Assuming that the noncentral χ^2 random variable in the numerator of Y has ν_1 degrees of freedom, λ_1 non-centrality parameter and the noncentral χ^2 variable in the denominator has ν_2 degrees of freedom and λ_2 non-centrality parameter, the PDF of Y is given by [60]

$$\begin{aligned} f_Y(y) = \sum_{j=0}^{\infty}\sum_{k=0}^{\infty} \left[\frac{e^{-\lambda_1/2}(0.5\lambda_1)^j}{j!}\right]\left[\frac{e^{-\lambda_2/2}(0.5\lambda_2)^k}{k!}\right]\Big[B\big(0.5\nu_1+j, 0.5\nu_2+k\big)\Big]^{-1} \\ \times y^{0.5\nu_1+j-1}(1+y)^{-0.5(\nu_1+\nu_2)-j-k}, \end{aligned} \tag{3.20}$$

where $B(.,.)$ is the beta function. It is worth mentioning that we use $\nu_1 = \nu_2 = 2$ and $\lambda_1 = \lambda_2 = 2K_r$ while employing the above PDF to evaluate the probabilities. Although the doubly infinite sum in (3.20) is undesirable, satisfactory convergence was found with only 18 terms. Hence, the approach is rapid and stable computationally. A comparison of simulated and analytical results is presented in Figs. 3.3 and 3.4. It can the seen that the analytical formulae for all the cases shown agree closely with the simulation results for different parameter values. A discussion of these results is presented in Sec. 3.4.

3.3 An Approximation For The Power Loss Parameter

In this section we focus on the power loss parameter, α, which governs how much of the transmit power the CR dedicates to relaying the primary message. The exact distribution of α appears to be rather complicated, even for fixed link gains (fixed values of $\Gamma_{cp}, \Gamma_{pc}, \Gamma_{pp}$ and Γ_{cc}). Hence, we consider an extremely simple approximation based on the idea that $|s||t|$ is usually small and $|s||t| >> |t|$. This approximation is motivated by the fact that the CP link is usually very weak compared to the PP link. This stems from the common scenario where the CRs will employ much lower transmit powers than the PU as the CC paths are usually much shorter. With this assumption it follows that $|t|^2(1+|s|^2)$ is small and we have

$$\begin{aligned}\sqrt{\alpha} &= \frac{|s|}{|t|}\left[\frac{\left(1+|t|^2(1+|s|^2)\right)^{1/2}-1}{1+|s|^2}\right] \approx \frac{|s|}{|t|}\left[\frac{1/2|t|^2(1+|s|^2)}{1+|s|^2}\right] \\ &= \frac{|s||t|}{2} = \sqrt{\alpha_{approx}}. \end{aligned} \tag{3.21}$$

Expanding α_{approx} we obtain

$$\alpha_{approx} = \frac{A_p A_c P_p P_c}{4N_p^2} e^{(X_{pp}+X_{cp})} r_{pp}^{-\gamma} r_{cp}^{-\gamma} |\tilde{p}|^2 |\tilde{f}|^2. \tag{3.22}$$

This approximation is very effective for low values of α_{approx}, but is poor for larger values since α_{approx} is unbounded whereas $0 < \alpha < 1$. To improve the approximation, we use the conditional distribution of α_{approx} given that $\alpha_{approx} < 1$. This conditional variable is denoted, $\hat{\alpha}$. The exact distribution of $\hat{\alpha}$ is difficult for variable link gains. However, the approximation has a simple representation which leads to considerable insight into the power loss and how it relates to system parameters. For example, α_{approx} is proportional to $|s|^2|t|^2$ so that high power loss may be caused by high values of $|s|$ or $|t|$ or moderate values of both. Now $|s|$ and $|t|$ relate to the PP and CP links respectively. Hence, the CR is forced to use high power relaying the PU message when the CP link is strong. This is obvious as the relay action needs to make up for the strong interference caused by the CR. The

second scenario is that the CR has high α when the PP link is strong. This is less obvious, but here the PU rate is high and a substantial relaying effort is required to counteract the efforts of interference on a high rate link. This is discussed further in Section 3.4. It is worth noting that the condition $|s||t| >> |t|$ holds good only for some specific values of channel parameters which support the assumption that the CP link is usually much weaker than the PP link. Hence, although it is motivated by a sensible physical scenario, it requires verification. Results in Figs. 3.5, 3.7 and 3.8 show that it works very well. For fixed link gains, the distribution of $\hat{\alpha}$ is:

$$\begin{aligned} & P\left(\alpha_{approx} < x | \alpha_{approx} < 1\right) \\ & = P(\hat{\alpha} < x) \\ & = \frac{P(\alpha_{approx} < x)}{P(\alpha_{approx} < 1)}. \end{aligned} \tag{3.23}$$

Thus, to compute the distribution function of $\hat{\alpha}$ we need to determine $P(\alpha_{approx} < x)$ which can be written as

$$P(\alpha_{approx} < x) = P(|s|^2|t|^2 < 4x). \tag{3.24}$$

Let $\mathbb{E}[|s|^2] = \mu_s$, $\mathbb{E}[|t|^2] = \mu_t$ with $\mu_s = P_p\Gamma_{pp}/N_p$ and $\mu_t = P_c\Gamma_{cp}/N_p$. Further, suppose that U, V and W are defined by $U = |\tilde{f}|^2$, $V = |\tilde{c}|^2$ and $W = |\tilde{p}|^2$. We wish to derive $P\big(WU < \frac{4x}{\mu_s\mu_t}\big)$, i.e., (3.24), subject to the condition $a < 1$, which implies that $U < V/d$, where $d = (N_c/N_p)(\Gamma_{cp}/\Gamma_{cc})$. Defining $\zeta = 4/\mu_s\mu_t$ the required conditional CDF is given by

$$\begin{aligned} & P\left(UW < \zeta x | U < \frac{V}{d}\right) \\ & = \frac{P\left(U \leq \frac{\zeta x}{W}, U < \frac{V}{d}\right)}{P\big(U < \frac{V}{d}\big)} \\ & = \frac{\int_w \int_v P(U < \min(\frac{\zeta x}{w}, \frac{v}{d}))f_W(w)f_V(v)dvdw}{\int_0^\infty P(U < \frac{v}{d})f_V(v)dv} \\ & = \frac{\int_{w=0}^\infty \int_{v=0}^{\zeta xd/w} P(U < \frac{v}{d})f_W(w)f_V(v)dvdw + \int_{w=0}^\infty \int_{v=\zeta xd/w}^\infty P(U < \frac{\zeta x}{w})f_W(w)f_V(v)dvdw}{\int_0^\infty P(U < \frac{v}{d})f_V(v)dv} \end{aligned}$$

$$= \frac{\int_{v=0}^{\infty}\int_{w=0}^{\zeta xd/v} P(U < \frac{v}{d}) f_V(v) f_W(w) dw dv + \int_{w=0}^{\infty}\int_{v=\zeta xd/w}^{\infty} P(U < \frac{\zeta x}{w}) f_W(w) f_V(v) dv dw}{\int_0^{\infty} P(U < \frac{v}{d}) f_V(v) dv}$$
$$= \frac{\int_{v=0}^{\infty} F_W(\zeta xd/v) F_U(v/d) f_V(v) dv + \int_{w=0}^{\infty} F_U(\zeta x/w)(1 - F_V(\zeta xd/w)) f_W(w) dw}{\int_0^{\infty} F_U(v/d) f_V(v) dv}. \quad (3.25)$$

In the above derivation $f_U(u)$ and $F_U(u)$ represent the PDF and CDF of U respectively with similar definitions for the PDFs and CDFs of V and W. With the general result in (3.25), the CDF of α_{approx} can be determined for any fading combinations across the links of the CR interference channel. In most cases where Rician fading occurs (3.25) has to be computed via infinite series expansions or numerical integration. In the Rayleigh fading scenario a closed form solution is possible. Since for this case all the distribution and density functions given in (3.25) are those of a standard unit mean exponential random variable, after a few algebraic manipulations (details given in Appendix B) and expanding $\zeta = 4/\mu_s\mu_t$ we get

$$P(\alpha_{approx} < x) = 1 - \sqrt{\frac{16(1+d)x}{\mu_s\mu_t}} K_1\left(\sqrt{\frac{16(1+d)x}{\mu_s\mu_t}}\right), \quad (3.26)$$

where $K_1(.)$ represents the modified Bessel function of the second kind. Using the expression given in (3.26), the CDF of $\hat{\alpha}$ follows from (3.23). Note that the CDF of R_{CR} in (3.5) can easily be obtained in the form of a single numerical integral for fixed link gains as

$$\begin{aligned} P(R_{CR} < x) &= P\left(|c|^2(1-\alpha) < (2^x - 1)\frac{N_c}{P_c}\right) \\ &= \mathbb{E}\left[P\left(\alpha > 1 - \frac{(2^x-1)N_c}{|c|^2 P_c}\right)\right] \\ &= \int_0^{\infty}\left(1 - F_\alpha\left(1 - \frac{(2^x-1)N_c}{|c|^2 P_c}\right)\right) f_c(c) dc, \end{aligned} \quad (3.27)$$

where in the second line the expectation is with respect to the conditioned variable c, $F_\alpha(.)$ is the CDF of α in (3.26) and $f_c(c)$ is the PDF of c.

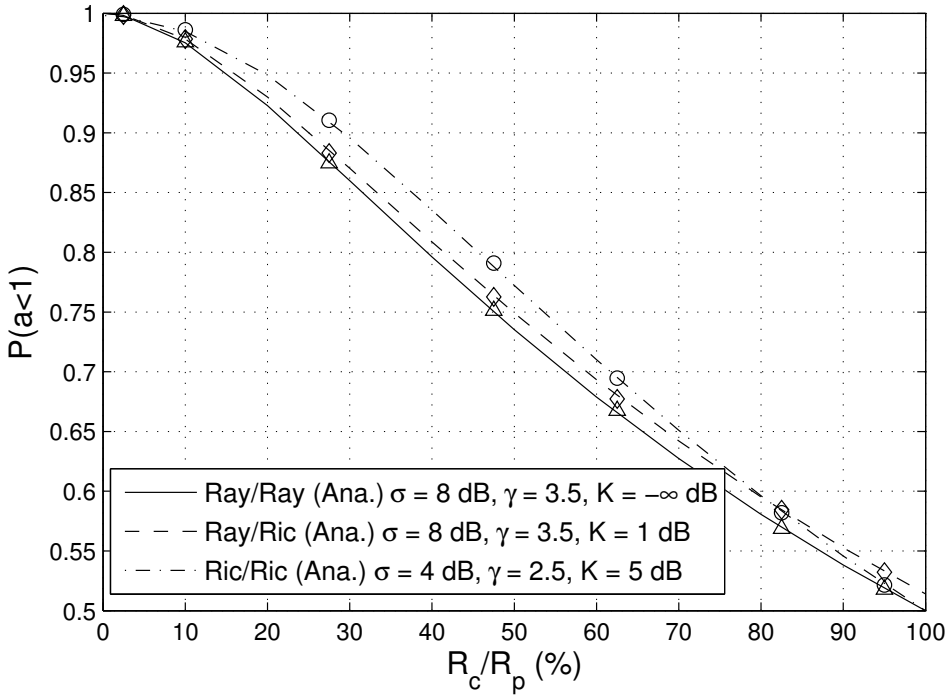

Figure 3.4: Probability of occurrence of the low interference regime as a function of the ratio R_c/R_p for different fading scenarios. Simulation values are shown by markers on the analytical curves.

3.4 Results

In this section, the default parameters are $\sigma = 8$ dB, $\gamma = 3.5$, $R_0 = 1$ m, $R_c = 100$ m, $R_p = 1000$ m and $N_p = N_c = P_p = P_c = 1$. The parameter A_p is determined by ensuring that the PP link has an SNR ≥ 5 dB 95% of the time in the absence of any interference. Similarly, assuming that both PU and CR devices have same threshold power at their cell edges, the constant $A_c = A_p(R_p/R_c)^{-\gamma}$. Unless otherwise stated these parameters are used in the following.

3.4.1 Low interference regime

In many cases where CRs are being considered, the focus is on link lengths which are usually short compared to the PU links. This situation coupled with typical values of γ and σ can be thought of as one type of practical deployment option. Results in Figs. 3.3 and 3.4 show that for this scenario the low interference regime, $a < 1$, is

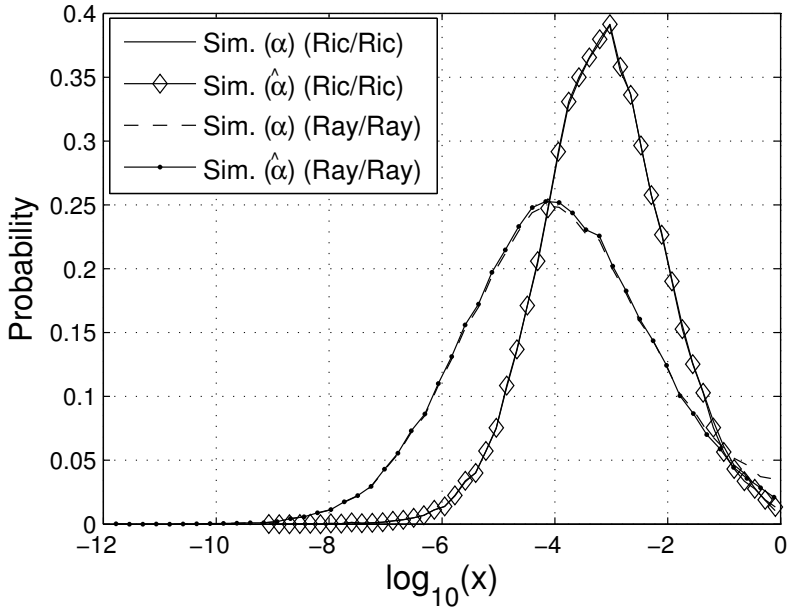

Figure 3.5: PDFs of $\log_{10}(\alpha)$ and its approximation $\log_{10}(\hat{\alpha})$. We have represented α and $\hat{\alpha}$ by a dummy variable x. We use the default parameters for the Ray/Ray curve, whereas, for Ric/Ric we have taken $\sigma = 4$ dB, $\gamma = 2.5$ and $K_r = 5$ dB. α represents the exact expression given in (3.6), while $\hat{\alpha}$ refers to its conditional approximation discussed in Sec. 3.3.

dominant. For typical values of $\gamma \in [3, 4]$ and $\sigma \in [6, 12]$ dB we find that $P(a < 1)$ is usually well over 90% when R_c is less than 20% of R_p. As expected, when R_c approaches R_p the probability drops and reaches $P(a < 1) = 0.5$ when $R_c = R_p$. Note that this is only the case when all the channel parameters are the same for the CC and CP links. From Fig. 3.4 we observe that the results are reasonably insensitive to the type of fast fading. This is due to the lesser importance of the fast fading compared to the large effects of shadowing and path loss. Figure 3.3 also verifies the analytical result in (3.15).

The relationship between $P(a < 1)$ and the system parameters is easily seen from (3.4) which contains the term $\left(r_{cc}/r_{cp}\right)^{\gamma/2} \exp\left((X_{cp} - X_{cc})/2\right)$. When $R_c << R_p$, this term decreases dramatically as γ increases (i.e., $P(a < 1)$ increases) and as σ increases the term increases (hence $P(a < 1)$ decreases). Also, as R_c increases r_{cc}/r_{cp} tends to increase which in turn decreases $P(a < 1)$. When $R_c \approx R_p$ the low and high interference scenarios occur with similar frequency (Fig. 3.4). This

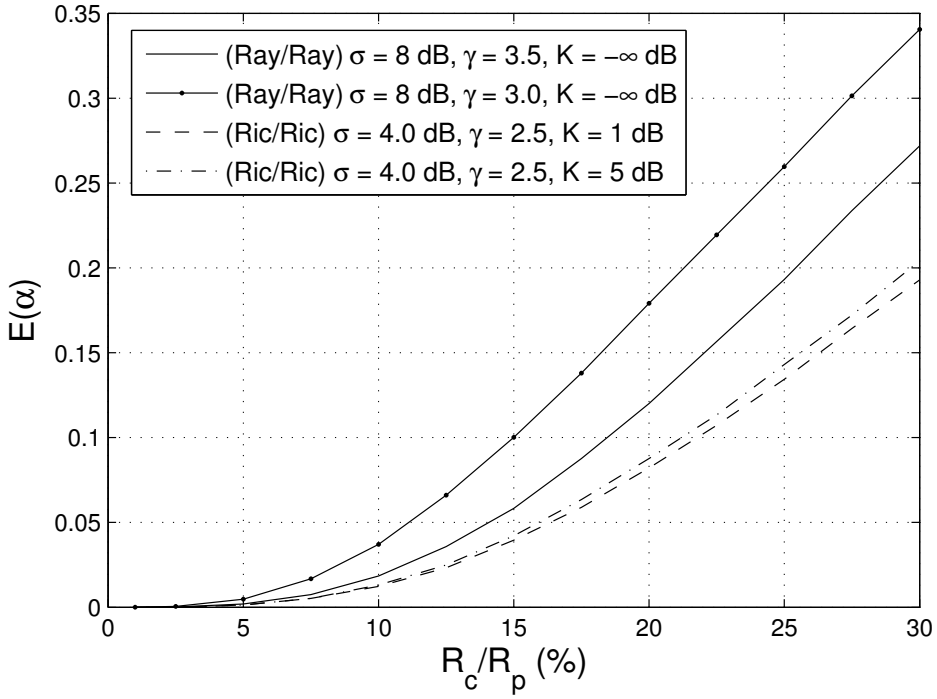

Figure 3.6: Mean value of the power loss parameter, α, as a function of the ratio $\frac{R_c}{R_p}$ for different fading scenarios.

may be a relevant system consideration if CRs were to be introduced in cellular bands where the cellular hot spots, indoor micro-cells and CRs will have roughly the same coverage radius. Note that a is independent of the transmit power, P_c. These conclusions are all verified in Figs. 3.3 and 3.4.

3.4.2 Statistics of the power loss parameter, α

Figures 3.5-3.7 all focus on the properties of α. Figure 3.5 shows that the probability density function (PDF) of α is extremely well approximated by the PDF of $\hat{\alpha}$ in both Rayleigh and Rician fading channels. In Fig. 3.6 we see that $\mathbb{E}[\alpha]$ increases with increasing values of R_c/R_p and decreasing values of γ. This can be seen from (3.22) where α_{approx} contains a $(r_{pp}r_{cp})^{-\gamma}$ term which increases as γ decreases, thus increasing the mean value of α. The increase of $\mathbb{E}[\alpha]$ with R_c follows from the corresponding increase in P_c to cater for larger R_c values. Increasing the line of sight (LOS) factor tends to increase $\mathbb{E}[\alpha]$ although the effect is minor compared to

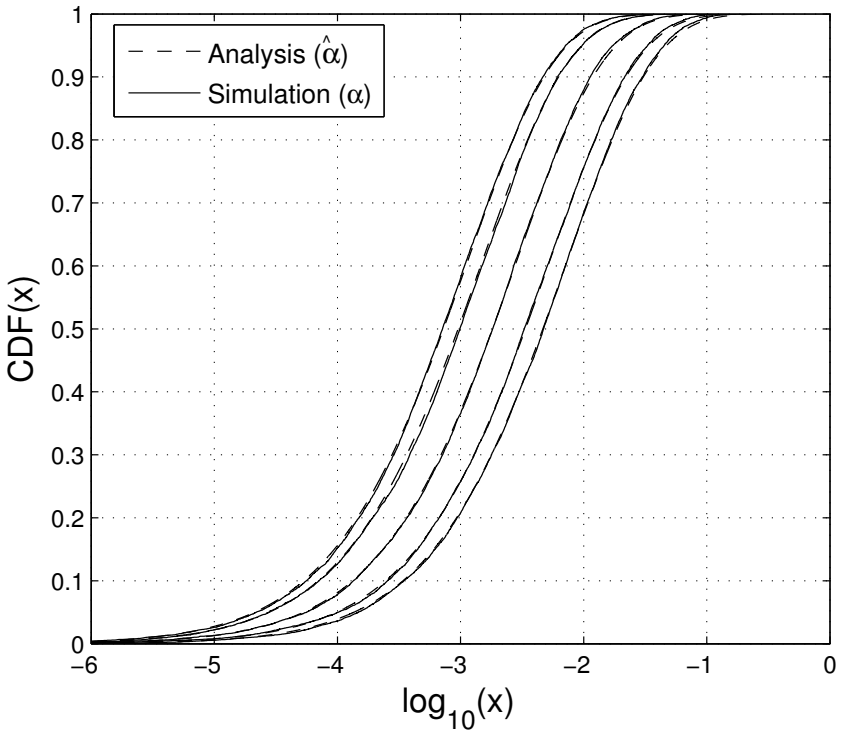

Figure 3.7: Comparison of the exact and analytical CDFs of the power loss factor on a logarithmic scale for fixed link gains. α represents the exact expression given in (3.6), while $\hat{\alpha}$ refers to its conditional approximation discussed in Sec. 3.3. Results are shown for 5 drops for the case of Ray/Ray fading.

changes in γ, σ or R_c/R_p. In Fig. 3.6 we have limited R_c/R_p to a maximum of 30% as beyond this value the high interference regime is also present with a non-negligible probability. In Fig. 3.7 we see the analytical CDF in (3.26) verified by simulations for five different scenarios of fixed link gains (simply the first five simulated values of Γ_{pp} and Γ_{cp}). Note that in the different curves each correspond to a random drop of the PU and CR transmitters. This fixes the distance and shadow fading terms in the link gains in (3.2), thereby the remaining variation in (3.1) is only Rayleigh. By computing a large number of such CDFs and averaging them over the link gains a single CDF can be constructed. This approach can be used to find the PDF of $\hat{\alpha}$ as shown in Fig. 3.5. Note that the curves in Fig. 3.7 do not match exactly since the analysis is for $\hat{\alpha}$ and the simulation is for α.

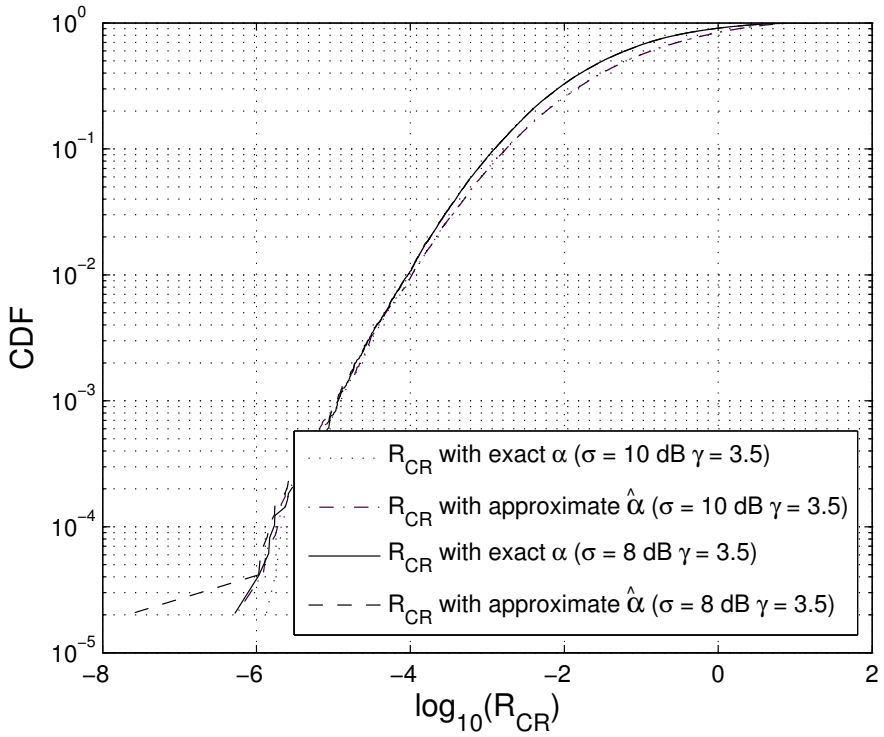

Figure 3.8: CDF of the CR rates with the exact α (3.6) and the approximate $\hat{\alpha}$ (Sec. 3.3) for Ray/Ray fading.

3.4.3 CR rates

Figures 3.8-3.10 focus on the CR rate R_{CR}. Figure 3.8 demonstrates that the use of $\hat{\alpha}$ is not only accurate for α but also leads to excellent agreement for the CR rate, R_{CR}. This agreement holds over the whole range and for all typical parameter values. Figure 3.9 shows the % loss given by $[R_{CR}(\alpha = 0) - R_{CR}(\alpha)]/[R_{CR}(\alpha = 0)]\%$. We call it mean loss in the figure since we average over several realizations of channels involved. We note that we term this quantity as loss in the CR rates since $\alpha = 0$ corresponds to the CR devoting no power for PU purposes and any non zero value of this parameter incurs are loss in the rates of the CR. The loss decreases as γ increases, as discussed above, and increases with σ. From (3.22) it is clear that increasing σ lends to larger values of $\exp(X_{pp} + X_{cp})$ which in turn increases α and the rate loss. Note that the rate loss is minor for $\sigma \in [8-10]$ dB with $R_c = R_p/10$. In chapter 5, we show that the interference to the PU increases with σ and decreases

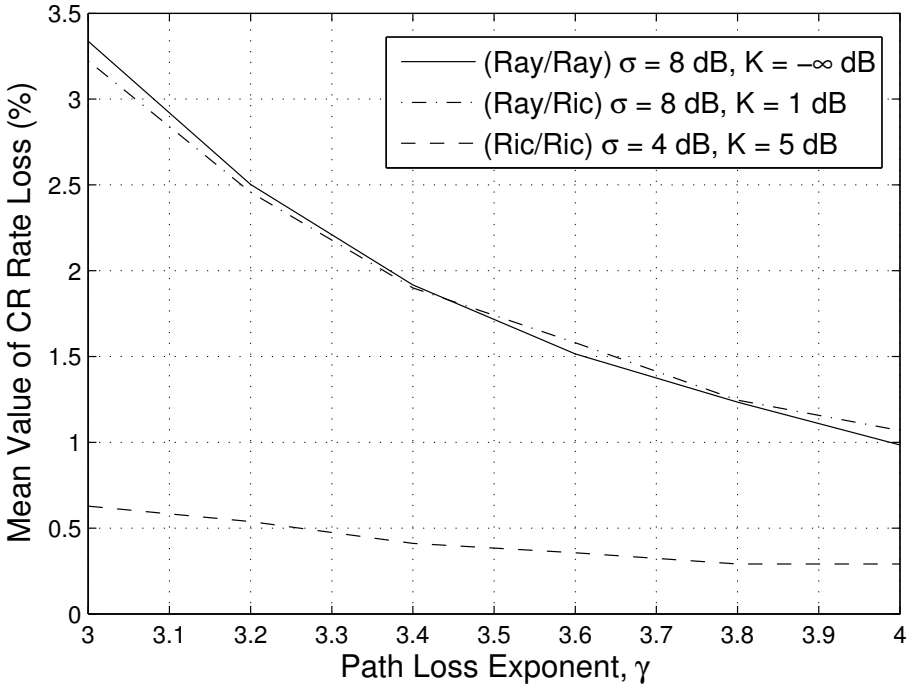

Figure 3.9: Mean value of the CR rate loss as a function of γ for different fading conditions. With slight abuse of notation, we take $K_r = K$ in the legend of above figure.

with γ. These results reinforce this observation, i.e., when the PU suffers more interference (σ is larger) the CR has to devote a higher part of its power to the PU. Consequently the percentage rate loss is higher. Again the effect of K_r, the LOS factor, is minor compared to that of γ and σ.

Finally, in Fig. 3.10 we investigate the gains available to the CR through increasing transmit power. The original transmit power, P_c, is scaled by the power inflation factor, β, and the mean CR rate is simulated over a range of β values. Due to the relaying performed by the CR, the PU rate is unaffected by the CR for any values of β and so the CR is able to boost its own rate with higher transmit power. Clearly the increased value of α for higher values of β is outweighed by the larger P_c value and so the CR does achieve an overall rate gain. In a very coarse way these results suggest that multiple CRs may be able to co-exist with the PU since the increased interference power might be due to several CRs and the rate gain might be spread over several CRs. Of course, this conclusion is speculative as the analysis

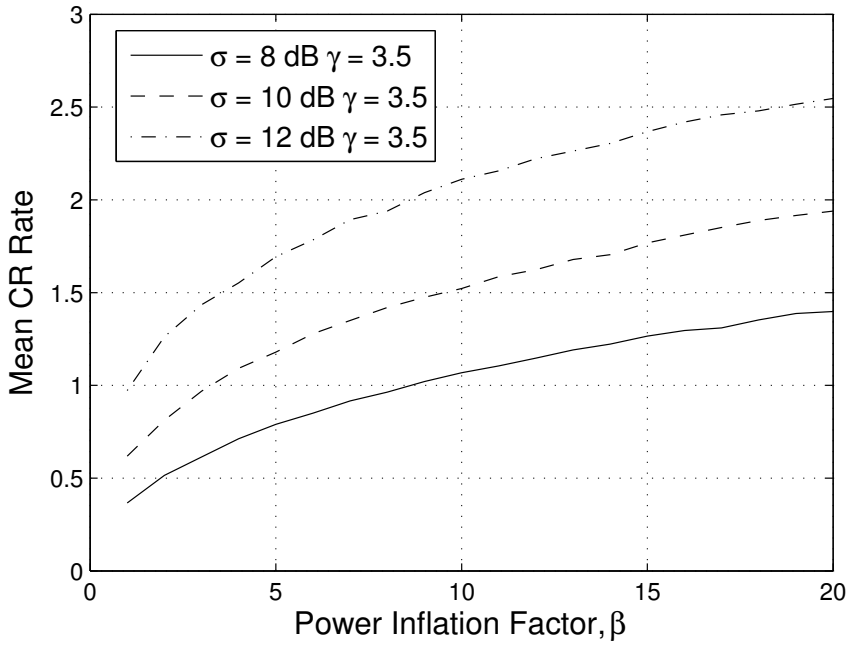

Figure 3.10: Variation of the mean CR rate with the power inflation factor, β for Ray/Ray fading case.

is only valid for a single CR.

3.5 Summary

In this chapter we derive the probability that the "low interference regime" holds and demonstrate the conditions under which this is the dominant scenario. We show that the probability of the low interference regime is significantly influenced by the system geometry. When the CR coverage radius is small relative to the PU radius, the low interference regime is dominant. On the other hand, when the CR coverage radius approaches a value similar to the PU coverage radius, the low and high interference regimes both occur with roughly equal probability. In addition, we have derived a simple, accurate approximation to α which gives considerable insight into the system capacity. The α approximation shows that the mean value of α is increased by small values of γ, large CR coverage zones and higher σ values. This in turn decreases CR rates due to small values of γ, large CR coverage zones and

σ. The effect of the LOS strength is shown to be minor and all results appear to be insensitive to the type of fast fading. Finally, we have shown that the CR can increase its own rate with higher transmit powers, although the relationship is only slowly increasing as expected.

Chapter 4

Interference and Level Crossing Statistics

We know from the discussion in earlier chapters that the CRs should try their best to protect the PUs from adverse interference. However, such efforts may jeopardize the quality of service (QoS) expected from the cognitive devices. Accurate spectrum sensing capabilities are being developed [8] for CRs and it is envisaged that either individually, or via collaboration, the cognitive devices will be able to detect the licensed users with an acceptably low probability of failure. It is evident that the statistics of the interfering signals will play an important role in the design of CR systems. Thus, modeling the total CR interference is an important issue and it is necessary to characterize the nature of the interfering signals along with their impact on the performance of the incumbent licensed users. Various results [61, 62] have appeared in this regard. [62] models the combined interference with heavy-tailed α[1]-stable distributions in an *infinite* field of interferers. [61] proposes a 3-parameter lognormal to accomplish this task. Later in the chapter we show that this approach is applicable only in certain scenarios.

While devising various CR scheduling strategies it is normal to consider an average interference constraint [63]. For example, the approaches in [64, 65, 63] allow

[1]This α should not be confused with the α used in Chapter 3 to represent the power loss parameter in the CR channel.

CRs to operate on the basis of average interference powers or SINR values and do not consider the instantaneous temporal variation of the interference. It is quite possible that an apparently plausible allocation strategy may result in the CR interference crossing a particular threshold on too many occasions when the interference process is considered over time. Thus the motivation to study the LCR of cumulative interference in conjunction with a particular CR allocation policy.

In this regard our contributions include the following. We derive the CDF of the interference due to a cognitive device assuming lognormal shadowing and path loss effects and investigate the nature of the distribution of the total interference due to multiple CRs. We derive a simplified expression for the cumulants of the total interference, which are in turn used in approximating the interference with a shifted lognormal distribution and determining the scenarios of applicability of this approach. Then, we compute the LCRs of the cumulative interference created by the CRs. We derive analytical formulae for the LCRs in Rayleigh and Rician fast fading conditions. We approximate Rayleigh and Rician LCRs using fluctuation rates of gamma and scaled noncentral χ^2 processes, respectively. The analytical results and the approximations used in their derivations are verified by Monte Carlo simulations and the analysis is applied to a particular CR allocation strategy.

4.1 System Model

In the system model we consider a PU receiver in the center of a circular region of radius R. The PU transmitter is located uniformly in an annulus of outer radius R and inner radius R_0 centered on the PU receiver. It is to be noted that we place the PU receiver at the center only for the sake of mathematical convenience (see Fig. 4.1). The use of the annulus restricts devices from being too close to the receiver. As seen in Chapter 3, this matches physical reality and also avoids problems with the classical inverse power law relationship between signal strength and distance [10]. In particular, having a minimum distance, R_0, prevents the signal strength from becoming infinite as the transmitter approaches the receiver. Similarly, we

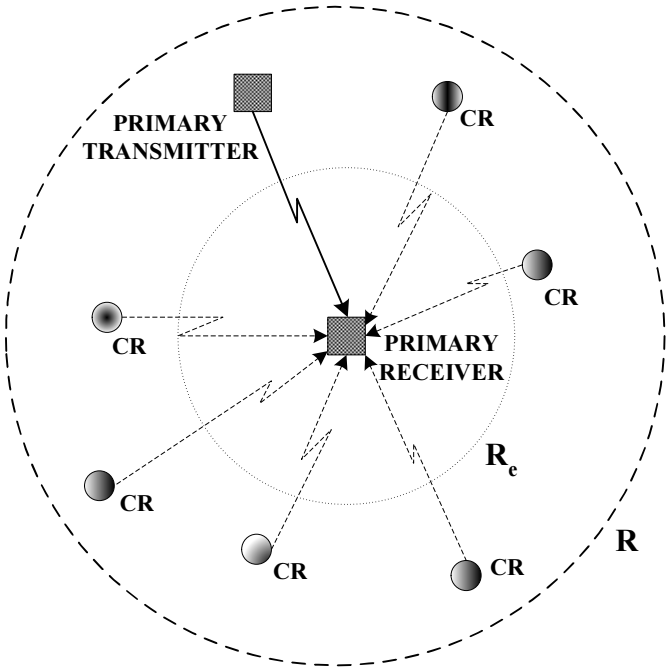

Figure 4.1: System model (R_0 not shown)

assume that multiple CR transmitters are uniformly located in the annulus. At any given time, each CR has a probability of seeking a connection, given by the activity factor, p. The number of CRs wishing to operate is denoted N_{CR}. Of these CRs, a certain number will be accepted depending on the allocation mechanism. Hence, a random number of CRs denoted $N \leq N_{CR}$ will transmit during the PU transmission and create interference at the PU receiver. The received signal strength for both the PU transmitter to PU receiver and CR transmitter to PU receiver is assumed to follow the classical distance dependent, lognormal shadowing model. For a generic interferer, this is given by

$$I = BLr^{-\gamma} = B10^{\tilde{X}/10}r^{-\gamma} = Be^{X}r^{-\gamma}, \tag{4.1}$$

where r is the random distance from the transmitter to the receiver, γ is the path loss exponent (normally in the range of 2 to 4) and L is a shadow fading variable. The lognormal variable, L, is given in terms of the zero mean Gaussian, $\tilde{X}$, which has standard deviation σ (dB) and $X = \beta\tilde{X}$ where $\beta = \ln(10)/10$. The standard deviation of X is denoted by σ_{sf}. The constant B is determined by the methods discussed in Chapters 2 and 3. The desired primary signal strength, S, has the same

form, with a different transmit power, so that $S = AL_p r_p^{-\gamma}$. Note that all the links are assumed to be i.i.d. and spatial correlation is ignored.

4.2 Statistical Characterization of Interference at the Primary Receiver

4.2.1 Interference Due to a Single Cognitive User

In this section we investigate the interference at the PU receiver due to one or more CRs. Firstly we characterize the interfering signal, given in (4.1), by computing the CDF, $F_I(x) = P(I < x)$. This can be done as follows

$$\begin{aligned} F_I(x) &= P\big(Be^X r^{-\gamma} < x\big) = P\left(e^{-X} r^{\gamma} > \frac{B}{x}\right) \\ &= P(e^U r^{\gamma} > y) = \mathbb{E}_U\Big[P\Big(r > y^{\frac{1}{\gamma}} e^{\frac{-U}{\gamma}}\Big)\Big] \\ &= \mathbb{E}_U\Big[1 - F_R\Big(y^{\frac{1}{\gamma}} e^{\frac{-U}{\gamma}}\Big)\Big]. \end{aligned} \tag{4.2}$$

In (4.2), $U = -X$, $\mathbb{E}_U[.]$ represents expectation over the random variable U and $y = B/x$. To evaluate the expectation in (4.2) we note that the CDF of r is given by

$$F_R(r) = \frac{r^2 - R_0^2}{R^2 - R_0^2}, \qquad R_0 \le r \le R. \tag{4.3}$$

Using this CDF, (4.2) can be rewritten as

$$F_I(x) = \mathbb{E}_U[G_R(U, y)], \tag{4.4}$$

where

$$G_R(U, y) = \begin{cases} 0 & U < w_0 \\ \left(\frac{R^2 - y^{\frac{2}{\gamma}} e^{\frac{-2u}{\gamma}}}{R^2 - R_0^2}\right) & w_0 < U < w_1 \\ 1 & U > w_1, \end{cases} \tag{4.5}$$

and $w_0 = \ln(yR^{-\gamma})$, $w_1 = \ln(yR_0^{-\gamma})$. Since $U = -X$ is Gaussian, $U \sim \mathcal{N}(0, \sigma_{sf}^2)$, with probability density function (PDF) $f(u)$, the CDF, $F_I(x) = \mathbb{E}_U[G_R(U, y)]$,

becomes

$$F_I(x) = \int_{w_0}^{w_1} \frac{R^2 - y^{\frac{2}{\gamma}} e^{\frac{-2u}{\gamma}}}{R^2 - R_0^2} f(u)du + \int_{w_1}^{\infty} f(u)du = \frac{R^2}{(R^2 - R_0^2)\sqrt{2\pi\sigma_{sf}^2}} \int_{w_0}^{w_1} e^{\frac{-u^2}{2\sigma_{sf}^2}} du$$
$$- \frac{(\frac{B}{x})^{2/\gamma}}{(R^2 - R_0^2)\sqrt{2\pi\sigma_{sf}^2}} \int_{w_0}^{w_1} e^{\frac{-2u}{\gamma} - \frac{-u^2}{2\sigma_{sf}^2}} du + \frac{1}{\sqrt{2\pi\sigma_{sf}^2}} \int_{w_1}^{\infty} e^{\frac{-u^2}{2\sigma_{sf}^2}} du. \quad (4.6)$$

All the integrals in (4.6) can be written in terms of integrals of Gaussian PDFs. Hence, (4.6) reduces to

$$F_I(x) = 1 - F_Z\left(\frac{w_1}{\sigma_{sf}}\right) + \frac{1}{R^2 - R_0^2}\left[\left\{R^2 F_Z\left(\frac{w_1}{\sigma_{sf}}\right) - R^2 F_Z\left(\frac{w_0}{\sigma_{sf}}\right)\right\}\right.$$
$$\left. - \left(\frac{B}{x}\right)^{\frac{2}{\gamma}} e^{\left(\frac{2\sigma_{sf}^2}{\gamma^2}\right)} \left\{F_Z\left(\frac{w_1 + 2\sigma_{sf}^2/\gamma}{\sigma_{sf}}\right) - F_Z\left(\frac{w_0 + 2\sigma_{sf}^2/\gamma}{\sigma_{sf}}\right)\right\}\right], \quad (4.7)$$

where $F_Z(.)$ is the CDF of a standard Gaussian. In order to validate the CDF given in (4.7), we compare the results of this expression with the complementary CDF obtained using Monte Carlo simulation as shown in Fig. 4.2. We note that although these results are expected to match exactly (since we are not approximating), the tails represent a simulation mismatch on account of fewer simulation samples. However, if there were any approximating techniques used then it would be more plausible to include confidence intervals on the graph. It can be seen that the analytical and simulated interference complementary CDFs agree over a wide range of propagation parameters. Hence, a complete characterization of the interference due to a single CR is possible. Next, we consider multiple CRs.

4.2.2 Interference Due to Multiple Cognitive Radios

In cognitive wireless networks the PU device under consideration may be affected by the interference due to many CRs. In this case, the total interference, denoted I_T, is given by

$$I_T = \sum_{i=1}^{N} B e^{X_i} r_i^{-\gamma} = \sum_{i=1}^{N} B L_i r_i^{-\gamma}, \quad (4.8)$$

where the parameters are as defined in (4.1). Equation (4.8) is a random sum of a finite number of lognormals with each lognormal being multiplied by a ran-

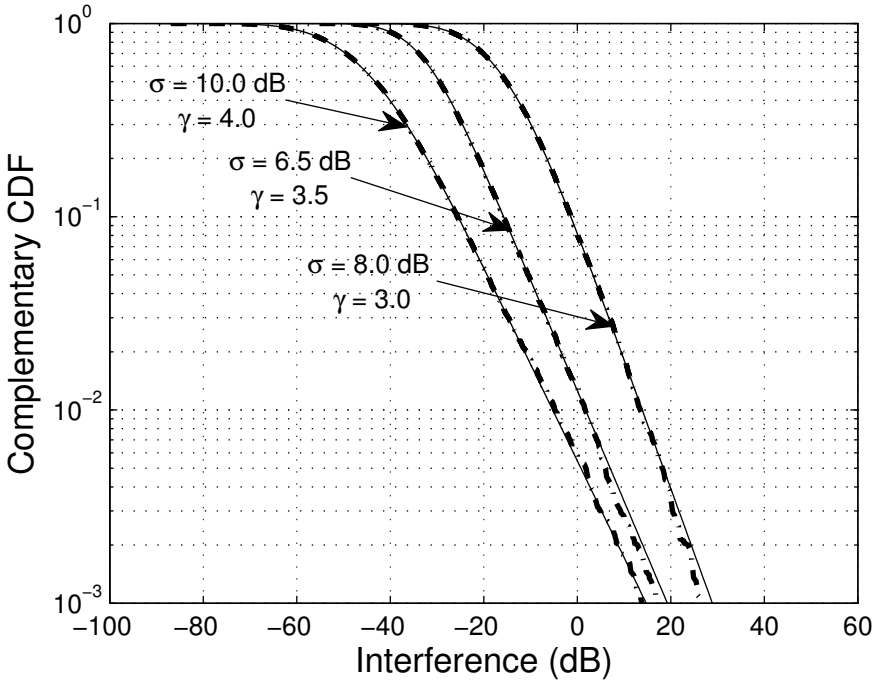

Figure 4.2: A comparison of analytical and simulated complementary CDFs of interference over a range of propagation parameters. Solid lines represent analytical results while dotted-dashed curves show simulated values.

dom distance factor. Problems similar to this, but involving a non random sum without incorporating the random distance factor, have been tackled in the past [66, 67, 68, 69, 70, 71, 72]. Historically, lognormal approximations to this summation have been envisaged. Approximations are definitely required since although (4.7) gives an analytical result for a single interferer, it is too complex to allow an exact approach for sums of interferers. Hence, one is tempted to use the same lognormal approximation for (4.8). However, as described below, we show that lognormal approximations are not accurate. We note that instead of showing discrepancy of the traditional approaches by displaying mismatch between the simulation and analytical results, we rely on mathematical analysis based on the shape determining factor of skewness. For convenience, consider a lognormal approximation to a single interferer, I, of the form given in (4.1). Let the moments of I be denoted by $\mathbb{E}[I^j] = m_j$. We seek to approximate I with the lognormal $Y = e^Z$ where $Z \sim \mathcal{N}(\mu_z, \sigma_z^2)$. The simplest approach to fitting Y is via the Fenton-Wilkinson approach [66, 68] which

computes the first two moments, so that

$$\mathbb{E}[Y^k] = \mathbb{E}[I^k] = m_k, \quad k = 1, 2. \tag{4.9}$$

Hence, the lognormal approximation has perfect moments up to order 2. To demonstrate the lack of fit we consider the skewness of Y and I which also involves the third moment. For any lognormal, say Y, the third moment is related to the first two by

$$\mathbb{E}[Y^3] = \left(\frac{\mathbb{E}[Y^2]}{\mathbb{E}[Y]}\right)^3. \tag{4.10}$$

Now, consider the skewness of I,

$$\begin{aligned} SK(I) &= \frac{\mathbb{E}[(I - m_1)^3]}{(m_2 - m_1^2)^{3/2}} \\ &= \frac{m_3 + 2m_1^3 - 3m_1 m_2}{(m_2 - m_1^2)^{3/2}}. \end{aligned} \tag{4.11}$$

Similarly, the skewness of Y can be written as

$$\begin{aligned} SK(Y) &= \frac{\mathbb{E}[Y^3] + 2\mathbb{E}[Y]^3 - 3\mathbb{E}[Y]\mathbb{E}[Y^2]}{(\mathbb{E}[Y^2] - \mathbb{E}[Y]^2)^{3/2}} \\ &= \frac{\mathbb{E}[Y^3] + 2m_1^3 - 3m_1 m_2}{(m_2 - m_1^2)^{3/2}}. \end{aligned} \tag{4.12}$$

Hence, the lognormal approximation is more skewed than the real interference if $\mathbb{E}[Y^3] > m_3$. Now, consider

$$\begin{aligned} \frac{\mathbb{E}[Y^3]}{m_3} = \frac{(m_2/m_1)^3}{m_3} &= \frac{\left(\frac{B^2\mathbb{E}[e^{2X}]\mathbb{E}[r^{-2\gamma}]}{B\mathbb{E}[e^X]\mathbb{E}[r^{-\gamma}]}\right)^3}{B^3\mathbb{E}[e^{3X}]\mathbb{E}[r^{-3\gamma}]} \\ &= \frac{\left(\frac{\mathbb{E}[e^{2X}]}{\mathbb{E}[e^X]}\right)^3}{\mathbb{E}[e^{3X}]} \frac{\left(\frac{\mathbb{E}[r^{-2\gamma}]}{\mathbb{E}[r^{-\gamma}]}\right)^3}{\mathbb{E}[r^{-3\gamma}]} = \frac{\left(\frac{\mathbb{E}[r^{-2\gamma}]}{\mathbb{E}[r^{-\gamma}]}\right)^3}{\mathbb{E}[r^{-3\gamma}]}. \end{aligned} \tag{4.13}$$

The above results follow since (4.10) also holds for the lognormal e^X. The moments of r in (4.13) can be found as

$$\mathbb{E}[r^{-k\gamma}] = \frac{2(R^{2-k\gamma} - R_0^{2-k\gamma})}{(R^2 - R_0^2)(2 - k\gamma)}. \tag{4.14}$$

Equation (4.14) is obtained using (4.3) as the CDF of r to compute the PDF and hence the moments. For large R (1000 m in our case), small R_0 (we use 1 m) and with $\gamma \geq 3$, (4.14) gives

$$\mathbb{E}[r^{-k\gamma}] \approx \frac{-1}{R^2}\left(\frac{2}{2-k\gamma}\right) = \frac{2}{R^2(k\gamma-2)}. \tag{4.15}$$

Thus, the ratio of the moments in (4.13) becomes:

$$\frac{\mathbb{E}[Y^3]}{m_3} \approx \left(\frac{\gamma-2}{2\gamma-2}\right)^3 \frac{R^2(3\gamma-2)}{2}. \tag{4.16}$$

It can be observed from the above expression that for typical values of the parameters, $\mathbb{E}[Y^3] >> m_3$, and the ratio is of the order of R^2. Thus the equivalent lognormal will be massively more skewed than the real interference. As skewness is a key shape determining factor (especially in the tails), the simple lognormal approximation will not be accurate. Note that this large discrepancy in skewness is due to the random distance factors. Exactly the same conclusions are reached when attempting to fit sums of interferers. Hence, it appears that a simple lognormal approximation will not suffice and further research is required. An alternate approach, one considered by [61], is to approximate interference of the form given in (4.8) with a *three parameter* lognormal random variable using cumulant matching. Such an approximation was shown to be highly accurate under typical operating conditions of the system considered in [61]. The parameters of the distribution can be expressed in terms of the cumulants of the interference which is now denoted $I_{T,N}$ to represent the dependence on the random number of interferers, N. For the sake of analytical tractability, instead of using a binomial random variable to model the interfering CRs, we use a Poisson random variable noting that the Poisson distribution is a limiting case of the binomial. These cumulants can be calculated by modeling the interferers by a marked Poisson process and invoking Campbell's theorem [73]. In what follows we provide a significantly simplified and more intuitive method of calculating the cumulants of $I_{T,N}$ than the one presented in [61]. We begin by noting that the moment generating function (MGF) of $I_{T,N}$ can be expressed as a function

of the MGF of I by means of conditioning on N. Hence,

$$\begin{aligned}\Phi_{I_{T,N}}(s) &= \mathbb{E}[e^{sI_{T,N}}] \\ &= \sum_{n=0}^{\infty} \mathbb{E}[e^{sI_{T,N}}|N=n]P(N=n) \\ &= \sum_{n=0}^{\infty} \mathbb{E}[e^{sI_{T,n}}]P(N=n) \\ &= \sum_{n=0}^{\infty} \left(\Phi_I(s)\right)^n P(N=n), \end{aligned} \tag{4.17}$$

where the last equality assumes i.i.d. interferers. We recognize that (4.17) is in the form of the *probability generating function* (PGF) of N, and thus

$$\Phi_{I_{T,N}}(s) = G_N\left(\Phi_I(s)\right), \tag{4.18}$$

where the PGF, G_N, for a Poisson distributed N with mean λ is given by

$$G_N(s) = e^{\lambda(s-1)}. \tag{4.19}$$

Before proceeding forward, we make an important remark. Using (4.19) one may be tempted to obtain the *exact* distribution of the cumulative interference. For example, it is plain to see that the characteristic function[2] of this variable is $\Phi_{I_{T,N}}(jt) = \exp\Big(\lambda(\Phi_I(jt)-1)\Big)$, where $j=\sqrt{-1}$. Further, the characteristic function of the individual interferer is given by

$$\Phi_I(jt) = \mathbb{E}[e^{jtBe^X r^{-\gamma}}] = \int_{R_0}^{R}\int_{-\infty}^{\infty} e^{jtBe^x r^{-\gamma}} f(x) f_R(r) dx dr, \tag{4.20}$$

where $f(x)$ is the PDF of a $\mathcal{N}(0,\sigma_{sf}^2)$ variable and $f_R(r)$ can be obtained by differentiating (4.3). With the CDF given in (4.7), it is easy to see that (4.20) may not be representable in terms of elementary functions or may not even allow a closed form solution. On top of this, evaluating the inverse Fourier transform of $\Phi_{I_{T,N}}(jt)$ may be a very difficult, if not an impossible, task. Thus the motivation behind fitting a simple distribution. We note that some progress is possible using stable

[2]We use characteristics function since this function always exists even when it is not possible to evaluate the MGF.

distributions [62] but this requires the assumptions that $R_0 \to 0$ and $R \to \infty$ giving rise to an infinite field of interferers.

Coming back to (4.19), we see that using (4.18) and (4.19) we can obtain the kth cumulant κ_k of $I_{T,N}$ as

$$\begin{aligned}\kappa_k &= \left[\frac{\partial^k}{\partial s^k} \ln \Phi_{I_{T,N}}(s)\right]_{s=0} \\ &= \lambda \left[\frac{\partial^k}{\partial s^k} \Phi_I(s)\right]_{s=0} \\ &= \lambda \mathbb{E}[I^k]. \end{aligned} \tag{4.21}$$

Thus, the cumulants of the aggregate interference can be easily obtained from the moments of the individual interferers.[3] Using (4.1), (4.14) and the moments of a lognormal the cumulants in (4.21) can be given as

$$\kappa_k = \lambda B^k e^{k^2\sigma_{sf}^2/2} \left(\frac{2}{2-k\gamma}\right)\left(\frac{R^{2-k\gamma} - R_0^{2-k\gamma}}{R^2 - R_0^2}\right). \tag{4.22}$$

Following [61] a shifted lognormal was fitted to the interference, $I_{T,N}$, by selecting the three parameters of the shifted lognormal to match the first 3 cumulants in (4.22). Although the fitting procedure was successful, the resulting shift parameter was found to be negative. Hence, in order to match the first 3 moments of $I_{T,N}$ the shifted lognormal yields negative interference values for some portion of the time. Investigation of this behavior showed that the negative shift is fundamentally a function of R_0. For one set of parameter settings, $R = 1000$ m, $\sigma = 8$ dB, $\gamma = 3.5$ and $\lambda = 1000$ CRs per square kilometer with an activity factor of 0.1, the percentage of the shifted lognormal distribution which is negative is given in Table 6.1. From Table 6.1 it is clear that for small R_0 values the shifted lognormal is completely inappropriate as a model for interference. However, for $R_0 \geq 20$ m the distribution is always positive and in this region it may be useful. Note that in [61] a high detection probability near the PU receiver's beacon means that CRs are very unlikely to be close to the PU. This is roughly equivalent to a larger R_0 value and

[3]The same result can be obtained via Campbell's theorem [73], as considered by [61], by appropriately modifying the expression for finite cell radius and disregarding the sensing-related component.

Table 4.1: The percentage of the shifted lognormal distribution which is negative for various R_0 values.

R_0 (m)	%
1.0	88%
10	72%
16	50%
20	0%

hence in the presence of a beacon the shifted lognormal may be useful as shown in [61]. However, in this work we are not necessarily assuming a beacon is present and so the shifted lognormal is not used.

4.3 Level Crossing Analysis

We observed in Chapter 2 that instantaneous variations in signal level are important from the perspective of designing and analyzing the performance of wireless communication systems. In the same way, small scale variations in the composite CR interference can degrade the PU performance even though the CR levels may be acceptable on average. Thus, the determination of the rate at which the instantaneous interference crosses a particular threshold and the duration for which it stays above or below it, is an issue of core importance. For example, the PU system may set an average interference constraint but if the interference exceeds this threshold for too long or crosses it too often for satisfactory QoS then the threshold may need to be reduced. From the perspective of CR system design, such an analysis can provide insight into issues such as CR allocation and power control. For example, how should the powers of CR devices be controlled keeping in mind the instantaneous fluctuations of the interfering signals at the PU receiver? Thus throughout the remaining part of this chapter SNR or SINR values represent long term average values while the interference is considered on an instantaneous scale.

4.4 Instantaneous CR performance

In any CR allocation policy, for example chapter 5, even if the target interference/SINR of the PU is exactly met, the fast fading will result in fluctuations of the instantaneous interference/SINR both above and below the target. As a first look at this problem we fix the PU signal power and consider the instantaneous variation of the interference only. Hence, in this section we focus on the instantaneous temporal behavior of the aggregate interference via the LCR.

4.4.1 LCRs for Rayleigh Fading

For a given set of CR interferers, the instantaneous aggregate interference, $I_{Ray}(t)$, is given by

$$I_{Ray}(t) = \sum_{i=1}^{N} I_i |h_i(t)|^2, \tag{4.23}$$

where I_i represents the long term interference power of the ith CR, $h_i(t)$ is the corresponding normalized channel gain so that in Rayleigh fading $|h_i(t)|^2$ is a standard exponential random variable with unit mean and N is the number of interfering CRs. Note that we fix the long term interference values, $I_1, \ldots, I_N$ and consider the variation of the fast fading terms, h_i. From (4.23), the aggregate interference is represented as a weighted sum of exponential variables. Such weighted sums can be approximated by a gamma variable [60]. The corresponding LCR results are shown to be accurate in Figs. 4.3-4.5, hence, justifying the approximation of cumulative interference in (4.23) by a gamma variable. Note that the exact LCR computation for such sums was given in [74] for the case of three and four branch maximal ratio combining (MRC) by providing special function integrals. Recently, more general expressions for arbitrary number of branches have been derived in [75]. However, the approach of [75] may result in numerical difficulties, especially for large values of N, which can be the case for CR systems. In particular, the hypergeometric functions in [75] are difficult to compute accurately for large negative arguments which is the case with weak CR interferers. Hence, an approximation is useful to overcome these

problems and to provide a much simpler solution. Thus, approximate LCRs for (4.23) can be found by approximating using a fitted gamma process. It is important to note that the following approximation is valid only for 2-D isotropic scattering, when the time autocorrelation function follows the classic Jakes' model [9]. The LCR for a gamma process has been calculated in [76]. Therefore, the LCR of (4.23) across a threshold, T, is

$$\mathrm{LCR}_{I_{Ray}}(T) = \frac{1}{2\Gamma(r)}\sqrt{\frac{2|\ddot{R}(0)|}{\pi}}(\theta T)^{r-0.5}\exp(-\theta T), \tag{4.24}$$

where $r = \mathbb{E}[I_{Ray}(t)]^2/Var(I_{Ray}(t))$, $\theta = \mathbb{E}[I_{Ray}(t)]/Var(I_{Ray}(t))$ and $\ddot{R}(0) = \ddot{\rho}_{Ray}(0)$ is the second derivative of the autocorrelation function (ACF) of $I_{Ray}(t)$ at time lag, $\tau = 0$. Computation of (4.24) only requires the mean, variance and ACF of the random process in (4.23). The first two moments of (4.23) are $\mathbb{E}[I_{Ray}(t)] = \sum_{i=1}^{N} I_i$ and $Var(I_{Ray}(t)) = \sum_{i=1}^{N} I_i^2$. To calculate the ACF, note that

$$h_i(t+\tau) = \rho_i(\tau)h_i(t) + \sqrt{(1-\rho_i^2(\tau))}e_i(t), \tag{4.25}$$

where $e_i(t)$ is independent of $h_i(t)$ and statistically identical to $h_i(t)$. Assuming a Jakes' fading process, $\rho_i(\tau)$ is the zeroth order Bessel function of the first kind, $J_0(2\pi f_{D_i}\tau)$ and f_{D_i} is the Doppler frequency of interferer i. Using (4.25) we have

$$\begin{aligned}
&\mathbb{E}[I_{Ray}(t)I_{Ray}(t+\tau)] \\
&= \sum_{i,j=1}^{N} I_i I_j \mathbb{E}[|h_i(t)|^2|h_j(t+\tau)|^2] \\
&= \sum_{i\neq j}^{N} I_i I_j + \left(\sum_{i=1}^{N} I_i^2 \mathbb{E}[|h_i(t)|^2(\rho_i^2(\tau)\times|h_i(t)|^2 + (1-\rho_i^2(\tau))|e_i(t)|^2)]\right) \\
&= \sum_{i\neq j}^{N} I_i I_j + \sum_{i=1}^{N} I_i^2 + \sum_{i=1}^{N} I_i^2\rho_i^2(\tau) \\
&= \left(\sum_{i=1}^{N} I_i\right)^2 + \sum_{i=1}^{N} I_i^2\rho_i^2(\tau),
\end{aligned} \tag{4.26}$$

where in the second to last step above, we have used the fact that cross products have zero mean and that $\mathbb{E}[|h_i(t)|^4] = 2$. The ACF of (4.23) is given by

$$\rho_{Ray}(\tau) = \frac{\mathbb{E}[I_{Ray}(t)I_{Ray}(t+\tau)] - \mathbb{E}[I_{Ray}(t)]\mathbb{E}[I_{Ray}(t+\tau)]}{\sqrt{Var(I_{Ray}(t))Var(I_{Ray}(t+\tau))}}, \tag{4.27}$$

and with the relevant substitutions, the ACF becomes

$$\rho_{Ray}(\tau) = \frac{\sum_{i=1}^{N} I_i^2 J_0^2(2\pi f_{D_i}\tau)}{\sum_{i=1}^{N} I_i^2}. \tag{4.28}$$

Finally, using the expansion $J_0(2\pi f_D\tau) = 1 - \pi^2 f_D^2\tau^2 + \ldots$, the second derivative of the ACF needed to compute the LCR in (4.24) is evaluated as

$$\ddot{\rho}_{Ray}(0) = -4\pi^2 \frac{\sum_{i=1}^{N} I_i^2 f_{D_i}^2}{\sum_{i=1}^{N} I_i^2}. \tag{4.29}$$

To the best of our knowledge the results in (4.28) and (4.29) are new. Hence, the three parameters, r, θ and $\ddot{R}(0)$, are available and (4.24) gives the approximate LCR.

4.4.2 LCRs for Rician Fading

The instantaneous aggregate interference, $I_{Ric}(t)$, for Ricean fading is given as

$$I_{Ric}(t) = \sum_{i=1}^{N} I_i |h_i(t)|^2, \tag{4.30}$$

where $|h_i(t)|$ is Rician, with Rician K-factor denoted by K, and $N, I_1, I_2, \ldots, I_N$ are as defined in (4.23). Hence, $I_{Ric}(t)$ is a weighted sum of noncentral chi-square (χ^2) random variables. Note that standard LCR results for Ricians [9, 77] and noncentral χ^2 variables [77] cannot be applied directly here. The work in [78] is for a single Rician and in [77] the LCR applies to the case where $I_1 = I_2 = \ldots = I_N$ and an exact noncentral χ^2 arises with integer degrees of freedom (dof). Instead, using the same approximation philosophy as that used in the Rayleigh case, we propose approximating (4.30) by a single noncentral χ^2. This approach is less well documented but has appeared in the literature (see [79]). Also note that a scaled, rather than a standard, noncentral χ^2 distribution is required for fitting and the resulting best-fitting distribution will almost certainly not have integer dof. A noncentral χ^2 variable with $v > 0$ dof, non-centrality parameter $\lambda \geq 0$ and scale parameter $\tilde{\alpha} > 0$ has the following PDF

$$p(x) = \frac{\tilde{\alpha}}{2} \exp\left(\frac{-(\lambda + \tilde{\alpha}x)}{2}\right) \left(\frac{\tilde{\alpha}x}{\lambda}\right)^{\frac{v-2}{4}} I_{\frac{v-2}{2}}\left(\sqrt{\lambda\tilde{\alpha}x}\right), \;\; x > 0 \tag{4.31}$$

where $I_{(v-2)/2}$ is a modified Bessel function of the first kind with order $(v-2)/2$. Fitting the PDF in (4.31) to the variable in (4.30) is performed using the method of moments technique so that the approximate noncentral χ^2 has the same first three moments as $I_{Ric}(t)$. The derivation details are outlined in Appendix C. Note that there can be numerical difficulties with the approach for certain values of $I_1, I_2, \ldots, I_N$. These difficulties arise when the parameter values obtained from (C.5) and (C.6) do not satisfy the constraints $v > 0, \lambda \geq 0, \tilde{\alpha} > 0$. However, when this approach does not work it is straightforward to perform a numerical minimization of the difference between the true moments of the CR interference and the moments of the $\tilde{\alpha}-$scaled noncentral χ^2 variable. Values of λ, v and $\tilde{\alpha}$ which minimize this difference can then be used. Finally, we note that this approach can easily be extended to the mixed interferer scenario where some channels are Rayleigh and the Rician channels have possibly different K factors. To handle this situation the 3 moments m_1, m_2, and m_3 derived in the Appendix C need to be recalculated for the case of unequal K values. This calculation is straightforward due to the independence of the channels.

The LCR of a noncentral χ^2 process with integer dof can be readily obtained from [77]. In particular, if we substitute $R = T$, $\sigma^2 = 1$, $M = v/2$, $s^2 = \lambda$ and $f_m = f_D$ in [77, Eq. (15)] we get the following expression for the LCR of the $\tilde{\alpha}-$scaled noncentral χ^2 variable

$$\mathrm{LCR}_{I_{Ric}} = \sqrt{\pi} f_D (\tilde{\alpha} T)^{\frac{v}{4}} \lambda^{\frac{-(v-2)}{4}} e^{\left(\frac{-\lambda-\tilde{\alpha}T}{2}\right)} I_{\frac{v-2}{2}}\left(\sqrt{\lambda\tilde{\alpha}T}\right). \tag{4.32}$$

The result in (4.32) holds good for a noncentral χ^2 process with integer dof. As elaborated in [77, 9], the above approximation holds under a set of conditions concerning Doppler frequencies and angles of arrival. For example, the result is valid under isotropic scattering when the LOS component has an angle of arrival of $\pi/2$ relative to the direction of the motion of mobile. In Appendix D we show that this formula is also valid for non-integer dof. Note that a similar extension for a central χ^2 with integer order [80] to a central χ^2 with fractional order [76] has also been shown to be correct. We observe that if $I_i = I$, $\forall i$ (the condition for which (4.24) holds exactly), then using $K = 0$ in (C.3) and (C.4) gives $\lambda = 0$, $\tilde{\alpha} = 2/I$ and

$v = 2N$ as a solution to (C.5) and (C.6). Using these values and the approximation, $I_v(z) \sim (z/2)^v/\Gamma(v+1)$ when $z \to 0$, in (4.32), some manipulations show that (4.32) reduces to the expression in (4.24).

4.4.3 Average Exceedance Duration

We define the AED for both Rayleigh and Rician environments as the average time that the aggregate interference stays above a given threshold T [9]. Mathematically,

$$AED = \frac{1 - F(T)}{LCR}, \tag{4.33}$$

where $F(T)$ gives the distribution function of the aggregate interference. Note that the exact CDFs of both $I_{Ray}(t)$ and $I_{Ric}(t)$ can be found in [81]. We note that the models in (4.23) and (4.30) and the analysis in (4.24), (4.32), (4.33) are valid for any scenario where interference caused by multiple Rayleigh or Rician interferers is of interest. Hence, the scope of the contribution is much wider than CR systems.

4.5 Results

In order to evaluate the accuracy of (4.24) and (4.32) it is important to use realistic values of $I_1, I_2, \ldots, I_N$. Hence, we use a particular CR access scheme chapter 5 to provide these values. The *decentralized selection* algorithm in chapter 5 employs a controller that considers CRs in their order of arrival. Each interferer is considered in turn and is accepted if the combined interference from previously accepted CRs and the current CR is less than some interference threshold. If a CR is not accepted, the next CR in the list is investigated. The I_i values are generated in chapter 5 from randomly located CRs in a circular region and include path loss and shadowing effects. In chapter 5 a threshold value is used which corresponds to the PU accepting a 2 dB loss in its SNR due to the presence of CRs.

From 1000 simulations, using the above selection procedure two sets of interferers were selected. The first set selected had the highest variance. Only 3 CRs were

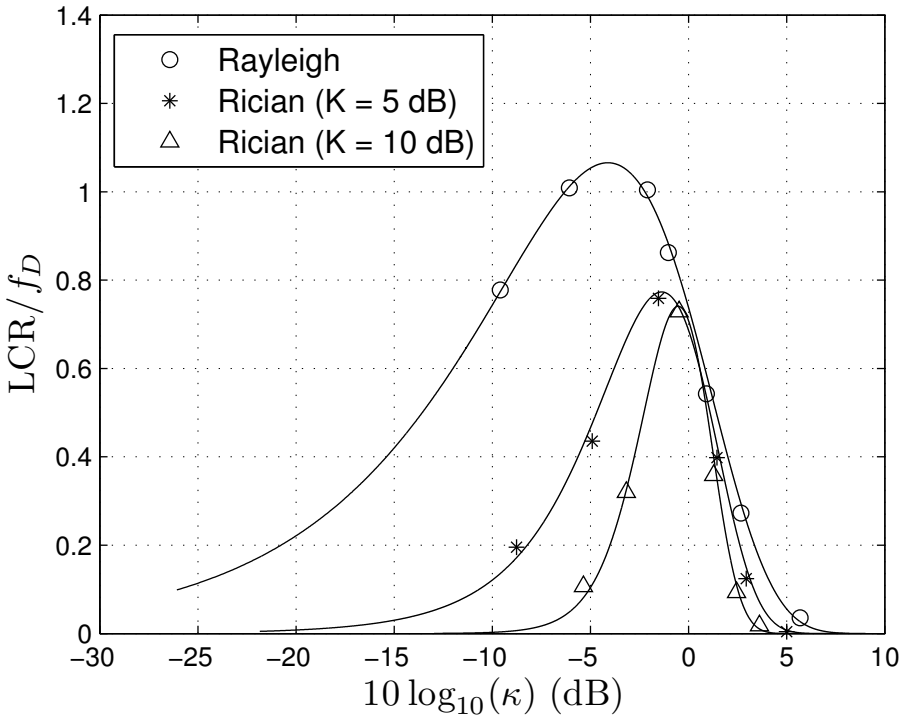

Figure 4.3: LCR results for different fading conditions with dominant interferers. The solid lines represent analytical results. Simulation values are shown by the circle, star and triangle symbols.

accepted and there was a dominant interferer which accounted for 95% of the interference power. The second set had the lowest variance, representing the no dominant interferer scenario. Here, 18 CRs were accepted with the largest interferer only accounting for 16%. Note that with equal values of $I_1, I_2, \ldots, I_N$ the results in (4.24), (4.32) are exact. Hence, the worst cases for fitting are when the interferers have a large variance. This is the first scenario. Thus, in addition to giving examples of engineering importance (presence or absence of a dominant interferer) these two cases also test the general applicability of (4.24) and (4.32) over a wide range of interferer profiles. These sets were obtained using the following parameter values: shadow fading standard deviation, $\sigma = 8.0$ dB, path loss exponent, $\gamma = 3.5$, radius of PU coverage area, $R = 1000$ m, radius of CR coverage area, $R_c = 100$ m, CR density of 1000 CRs per square kilometer, an activity factor of 0.1 and a common Doppler frequency of $f_D = 25$ Hz. Coverage areas are defined to be the areas in which the

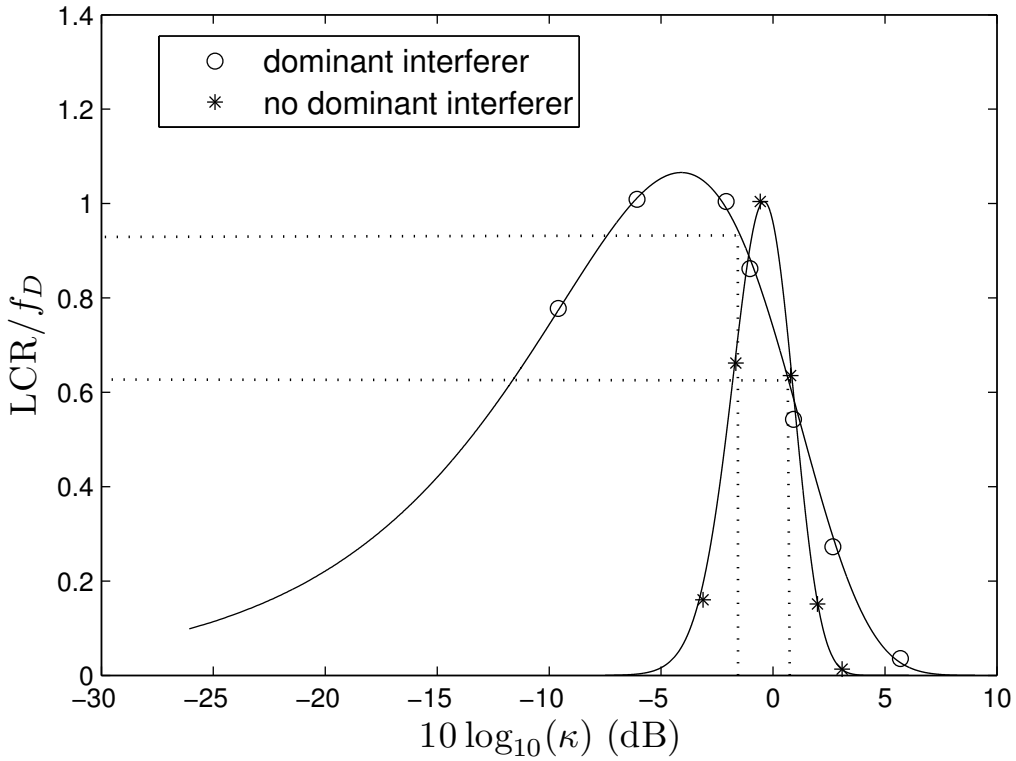

Figure 4.4: LCR results for the dominant and no dominant interferer cases in a Rayleigh fading scenario. The solid lines represent analytical results. Simulation values are shown by the circle and star symbols. The interference threshold values and their LCRs are shown by dotted lines.

received SINR is greater than a certain threshold at least 95% of time. We simulate LCRs by generating 10^5 independent channel pairs for each interferer, where each pair consists of $(h_i(t), h_i(t+\tau))$ where $h_i(t)$ and $h_i(t+\tau)$ are correlated according to the channel ACF which depends on the Doppler frequency. This approach enables an exact generation of the pairs and a rapid evaluation of LCR. Approaches that generate a single, long process over time are slower and require approximate models.

LCR and AED of CR-PU Interference

Figures 4.3, 4.4 and 4.5 show the LCR (normalized by Doppler frequency) of the interference for different types of fading and interference profiles. The x-axis is also normalized by the rms value of the process so that $\kappa = T/\sqrt{m_2}$ is plotted,

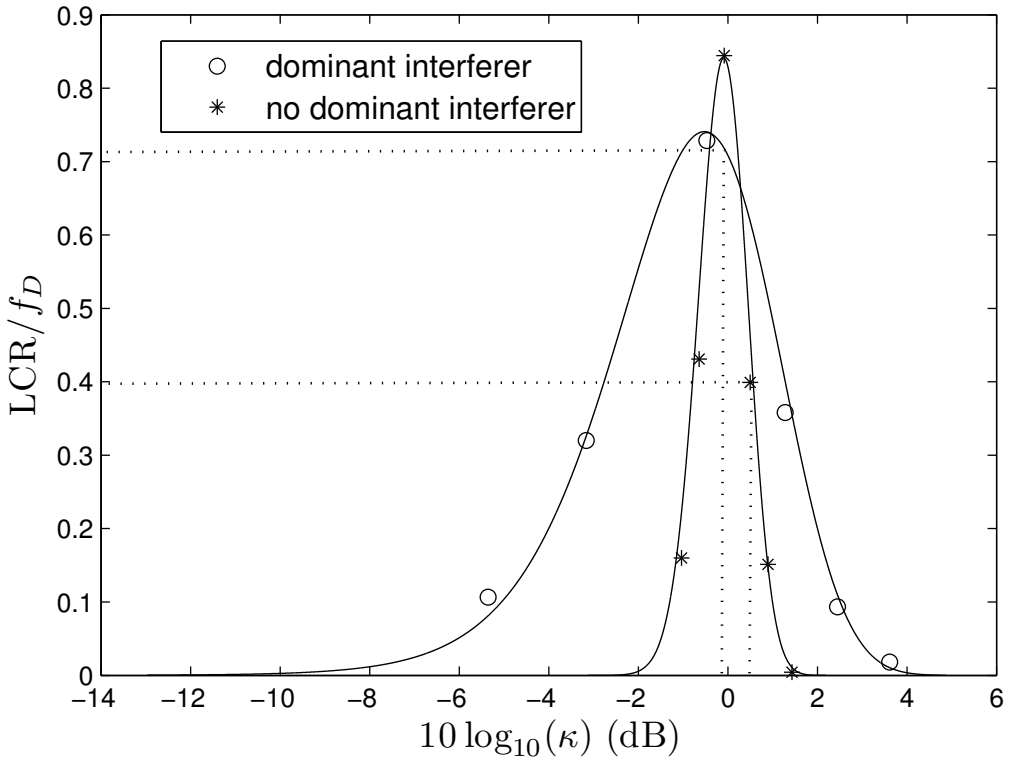

Figure 4.5: LCR results for the dominant and no dominant interferer cases in a Rician ($K = 10$ dB) fading scenario. The solid lines represent analytical results. Simulation values are shown by the circle and star symbols. The interference threshold values and their LCRs are shown by dotted lines.

where T is the interference power level and m_2 is the mean-square interference (see Appendix C). Figure 4.3 shows the effect on LCR of increasing the Rician K-factor, with the strong LOS case being considerably narrower than the non-LOS case. Figures 4.4 and 4.5 also show the value of the normalized interference threshold that restricts the long term average interference value in the CR system (as shown by the dotted lines). Note that there are multiple thresholds since the normalization is different for different channels. For all types of fading, the maximum LCR is observed close to this threshold value. This is because the CR allocation method gives a mean interference level close to the threshold. Even in strong LOS conditions ($K = 10$ dB), the interference shows a significant number of level crossings across the buffer due to the scattered component. Figure 4.4 shows the case of Rayleigh fading where the interference budget is dominated by a single large interferer with a number

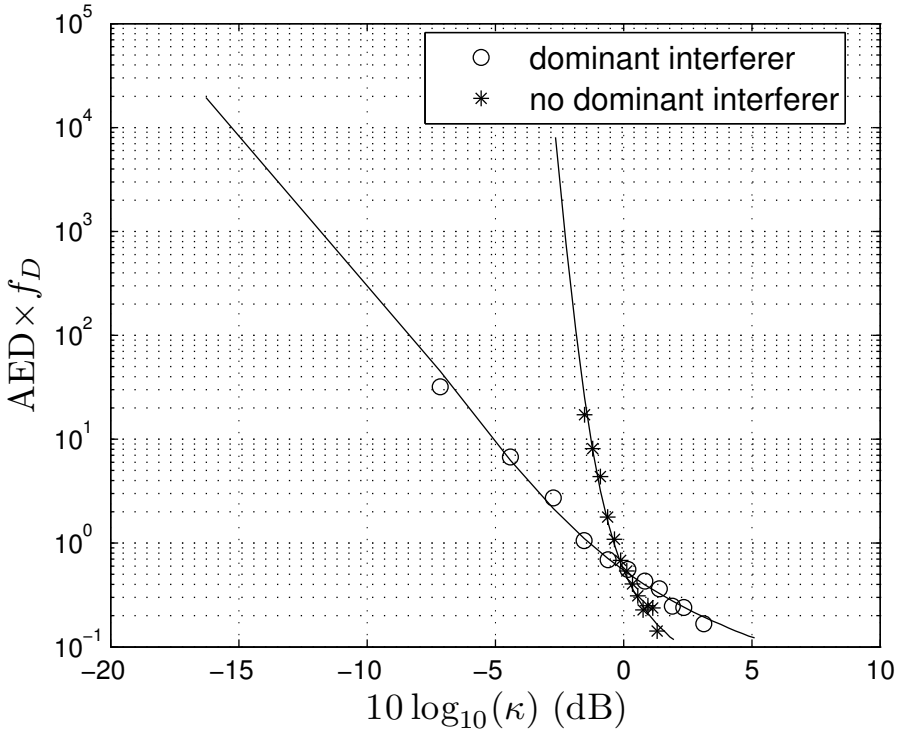

Figure 4.6: AED results for the dominant and no dominant interferer cases in a Rician ($K = 10$ dB) fading scenario. The solid lines represent analytical results. Simulation values are shown by the circle and star symbols.

of smaller additional interferers. Also shown is the no dominant interferer case. Figure 4.5 shows the same results for a Rician channel with $K = 10$ dB. Figures 4.4 and 4.5 show that when there are many small interferers, the interference is more stable compared to the dominant interferer case. The results in Fig. 4.5 are quite promising. In near LOS conditions, the interference has a much lower level crossing rate across the interference buffer for the no dominant interferer case. Hence, it may be a desirable part of the CR allocation policy to avoid any single user which takes up a significant part of the buffer. Finally, for completeness, we show the AED results corresponding to Fig. 4.5 in Fig. 4.6. As expected, the time spent by the interference above a threshold decreases as the threshold value increases. Therefore, for the no dominant interferer case, the interference seldom crosses the threshold (see Fig. 4.5), and when it does, it only exceeds the threshold for a small period of time. Since the LCR curve for the no dominant case is much sharper in Fig. 4.5,

the corresponding AED is much steeper. For example, -2 dB is rarely crossed in Fig. 4.5 and this corresponds to a very high AED value at the same threshold. All figures show an excellent agreement between the analytical approximations and the simulations.

4.6 Summary

In this chapter we have shown that the interference due to a single CR can be characterized in closed form for the scenario considered. However, the total interference due to multiple CRs is more difficult. Simple lognormal approximations are shown to be inaccurate and more complex models are required. Then we determine the LCR and AED for the CR-PU interference for Rayleigh and Rician channels. We have shown that LCRs in Rayleigh environment can be accurately approximated by LCRs of a gamma process. Similarly, while deriving LCR approximations in Rician conditions we have shown that the LCR of a noncentral χ^2 process with non-integer dof has the same form as that of a noncentral χ^2 process with integer dof. The LCR results show that in near LOS conditions, it is desirable for any CR allocation method to give priority to several small interfering CRs rather than a dominant interfering CR. The LCR of the former shows a greatly reduced crossing rate at and above the interference threshold. The AED results also show that the for the no dominant interferer case, the interference only exceeds the threshold for small period of time.

Chapter 5

Cognitive Radio Allocation Schemes

In addition to sensing techniques, a number of schemes aimed at avoiding harmful interference due to CRs at PUs have recently been developed, either based on a *primary exclusion zone* (PEZ) approach [58] or on the exploitation of *radio environment map* (REM) [82] information. The former utilizes the knowledge of interference statistics to define an exclusion zone inside which CRs are not permitted to operate, while the latter, which assumes a more complete knowledge of the interferers including their geographical position, permits only selected CRs to operate in order to maintain a specific SINR.

From our discussion in Chapter 4, it is clear that we cannot approximate the cumulative CR interference with a simple distribution. The availability of such a result would have helped in calculating, for example, an exact expression for the exclusion zone radius in PEZ schemes or the number of allowable CRs in the REM based techniques. This would have further shed light on the dependence of system performance on various different parameters. Hence, as a first look at this problem we study various CR scheduling schemes based on results obtained by computer simulations. We also stress here that we do not deal with the issue of how the CRs would communicate with each other and pass on the information about their

activity as this is beyond the scope of the current work. This, for example, can involve the CRs communicating with a controller upon obtaining permission for using the spectrum. Hence, in this chapter our contributions include analyzing a PEZ approach that allows access to CRs when the primary device is willing to pay a price in the form of a reduction in its threshold SNR. We determine the permissible number of CRs when the REM is *a priori* known to the CRs and establish how these numbers vary in different fading environments. In the presence of coarse REM information we show that when the REM for a given area is discretized then the total CR interference is significantly underestimated when realistic grid sizes are considered. We also determine the interaction between shadow fading correlation and REM grid size and evaluate their impact on interference estimation. Finally, we determine the scenarios (CR density, fading parameters) under which REM equipped CR systems outperform PEZ based cognitive wireless systems. To the best of our knowledge, we present the first comparative study of the PEZ and the proposed REM schemes with and without perfect REM information in shadowing environments.

In the simulations and results to follow, we assume that CRs are located uniformly in the primary coverage area. The number of active CRs, N_{CR}, is binomially distributed[1] with a maximum number of CRs given by $\pi R^2 D_{CR}$, where D_{CR} is the density of the CRs (number of CRs per m^2) and we ignore the negligible hole in the circle of radius R_0. The binomial probability that a CR wishes to transmit is given by the activity factor, $p = 0.1$. The primary receiver is at the center of the coverage area and the primary transmitter is also uniformly located in the primary coverage area. We consider two fundamentally different schemes for managing the interference at the PU receiver. The REM approach utilizes complete knowledge of all the interference values whereas the PEZ approach only uses average information of all interferers within a certain distance of the PU receiver. There are N_{CR} CR transmitters which desire a connection. Each of the N_{CR} CRs has an interference

[1]We mention that to arrive at (4.19) we used a Poisson variable to model the interfering CRs (in the limiting case when the number of CRs tends to infinity and the probability of each interfering CR is small enough) for the sake of mathematical tractability. Here, without loss of generality, we assume a binomial random variable modeling the finite number of such CRs.

power at the primary receiver given by (4.1) and denoted $I_1, I_2, \ldots, I_{N_{CR}}$. Based on these interference values, the PEZ and REM approaches are described below.

5.1 PEZ Approach

The PEZ approach [58] only uses location information to control the access of CRs. A simple exclusion zone is created with radius R_e around the primary receiver. No CR is allowed to transmit inside the PEZ and all CRs outside the PEZ are permitted. The radius, R_e, is set so that the cell-edge SINR is degraded by a certain amount. Specifically, the primary coverage area is defined to give an SNR greater than 5 dB, 95% of the time. By allowing CRs to operate we accept a new SINR target, less than 5 dB, which is achieved at least 95% of the time.

5.2 REM Approach

The REM approach [82] assumes that $I_1, I_2, \ldots, I_{N_{CR}}$ (defined to be same as in the previous chapter) are known and selects those CRs for transmission which satisfy an SINR constraint. The constraint chosen is that the added interference must not decrease the SNR by more than Υ dB. For example, if SNR = 10 dB in the absence of CRs, then those CRs chosen must give SINR $\geq (10 - \Upsilon)$ dB. Two methods are chosen for selection, a centralized approach and a decentralized approach.

- *Centralized Selection:* Here we assume that a centralized controller knows $I_1, I_2, \ldots, I_{N_{CR}}$ instantaneously and creates a list of the ordered interferers as $I_{(1)} \leq I_{(2)} \leq \ldots \leq I_{(N_{CR})}$. The first n CRs are selected such that $\sum_{i=1}^{n} I_{(i)} \leq \Upsilon$ dB and $\sum_{i=1}^{n+1} I_{(i)} > \Upsilon$ dB.

- *Decentralized Selection:* Here we assume that the CRs are considered in their original order which can be interpreted as their order of arrival. Each interferer is considered in turn and is accepted if the combined interference from previously accepted CRs and the current CR is less than Υ dB. If a CR is not accepted,

the next CR in the list is investigated.

The usefulness of REM based techniques hinges around the quality of the information available. Thus we discriminate between perfect and imperfect REM information in the following.

A Perfect REM

A REM can hold a wide variety of information [83] and it is not clearly understood at present what constitutes a practical and effective REM. In this work we assume that the REM contains signal strength data. In a perfect REM the signal strength from all source coordinates to all destination coordinates is known. With this perfect REM a CR controller can select those CRs for operation which satisfy a given interference constraint. The CR controller requires positional information for the PU and the CRs, and can then use the REM to compute the overall SINR of the PU where

$$\text{SINR} = \frac{S}{\sum_{i=1}^{N} I_i + \sigma^2}. \tag{5.1}$$

In (5.1), S is the signal strength of the PU, σ^2 is the noise power and $\sum_{i=1}^{N} I_i$ is the aggregate interference of the N selected CRs. The interference constraint used is that the CR interference must not reduce the PU SNR by more than $\Upsilon = 2$ dB. All results shown in the paper are for a 2 dB buffer. The value of 2 dB was chosen arbitrarily.

Modeling of REM Imperfections

In practice, it is unrealistic to assume a perfect REM and the REM information is discretized in the form of a grid of points with grid size, Δ. Hence, the central controller allocating CRs will formulate its decisions on the basis of REM information obtained from the grid points, rather than from exact signal strength data. Therefore, an interfering signal strength, I, will be estimated as $\hat{I}$ from the REM. The estimate is obtained from the grid-to-grid path in the REM which is closest to the actual signal path.

We consider the CR signal strength to be of the form given in (4.1). The REM predicted signal strength is given by

$$\hat{I} = Be^{\hat{X}}\hat{r}^{-\gamma}, \tag{5.2}$$

where $\hat{r}$ is the distance between the transmitter and the receiver in the REM grid and $\hat{X}$ is correlated with X by

$$\hat{X} = \rho X + \sqrt{1-\rho^2}E. \tag{5.3}$$

In (5.3) E is i.i.d. with X. Assuming a distance, d_i, between the actual and REM based position of the CR and a distance, d_p, between the actual and REM based location of the PU receiver, the correlation coefficient ρ can be obtained using an extension of Gudmundson's model [16] as

$$\rho = 0.5^{d_i/D_d} \times 0.5^{d_p/D_d}. \tag{5.4}$$

In (5.4) D_d is the so called *decorrelation distance* i.e., the distance at which the correlation between X and $\hat{X}$ drops to 0.5. The effect of flawed REM information on the signal strength between the primary transmitter and its receiver can be modeled using (5.2), (5.3) and (5.4). Simulation results of this model based on parameter values of a suburban macrocellular environment are given in Section 5.3.

Optimal Interpolation: The above models for REM imperfections allow the effects of errors in the REM to be simulated. However, REM accuracy is of key importance as shown in Sec. 5.3 and hence it is useful to take a closer look at this issue. In what follows we derive the distribution of the errors resulting from the imperfect REM under certain idealized conditions.

Consider a REM with grid size, Δ, where the receiver is exactly located at one grid point and the transmitter location, P, is arbitrary, falling in one square of the grid pattern. We further assume that the signal strength model in (4.1) is exact and that, B, r, γ are exactly known. Hence, only the shadow fading is unknown and this information is exactly known at the grid points. We further assume that Gudmundson's model (5.4) holds with $d_p = 0$. Clearly this situation is extremely

optimistic and leads to a lower bound on realistic REM errors. Now consider the signal strength from P to the PU receiver where P falls inside one of the grid boxes. Since all the five points (the four corners of the box and P) experience correlated shadow fading, we model the correlation between the normal random variables, X_i, associated with the lognormal shadowing at the five points using Gudmundson's model [16]. Thus,

$$\rho(X_i, X_j) = a^{d_{ij}}, \qquad i, j = 1, \ldots, 5, \tag{5.5}$$

where $\rho(X_i, X_j)$ represents the corrrelation between X_i and X_j, and d_{ij} is the distance between X_i and X_j. Using Gudmundson's results we choose $a = 0.998$ for suburban environments and $a = 0.886$ for urban environments. Furthermore, we assume that X_1 to X_4 form the corner points of the square with the principal diagonal between X_1 and X_3 and the other diagonal between X_2 and X_4. Hence, we have the following correlation matrix for $(X_1, \ldots, X_5)^T$:

$$\mathbf{R} = \begin{bmatrix} 1 & r & r^{\sqrt{2}} & r & r^{d_1} \\ r & 1 & r & r^{\sqrt{2}} & r^{d_2} \\ r^{\sqrt{2}} & r & 1 & r & r^{d_3} \\ r & r^{\sqrt{2}} & r & 1 & r^{d_4} \\ r^{d_1} & r^{d_2} & r^{d_3} & r^{d_4} & 1 \end{bmatrix}, \tag{5.6}$$

where $r = a^{\Delta}$, $\rho(X_5, X_i) = a^{d_i \Delta} = r^{d_i}, \forall i$ and d_i is the distance from the point P to the ith corner of the square. Performing the Cholesky decomposition we have $\mathbf{R} = \mathbf{A}\mathbf{A}^{\dagger}$, where $\mathbf{A}$ is a lower triangular matrix. Clearly, $\mathbf{A}$ can be factored as,

$$\mathbf{A} = \left[\begin{array}{c|c} \mathbf{A}_{11} & \mathbf{0} \\ \hline \mathbf{a}^T & b \end{array}\right], \tag{5.7}$$

where $\mathbf{A}_{11}$, $\mathbf{0}$ and $\mathbf{a}^T$ represent a sub-matrix, a column vector of zeros and a row vector of appropriate sizes, respectively. Further, b represents a scalar lying between

0 and 1. With this notation, it can be shown that,

$$X_5 = \mathbf{a}^T \mathbf{A}_{11}^{-1} \begin{bmatrix} X_1 \\ X_2 \\ X_3 \\ X_4 \end{bmatrix} + bu_5, \tag{5.8}$$

where u_5 is $\mathcal{N}(0, \sigma_{sf}^2)$. The first term in (5.8) represents the optimal estimator of X_5 using the REM and the second term gives the estimation error which is $\mathcal{N}(0, b^2\sigma_{sf}^2)$. Note that this is standard theory [84]. Further it is worth emphasizing that this analysis can easily be extended to interpolation using more than 4 REM grid values.

It is evident that the performance of the above scheme heavily depends on the behavior of the error term which in turn relies on Δ and σ_{sf}. One way to evaluate this is to compute the probability of underestimating signal strength (interference) from the CR devices. Based on (5.5)-(5.8) the probability of underestimating the interfering signal strength by an amount, E, is given by

$$\begin{aligned} P_E &= \text{Probability of underestimating the signal strength by more than } E \text{ dB} \\ &= P(\text{estimation error} < -E \text{ dB}) = Q\left(\frac{E}{b\sigma}\right), \end{aligned} \tag{5.9}$$

where $Q(.)$ gives the tail probability of a standard Gaussian. Hence, the Cholesky decomposition of $\mathbf{R}$ gives b which directly leads to (5.9), a simple closed form result for the effects of imperfect REM.

5.3 Simulation Results

Unless otherwise stated, we assume a PU coverage radius of $R = 1000$ m, and the transmit power is adjusted such that the SNR at the cell edge is 5 dB (i.e., in the coverage area the SNR exceeds 5 dB with probability 0.95). The CR transmit power is also chosen to meet a cell edge SNR of 5 dB for a given CR coverage radius, $R_c = 100$ m. Two kinds of CR penetration densities were chosen, a high density of $10,000$ CRs per sq. km and a corresponding moderate density of 1000 CRs per

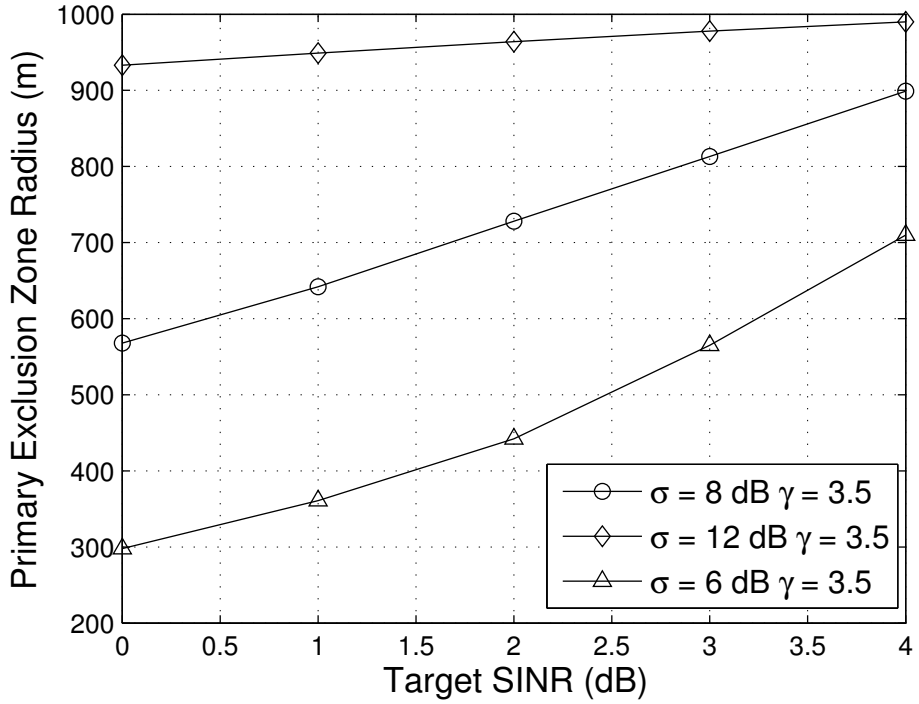

Figure 5.1: The effect of σ and the target SINR on the PEZ radius for a medium density of CRs.

sq. km. Additionally, it was assumed that only 10% of the CRs wish to be active at any one time. The values of the propagation constants, γ and σ are given on the relevant figures. The shadow fading variance and path loss exponent should be taken as 8 dB and 3.5, respectively, when they are not explicitly mentioned.

5.3.1 Exclusion Zone Results

Given a variety of target SINRs, Fig. 5.1 shows the PEZ radius for different values of σ. For example, if the interference degrades the target SNR from 5 dB to an SINR of 4 dB, then the PEZ radius is approximately 700 m, for $\sigma = 6$ dB and $\gamma = 3.5$. It is interesting to note that the PEZ radius excludes virtually the entire PU coverage area for all target SINRs in $[0, 5]$ dB when $\sigma = 12$ dB, corresponding to dense urban areas. This result implies that for a given target SINR, environments with larger σ will result in higher interference and an increased R_e. This observation is consistent with previous observations reported in [85].

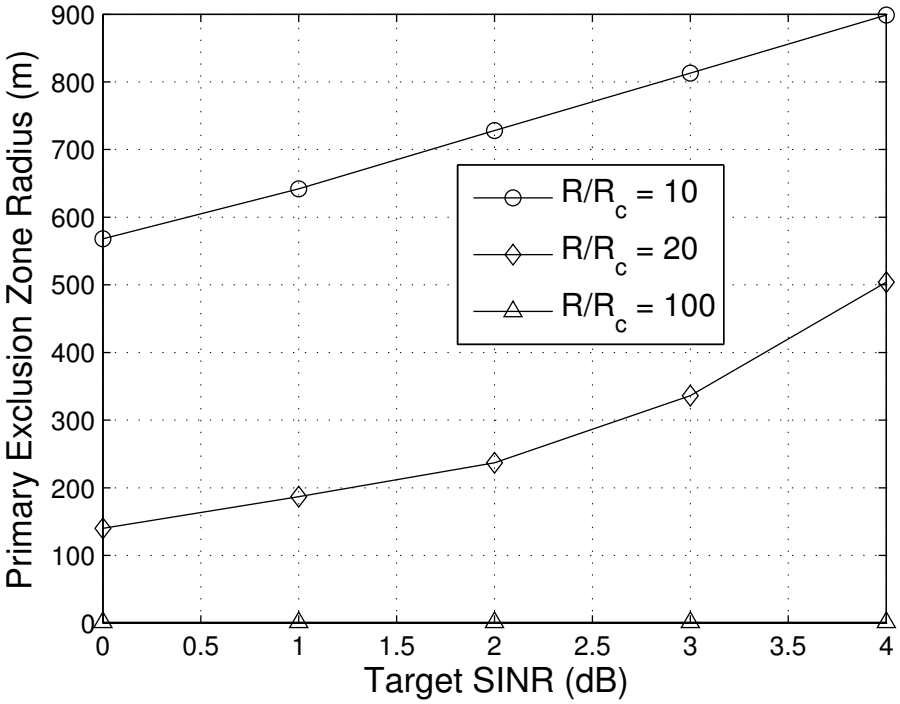

Figure 5.2: PEZ radius vs target SINR for different values of the ratio of primary to secondary device coverage areas ($\sigma = 8$ dB, $\gamma = 3.5$).

Increasing the CR transmit power or increasing R_c will correspondingly increase the interference and hence the PEZ radius. Figure 5.2 shows the PEZ radius vs target SINR for three different values of R/R_c. Reducing the CR transmit power will obviously result in a lower PEZ radius.

5.3.2 Comparison of Numbers of CRs

Figures 5.3 and 5.4 show CDFs of the number of CRs for the two different types of REM approach and the impact of varying the fading parameters. In both these figures, the centralized approach is superior, since it is designed to pick up the maximum number of CRs that aggregate to make up the acceptable interference degradation. We also note from Fig. 5.3 that increasing γ increases the number of permissible CRs. This is because environments where $\gamma = 4$ will experience less interference compared to environments where $\gamma = 3$ due to increased path loss. Looking at Fig. 5.4, increasing σ decreases the permissible number of CRs. This

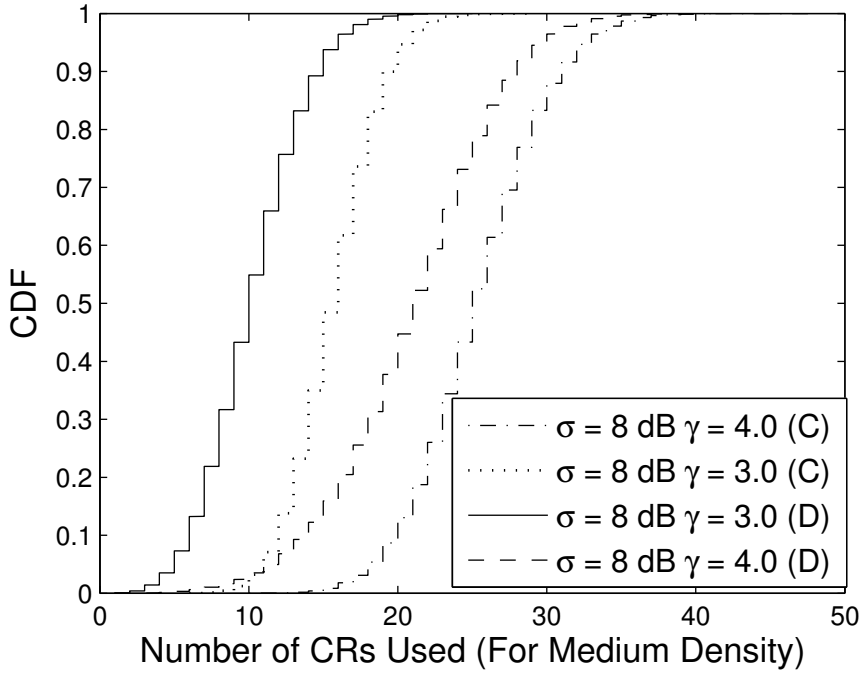

Figure 5.3: CDF of the number of CRs obtained using REM based approaches for various γ values. D and C denote decentralized and centralized approaches.

result reinforces the conclusion of Fig. 5.1 where increasing σ increased the PEZ radius - effectively reducing the area in which CRs operate and also reducing the permissible number of CRs. Note that dense urban environments are characterized by γ values of 4 and above and σ values of 8 dB and above. These two parameters have opposing effects on the permissible number of CRs.

Figure 5.5 compares the PEZ and REM approaches in terms of the percentage of CRs that gain access in a high density environment. The centralized approach is far superior, showing the potential advantage gained if the CR knows the radio environment. This advantage is dissipated by the decentralized approach as effectively a few CRs consume the permissible interference budget (2 dB in this case). The PEZ approach is worse than the decentralized strategy. It is an important result that the decentralized REM approach, which can be thought of as a first-come-first-served mechanism, results in better access for the CRs than the PEZ approach. Hence, the overhead of obtaining the REM can result in improved access. However, it is critical that the REM information be used in an intelligent allocation process if real gains

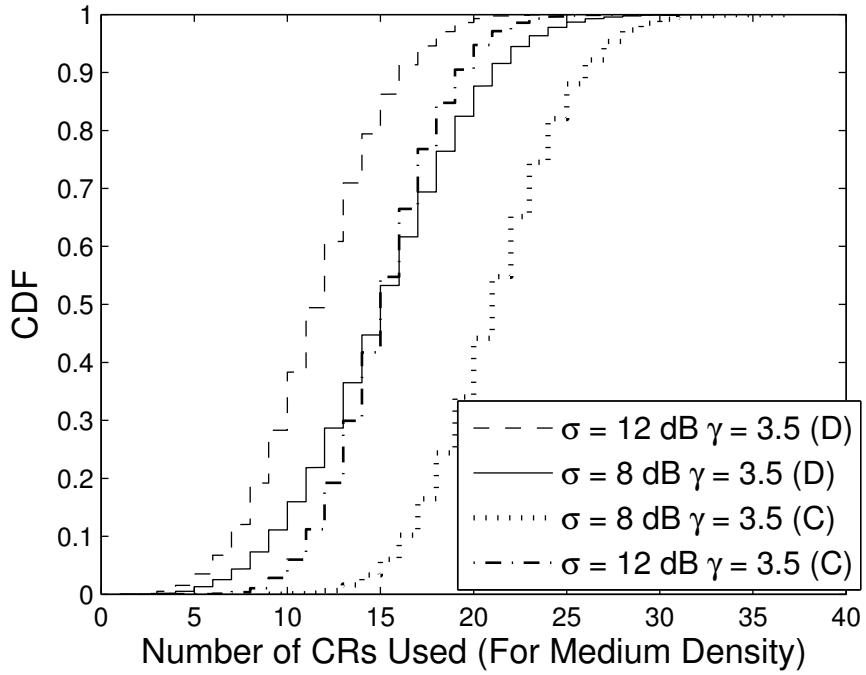

Figure 5.4: CDF of the number of CRs obtained using REM based approaches for various σ values. D and C denote decentralized and centralized approaches.

over PEZ are to be achieved. Figure 5.6 revisits the results in Fig. 5.5 for a lower CR density. Here too the centralized approach is better, but now the decentralized approach shows an even bigger advantage over the PEZ approach for higher values of the CDF. In addition to this, we also investigate the case of CRs with different coverage areas. In particular, we consider a coverage circle with radius uniformly distributed in [50 m, 150 m]. Such scenarios may correspond to heterogenous CR systems with application specific coverage zones. Clearly, in this case the mean value of the number of CRs given access remains nearly the same as before in the two REM based schemes. However, as expected, the variation in the percentage of CRs given access tends to increase. We note that the PEZ scheme outperforms the REM based strategies in Fig. 5.5 by a bigger margin than an Fig. 5.6 on account of the higher CR density employed in Fig. 5.5.

The results in Figs. 5.3-5.6 taken collectively are the important contributions of this chapter. They clearly show the advantage in terms of permissible CR numbers

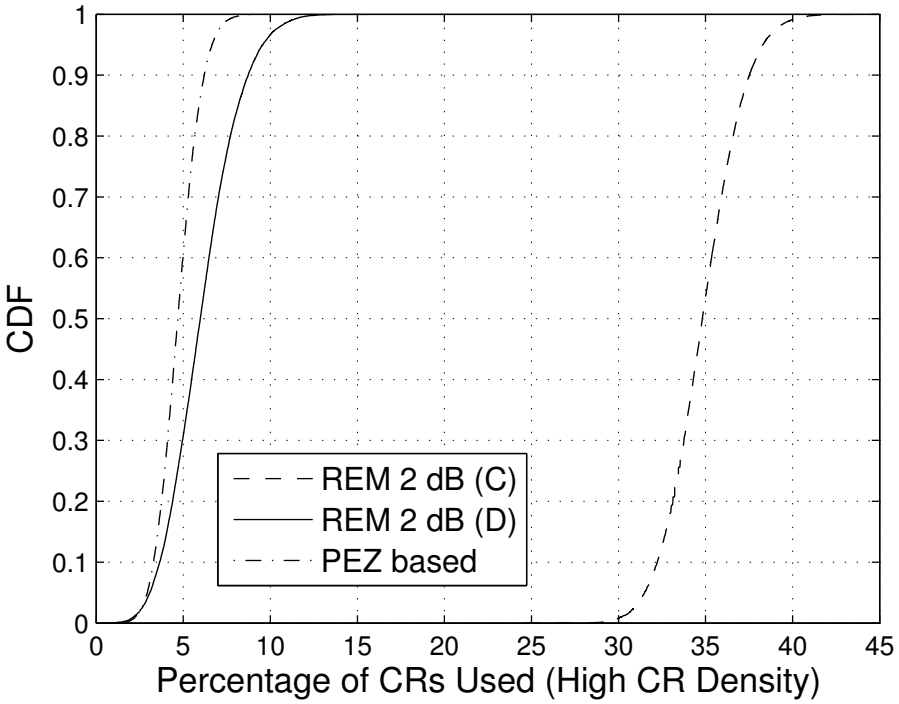

Figure 5.5: Percentage of CRs given access for a high CR density ($\sigma = 8$ dB, $\gamma = 3.5$).

if a knowledge of the radio environment is made available to the CRs. Furthermore, they show that the full REM gains are only obtained if a smart access control algorithm is used which chooses many CRs with low interference instead of a few stronger interferers which might subsume the interference budget.

5.3.3 Imperfections in the REM

In practice, the radio environment is often modeled by dividing an area into a regular grid (typically composed of 100 m $\times$ 100 m grid boxes) and assuming that the fading conditions in any grid box can be approximated by a single point at the center of the box. For example, drive testing of cellular networks to validate path loss models and predicted signal coverage follows this approach. Clearly, larger grid sizes result in errors between measurement and prediction. On the other hand, reducing the grid size results in a large data overhead. Figure 5.7 shows the CDF of the magnitude of the actual CR-PU interference when the REM is estimated via a grid size ranging

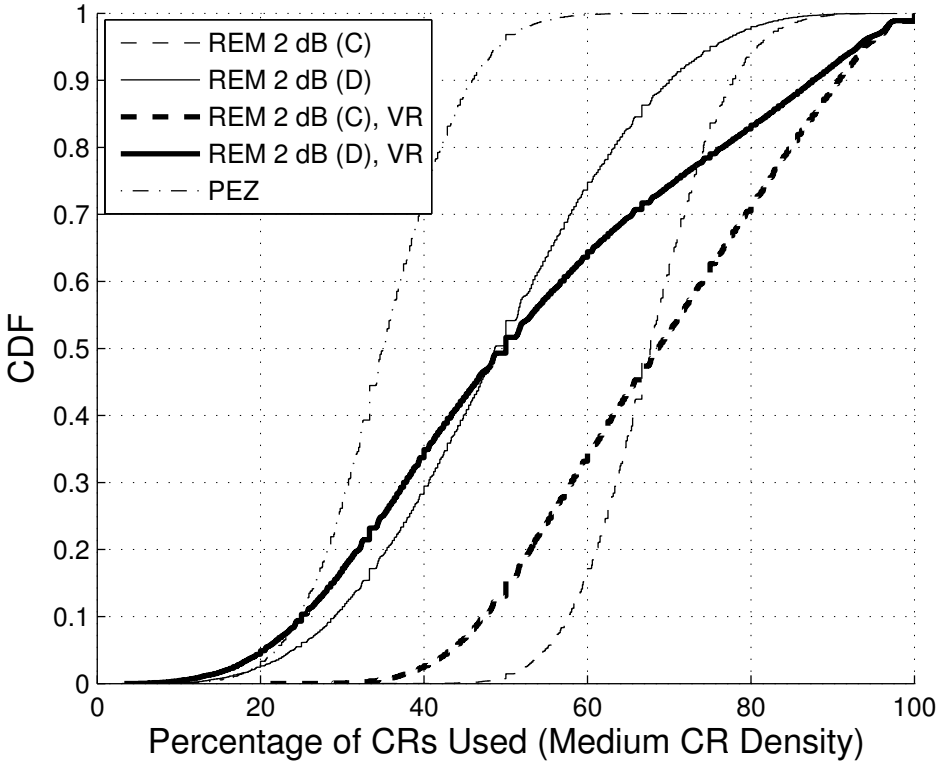

Figure 5.6: Percentage of CRs given access for a medium CR density ($\sigma = 8$ dB, $\gamma = 3.5$). VR denotes a variable CR radius uniformly distributed between 50 m and 150 m.

from 1 m $\times$ 1 m to 100 m $\times$ 100 m. The REM approach aims to maintain a 2 dB SINR buffer for the primary, but this is only possible with a perfect REM. When $\Delta = 1$ m the 2 dB buffer is nearly achieved (exceeded only 13% of time) but for a grid size of 50 m $\times$ 50 m, the interference exceeds 2 dB for approximately 70% of the time. For a grid size of 100 m $\times$ 100 m, 2 dB is exceeded 85% of the time and 5 dB is exceeded 10% of the time. In effect this means that if REM information is derived from a coarse grid, the buffer size must be increased or the CRs must back off from the buffer.

The effects of increasing the buffer or backing off the CRs are shown in Figs. 5.8 and 5.9, respectively. In Fig. 5.8 the PU has a target 2 dB buffer but due to the imperfect REM it will not always be achieved. Hence, an extra buffer is permitted beyond which the CRs are only allowed, 5% of the time. In Fig. 5.8 this scenario is

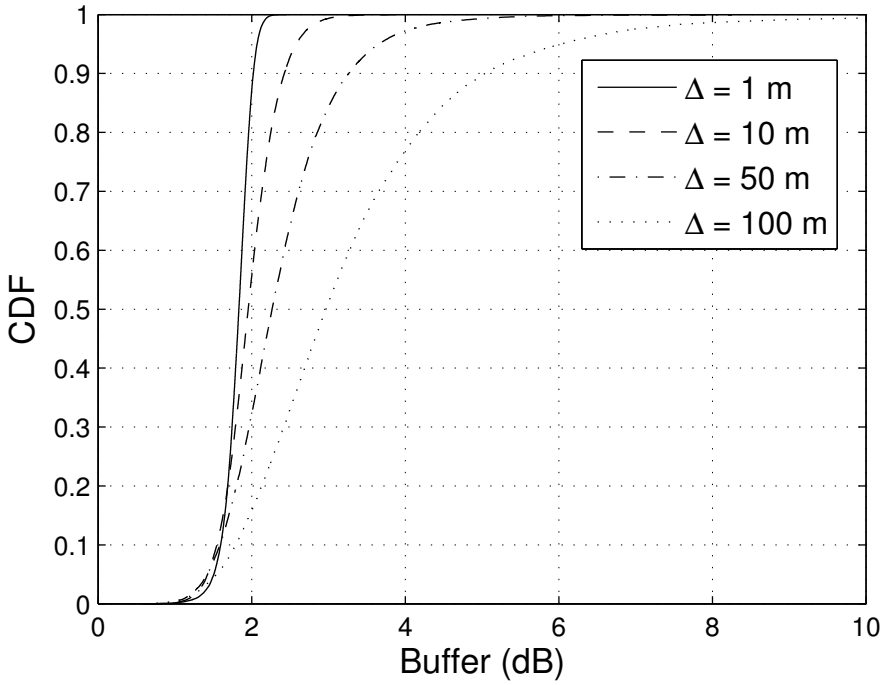

Figure 5.7: Interference CDF for an REM enabled CR network for several values of Δ and decorrelation distance, $D_d = 100$ m.

denoted by the legend, Threshold = (original + extra) dB. The effects of spatially correlated shadow fading are also considered in Fig. 5.8. Shadow fading is correlated over any given area and the level of this correlation has a simple effect on the REM grid size. For highly correlated areas a coarse grid (large Δ) will be acceptable whereas in areas of low correlation, a fine grid (small Δ) will be required. Figure 5.8 shows the REM grid size vs the decorrelation distance of the shadow fading. For a given interference degradation (say the buffer value plus an additional 2 dB) a large decorrelation distance (say 500 m) enables a coarser grid size 130 m $\times$ 130 m relative to a decorrelation distance of 100 m (typical for dense urban areas) when the grid size is 38 m $\times$ 38 m.

In Fig. 5.9 we consider a back off in the CR allocation policy. In order to meet the nominal 2 dB SINR buffer at least 99% of the time, the CRs have to target a reduced buffer which is less than 2 dB. Figure 5.9 shows this buffer vs Δ for various values of D_d. For a grid size of 25 m $\times$ 25 m and a decorrelation distance of 100 m, the interference buffer is 0.88 dB. Figures 5.8 and 5.9 are instructive in determining

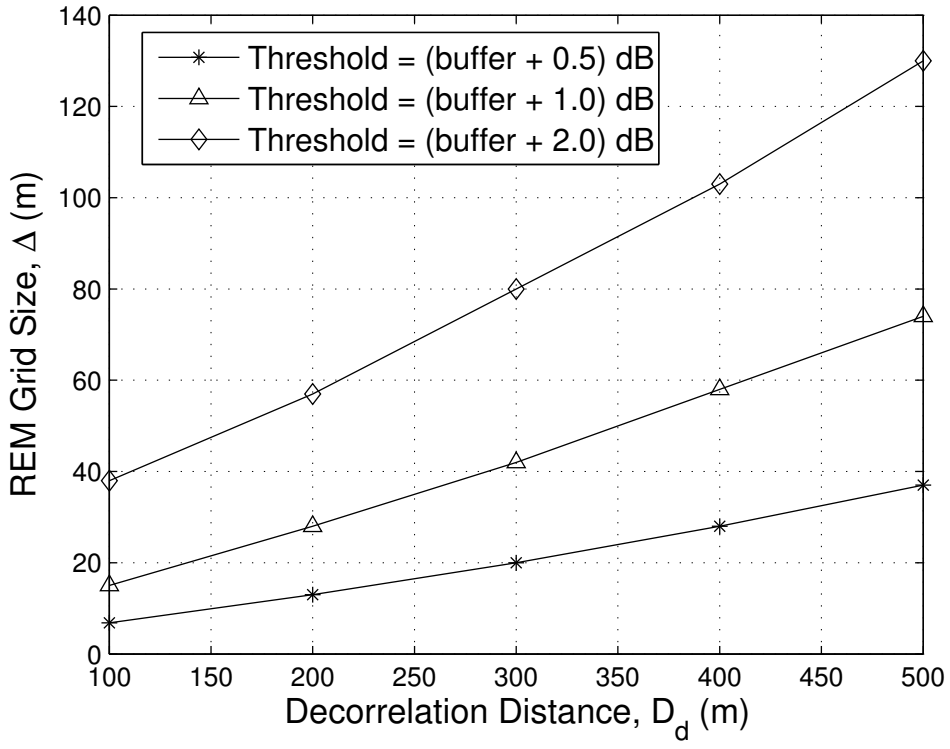

Figure 5.8: REM grid size, Δ, vs decorrelation distance, D_d, for different threshold buffer sizes.

the grid sizes for different radio environments.

To study the effect of linearly interpolating signal strength from the position of a source point in a REM grid, we simulate the estimation error introduced in Sec. 5.2 for different environments. In particular, we plot the probability of this error being less than a threshold of -3 dB (i.e., when we underestimate the interference by more than 3 dB) for urban and suburban environments based on meshes of 4 and 16 points for shadow fading variances of 6 dB and 12 dB as shown in Fig. 5.10. It is clear from the figure that linearly interpolating the signal strength using the nearest 16 points in the REM grid is no better than using the closest 4 grid points. Furthermore, it is seen that owing to smaller decorrelation distances, finer grid sizes would be needed in urban environments ($a = 0.886$). In addition to this, shadowing has a negative impact on the performance of such REM systems in terms of underestimating the true interference produced by the CRs. The scale of the underestimation problem

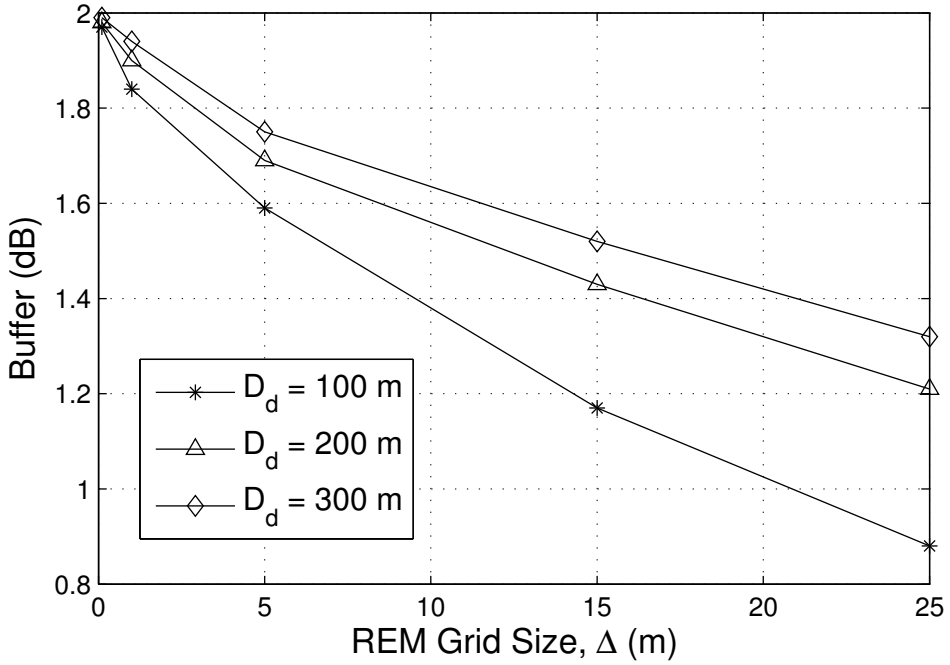

Figure 5.9: Variation of actual buffer with REM grid size, Δ, for different values of the decorrelation distance, D_d.

can be seen from a few examples in Fig. 5.10. In urban environments with 6 dB shadowing, 30% of time the interference is underestimated by more than 3 dB for a grid size of 31.6 m. Even with a much smaller 10 m grid this probability is still greater than 20%. Hence, despite underestimating the real REM errors, it can be seen that extremely small grid sizes may be needed to avoid harmful interference.

5.4 Summary

In this chapter two interference management approaches have been considered based on REM and PEZ ideas. The REM approach requires considerable higher overheads but can perform substantially better than the PEZ one. To achieve these gains an intelligent allocation method is essential since providing access to CRs on a first-come-first-served basis can be worse than the PEZ method. However, the PEZ approach results in large exclusion zones especially for high σ and large R_c values. We have shown that interference degradation to the PU can be significantly un-

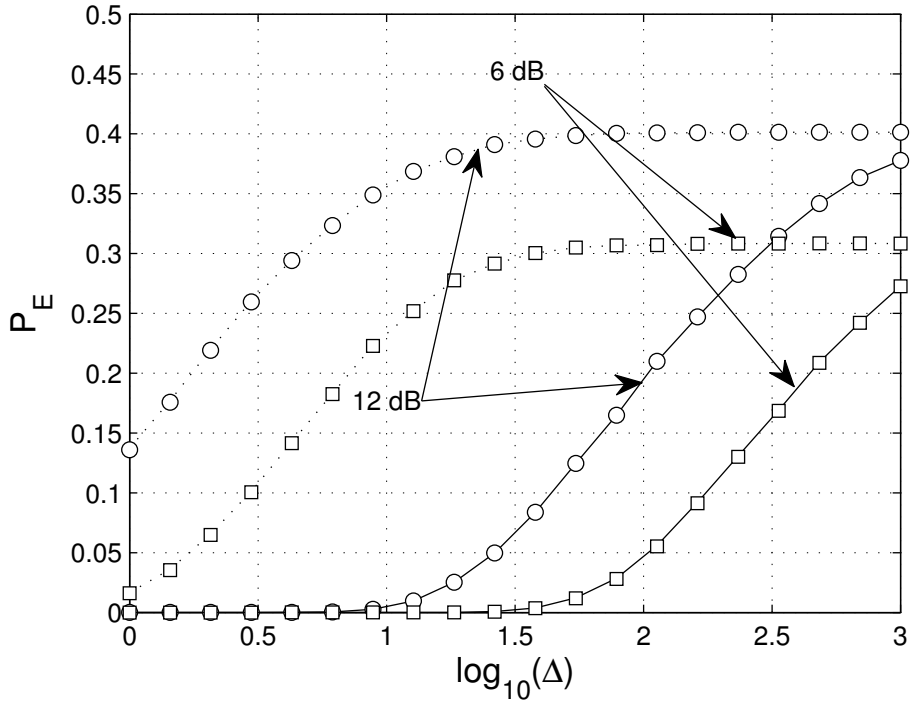

Figure 5.10: Variation of the probability of underestimating the interference versus grid size. Solid lines are for suburban and dotted lines are for urban environments. The lines (solid and dotted) represent 4 point while the points (circles and squares) depict 16 point interpolation.

derestimated if the channel state information needed to estimate interference levels is derived from a coarse REM. In particular, the probability of interference underestimation has been shown to be very high for urban environments. For practical deployments, this may mean that the PU has to accept a much larger interference from the CRs or the CRs may need to set a more conservative interference target. This will reduce the number of CRs allowed.

Chapter 6

MIMO Cognitive Radios with Antenna Selection

The concept of MIMO CR systems has triggered significant interest in the research community [86, 87, 88, 89]. In CR systems, multiple antennas in addition to providing rate benefits, can also help in enabling interference control at the PU RX [87]. However, along with the gains, comes hardware complexity at the radio front end owing to the requirement to have costly RF chains (consisting of low noise amplifiers, downconverters and analog-to-digital converters) that scale with the number of antennas being used. Even more costly is the provision of power amplifiers and up converters at the transmit end.

It is well known that antenna selection techniques present an elegant solution to such problems, see, for example, [90, 91, 92] and the references therein. Recent work in this area includes [93] where transmit antenna selection was considered for a MISO CR operating in the presence of a SISO PU. In this chapter, we consider the problem of joint selection of transmit/receive antennas in a MIMO CR system. The selection procedure aims to maximize the achievable rate of the CR while satisfying any interference constraints due to the PU RX(s) (either equipped with a single antenna or multiple antennas) operating in the vicinity. The work in [93] has similarities in that the SINR results in [93] can be transformed to rates, and

they also impose interference constraints and consider a range of selection strategies including norm based approaches. We note, however, that the approach in [93] is analytically based whereas our techniques are more focused on optimization and potential implementation. Furthermore, in this chapter we also include the effects of interference from the PU to the CR and power control at the CR TX. After formulating the antenna selection problem in the context of CR networks, we propose two solutions in addition to the brute force, optimal full search method. A comparison of the proposed algorithms, based on their performance, is also presented. In certain situations, the optimal exhaustive search method can be analyzed and these results in addition to simulations incorporating shadow fading and path loss effects are also provided. Our key contributions are following:

- An approximate solution to the original non-convex optimization problem based on iteratively solving a series of convex problems. The results are found to be stable and in close agreement with those obtained from the optimal search.

- A norm-based heuristic that performs transmit and receive antenna selection, to increase the rate while satisfying the interference constraints. The heuristic has massively reduced computational complexity and gives very accurate results when compared with the optimal search.

- A demonstration that even under interference constraints, the CR system is still able to achieve substantial rate gains due to selection (especially when the strength of the CR-PU interference channel is lower than that of the CR-CR channel) and thus retain the traditional spatial multiplexing benefit of MIMO systems.

- An analytical characterization of the optimal selection process for the special case where a single SISO link is selected. These analytical results are supported by simulations of a more complete channel model including shadowing, path loss and random numbers of PU RXs.

In this chapter we use $||.||_2$ to denote the norm operator, $\mathbf{M}(i,:)$ and $\mathbf{M}(:,j)$ to

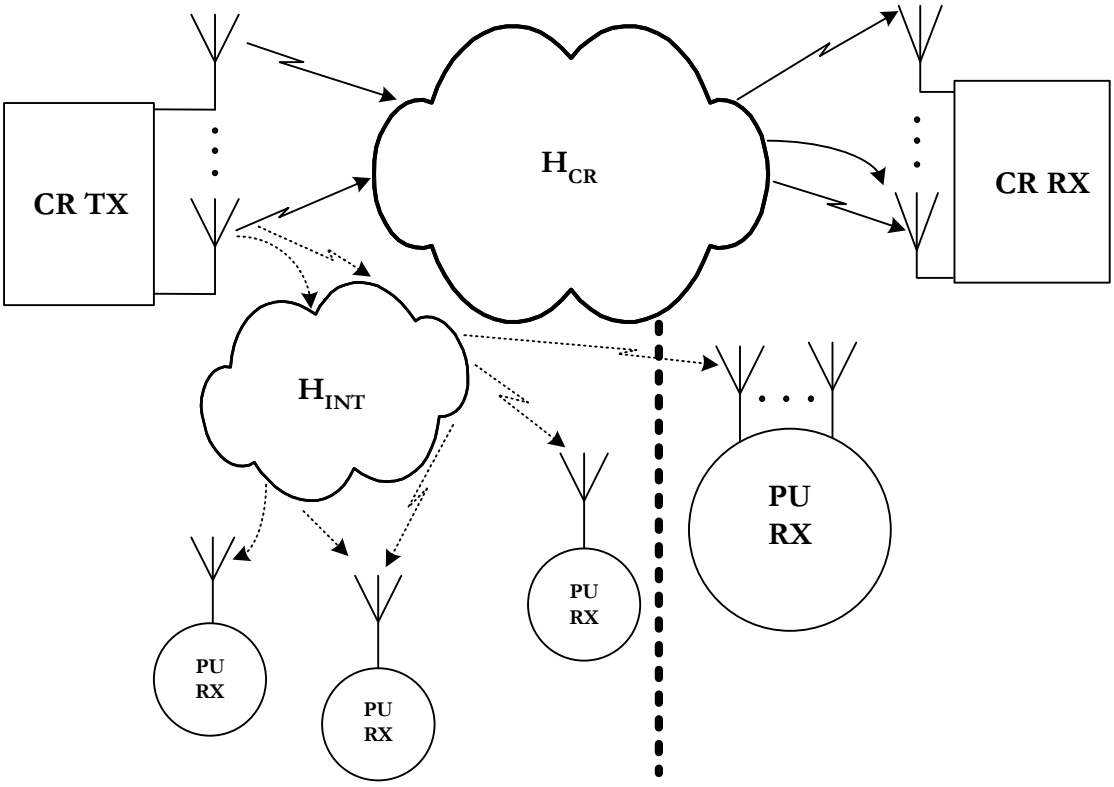

Figure 6.1: System model. The vertical dotted line indicates that the multiple antenna and single antenna PU systems are considered separately. PU TXs are not shown for the sake of clarity.

represent the ith row and jth column of a matrix, $\mathbf{M}$, respectively. (x, y) and (X, Y) are used to denote y and x antennas chosen out of Y and X receive and transmit antennas, respectively. Diag(.) gives the diagonal elements of a matrix. diag($[\mathbf{x}], 0$) represents a diagonal matrix with vector $\mathbf{x}$ along the diagonal. Finally, $f(n) \in \mathcal{O}(g(n))$ is used to characterize the order of $f(n)$ such that for sufficiently large n, $f(n)$ is upper bounded by a constant times $g(n)$.

6.1 System Model

The proposed system model is shown in Fig. 6.1. We assume that the CR TX and RX are equipped with N_{CR} and M_{CR} antennas, respectively. The incumbent PU has N_{PU} transmit (not shown in Fig. 6.1) and M_{PU} receive antennas in the case of a single MIMO PU. We also consider the case of multiple single receive antenna

PUs operating in the vicinity of the CR system. In this case M_{PU} is the number of PUs. These scenarios are referred to as single user (SU) and multi-user (MU), respectively. The channels between all nodes are assumed to experience frequency flat Rayleigh fading. The signal at the CR RX is given by

$$\mathbf{y}_{\mathrm{CR}}(n) = \mathbf{H}_{\mathrm{CR}}\mathbf{x}(n) + \mathbf{i}(n) + \mathbf{z}(n), \tag{6.1}$$

where $\mathbf{H}_{\mathrm{CR}} \in \mathbb{C}^{M_{CR} \times N_{CR}}$ is the channel gain matrix with (zero mean circularly symmetric complex Gaussian) ZMCSCG entries, $\mathbf{y}_{\mathrm{CR}}(n)$ and $\mathbf{x}(n)$ are the received and the transmitted signal vectors respectively, $\mathbf{z}(n) \sim \mathcal{CN}(0, \mathbf{I}_{M_{CR}})$ is the additive white Gaussian noise (AWGN), $\mathbf{i}(n)$ is the interference (assumed to be independent of $\mathbf{z}(n)$) received from the PU TX(s) and the index n represents the nth time sample. Further, the transmit covariance matrix of the CR user is denoted $\mathbf{Q}_{\mathrm{CR}} = \mathbb{E}[\mathbf{x}(n)\mathbf{x}(n)^{\dagger}]$. We assume that the total average CR transmit power is limited to its long term SNR, P_{CR} i.e., $\mathrm{Tr}(\mathbf{Q}_{\mathrm{CR}}) \leq P_{CR}$. Since a normalized CR-CR channel is considered, we have $\mathbb{E}[|(\mathbf{H}_{\mathrm{CR}})_{ij}|^2] = 1$ and the receive SNR across a receive antenna (in the absence of any interference) at the CR RX is given by $\mathrm{SNR} = P_{CR}$. The PU system has an SNR at the receiver end denoted $\mathrm{SNR}_{\mathrm{PU}}$. $\mathrm{SNR}_{\mathrm{PU}}$ could either represent one value in the SU case or a set of values in the MU case all of which could be assumed to be the same without loss of generality. The covariance matrix of the interference-plus-noise is defined by $\mathbf{K} = \mathbb{E}[\mathbf{i}(n)\mathbf{i}(n)^{\dagger} + \mathbf{z}(n)\mathbf{z}(n)^{\dagger}] = \mathbf{I}_{M_{CR}} + \mathbf{H}_{\mathrm{PC}}\mathbf{H}_{\mathrm{PC}}^{\dagger}$ where we have assumed the PU TX(s) have channel $\mathbf{H}_{\mathrm{PC}}$ to the CR RX and transmit unit power uncorrelated signals. For the CR to PU interference channel, $\mathbf{H}_{\mathrm{INT}}$ (see Fig. 6.1), we assume $\mathbb{E}[|(\mathbf{H}_{\mathrm{INT}})_{ij}|^2] = 1/\lambda_i$ where $1/\lambda_i = \bar{\alpha}$ for the SU case and $1/\lambda_i = \bar{\alpha}^i,\ i = 1, \ldots, M_{PU}$ for the MU case. The constant $\bar{\alpha} \geq 0$ represents the strength of the dominant interference channel relative to the CR-CR channel and in the MU case it is assumed that the CR interference power decays exponentially across the PU receivers [94]. This simple model allows the signal strength of the M_{PU} interfering channels to be modeled with a single parameter, $\bar{\alpha}$. Perfect channel state information (CSI) ($\mathbf{H}_{\mathrm{CR}}$, $\mathbf{H}_{\mathrm{INT}}$ and $\mathbf{H}_{\mathrm{PC}}$) is assumed to be available at both the CR TX and CR RX for antenna selection purposes. We also assume that the

antennas are spatially uncorrelated. For satisfactory operation of the incumbent PU in the presence of the CR TX, the interference seen at the PU RX should not exceed a predefined threshold. This gives rise to two types of interference constraints depending on whether the PU is SU or MU. In the SU case, the interference constraint can be written as

$$\sum_{i=1}^{M_{PU}} \mathbf{H}_{\mathrm{INT}}(i,:)\mathbf{Q}_{\mathrm{CR}}\mathbf{H}_{\mathrm{INT}}(i,:)^{\dagger} \leq \Omega \;\Rightarrow \mathrm{Tr}(\mathbf{H}_{\mathrm{INT}}\mathbf{Q}_{\mathrm{CR}}\mathbf{H}_{\mathrm{INT}}^{\dagger}) \leq \Omega, \tag{6.2}$$

where $\mathbf{H}_{\mathrm{INT}}(i,:) \in \mathbb{C}^{1\times N_{CR}}$ represents the channel from the CR TX to the ith receive antenna of the PU RX and Ω is the maximum tolerable total interference power at the PU RX. For the MU case the interference constraint is given by

$$\mathbf{H}_{\mathrm{INT}}(i,:)\mathbf{Q}_{\mathrm{CR}}\mathbf{H}_{\mathrm{INT}}(i,:)^{\dagger} \leq \omega_i \quad i = 1, 2, \ldots, M_{PU}, \tag{6.3}$$

where ω_i is the interference constraint for the ith user. For notational convenience (6.3) is rewritten as $\mathrm{Diag}(\mathbf{H}_{\mathrm{INT}}\mathbf{Q}_{\mathrm{CR}}\mathbf{H}_{\mathrm{INT}}^{\dagger}) \leq (\omega_1, \ldots, \omega_{M_{PU}})$, where the inequality is to be interpreted elementwise.

6.2 Analytical Framework

With an aim to performing constrained joint transmit-receive antenna selection at the CR, we start with the well known fact that the achievable rates of the CR system using all antennas are [19]

$$R(\mathbf{H}_{\mathrm{CR}}, \mathbf{Q}_{\mathrm{CR}}) = \log_2 \det\big(\mathbf{I}_{M_{CR}} + \mathbf{H}_{\mathrm{CR}}\mathbf{Q}_{\mathrm{CR}}\mathbf{H}_{\mathrm{CR}}^{\dagger}\mathbf{K}^{-1}\big). \tag{6.4}$$

Similar to the approach of [95], we define diagonal selection matrices $\mathbf{S}_1, \mathbf{S}_2$ of dimension $M_{CR} \times M_{CR}$ and $N_{CR} \times N_{CR}$ respectively with binary diagonal entries. Specifically, we define their elements as

$$(\mathbf{S}_i)_{kk} = \begin{cases} 1 & \text{if the } k\text{th antenna element is selected} \\ 0 & \text{otherwise,} \end{cases} \tag{6.5}$$

where $i = 1, 2$. The diagonal entries of $\mathbf{S}_1, \mathbf{S}_2$ specify the indices of the antennas selected at the CR RX and CR TX respectively. Hence, if $m_{cr} \leq M_{CR}$ receive

antennas and $n_{cr} \leq N_{CR}$ transmit antennas are selected we obtain a new CR channel matrix $\bar{\mathbf{H}}_{\mathrm{CR}}$ with $M_{CR} - m_{cr}$ rows and $N_{CR} - n_{cr}$ columns in $\mathbf{H}_{\mathrm{CR}}$ replaced with zeros. The rate expression of (6.4) then reduces to

$$R(\bar{\mathbf{H}}_{\mathrm{CR}}, \bar{\mathbf{Q}}_{\mathrm{CR}}) = \log_2 \det\big(\mathbf{I}_{M_{CR}} + \bar{\mathbf{H}}_{\mathrm{CR}} \bar{\mathbf{Q}}_{\mathrm{CR}} \bar{\mathbf{H}}_{\mathrm{CR}}^{\dagger}\big) \tag{6.6}$$

where $\bar{\mathbf{H}}_{\mathrm{CR}} = \bar{\mathbf{K}}^{-1/2} \mathbf{S}_1 \mathbf{H}_{\mathrm{CR}} \mathbf{S}_2$ and we define $\bar{\mathbf{K}}$ and $\bar{\mathbf{Q}}_{\mathrm{CR}}$ as follows. The selection of receive antennas reduces interference and noise vector dimensions to $m_{cr} \leq M_{CR}$ resulting in interference and noise covariance matrix, $\mathbf{K}_{\mathrm{red}}$, of dimension $m_{cr} \times m_{cr}$. This matrix is inflated to form $\bar{\mathbf{K}}$, an $M_{CR} \times M_{CR}$ matrix, by adding rows and columns of zeros corresponding to the non-selected receive antennas. Similarly, a reduced $\mathbf{Q}_{\mathrm{red}}$ matrix ($n_{cr} \times n_{cr}$) is formed corresponding to the selected transmit antennas which is inflated to form $\bar{\mathbf{Q}}$ ($N_{CR} \times N_{CR}$) by inserting rows and columns of zeros corresponding to the unselected transmit antennas. Thus, the problem of joint transmit-receive antenna selection together with CR power allocation can be mathematically cast in the SU case as the constrained optimization problem **P1**, in the form

$$\begin{aligned}
\textbf{P1:} \underset{\mathbf{S}_1, \mathbf{S}_2, \mathbf{Q}_{\mathrm{CR}}}{\text{maximize}} \quad & \log_2 \det\big(\mathbf{I}_{M_{CR}} + \bar{\mathbf{K}}^{-1/2} \mathbf{S}_1 \mathbf{H}_{\mathrm{CR}} \mathbf{S}_2 \mathbf{Q}_{\mathrm{CR}} \mathbf{S}_2^{\dagger} \mathbf{H}_{\mathrm{CR}}^{\dagger} \mathbf{S}_1^{\dagger} \bar{\mathbf{K}}^{-1/2}\big) \\
\text{subject to} \quad & (\mathbf{S}_i)_{jj} \in \{1, 0\},\ j = 1, \ldots, M_{CR} \text{ if } i = 1 \\
& \text{and } j = 1, \ldots, N_{CR} \text{ if } i = 2 \\
& \mathrm{Tr}(\mathbf{Q}_{\mathrm{CR}}) \leq P_{CR}, \mathrm{Tr}(\mathbf{S}_1) = m_{cr}, \mathrm{Tr}(\mathbf{S}_2) = n_{cr} \\
& \mathrm{Tr}(\mathbf{H}_{\mathrm{INT}} \mathbf{S}_2 \mathbf{Q}_{\mathrm{CR}} \mathbf{S}_2^{\dagger} \mathbf{H}_{\mathrm{INT}}^{\dagger}) \leq \Omega, \quad \mathbf{Q}_{\mathrm{CR}} \succeq \mathbf{0}
\end{aligned}$$

Note that in **P1** we have slightly modified the interference constraint of (6.2) to represent the effective interference seen at the PU RX due to only the selected CR transmit antennas. We also note that $\bar{\mathbf{Q}}_{\mathrm{CR}}$ in (6.6) has been replaced by $\mathbf{Q}_{\mathrm{CR}}$ in **P1**. This can be done since the maximization in **P1** will not allocate any power to antennas that are not selected by $\mathbf{S}_2$. The problem can be written for the MU case by simply replacing the interference constraint with (6.3) and incorporating the column selection matrix $\mathbf{S}_2$. Furthermore, it is straightforward to extend **P1** to the case of multiple multi-antenna PU RXs. Assuming that the ith PU RX has the

interfering channel $\mathbf{H}_{\mathrm{INT},i}$ and constraint Ω_i, then the final constraint in **P1** can be written as $\mathrm{Tr}(\mathbf{H}_{\mathrm{INT},i}\mathbf{S}_2\mathbf{Q}_{\mathrm{CR}}\mathbf{S}_2^{\dagger}\mathbf{H}_{\mathrm{INT},i}^{\dagger}) \leq \Omega_i$. With this alteration, **P1** will handle the multiple multi-antenna PU case. Of course, as the number of PU RXs grows, the CR rates will usually fall. As a result, the CR will need to explore a range of time and frequency options in order to find channels in which coexistence at reasonable rates is achievable. In the log-determinant of **P1** it is important to note that the effect of the interference and noise covariance matrix is separated from the channel, $\mathbf{H}_{\mathrm{CR}}$, by the selection matrix, $\mathbf{S}_1$. In systems with a fixed number of antennas it is common to construct an equivalent channel which, in (6.4), would correspond to $\mathbf{K}^{-1/2}\mathbf{H}_{\mathrm{CR}}$. Then, the analysis proceeds simply by considering $\mathbf{K}^{-1/2}\mathbf{H}_{\mathrm{CR}}$ rather than $\mathbf{H}_{\mathrm{CR}}$. In our situation the interference and noise covariance matrix changes for every $\mathbf{S}_1$ and so we cannot select rows or columns of the equivalent channel. Instead, selection from $\mathbf{H}_{\mathrm{CR}}$ is performed first, followed by the use of the corresponding $\bar{\mathbf{K}}^{-1/2}$ and then we maximize the resultant expression subject to the constraints shown. This makes the problem more difficult as discussed in Sec. 6.2.2. To further clarify this subtle but important point, we illustrate with a toy example.

Suppose, we have a 2×1 single-input multiple-output (SIMO) system from which we wish to obtain the best SISO link. We assume the link gains to the first and second RX antennas are 1 and 2, respectively. Furthermore, we arbitrarily take the channel coefficients at the first and the second RX antennas to be 0.55 and -2, respectively. With this data, SINR at the first antenna (assuming unit variance noise at both RXs) is 0.7678 and at the second antenna it is found be 0.8 (both in absolute scale). Clearly, we should choose the second antenna. If instead we consider the equivalent channel method, then we need $\mathbf{K}$ which is found to be $\begin{pmatrix} 1.3025 & -1.1 \\ -1.1 & 5 \end{pmatrix}$. This results in equivalent channel $\mathbf{K}^{-1/2}\begin{pmatrix} 1 \\ 2 \end{pmatrix} = \begin{pmatrix} 1.2495 \\ 1.0927 \end{pmatrix}$, which indicates the first antenna should be selected. It is evident from the direct and interfering link gains used in the setup that this will be the incorrect choice. Therefore, selecting antennas on the basis of the equivalent channel rather than assessing the effect of interference

on the selected antennas, can lead to different results and a lower achievable rate.

6.2.1 Exhaustive Search

A straightforward way to solve **P1** is to perform an exhaustive search (ES) over all possible combinations of antenna elements and to only optimize over $\mathbf{Q}_{\mathrm{CR}}$. Hence, ES amounts to optimizing $\mathbf{Q}_{\mathrm{CR}}$, $\binom{N_{CR}}{n_{cr}} \times \binom{M_{CR}}{m_{cr}}$ times subject to interference and total transmit power constraints. Each optimization over $\mathbf{Q}_{\mathrm{CR}}$ is a convex problem that can be efficiently solved in polynomial time using interior-point methods [36]. However, the need to iterate over all possible combinations gives a complexity which explodes for higher dimensional systems. Throughout the paper we obtain numerical solutions to the optimization problems using the `cvx` software package [46].

6.2.2 Convex Approximation

Overall, problem **P1** is highly non-convex and can be classified as an example of an *integer programming* problem, since two of the variables $\mathbf{S}_1$ and $\mathbf{S}_2$ are binary [37]. The non-convexity of the problem arises due to the nature of the objective function, interference and the binary constraints. Furthermore, the binary variables in $\mathbf{S}_1$ and $\mathbf{S}_2$ render the problem NP-hard [95]. In order to produce a more computationally efficient approach we modify the problem in the following ways. Firstly, the binary structure of $\mathbf{S}_1$ and $\mathbf{S}_2$ can be relaxed so that the antenna selection variables take on values in the interval 0 to 1. This makes the problem far easier to solve than the original integer program [36]. In addition to this, we transform the interference constraint in **P1** from being applicable only over the selected transmit antennas to apply to all CR transmit antennas. This yields a simpler constraint for optimization and also corresponds to the relaxation approach where the selection matrices are fractional rather than binary. Finally, we note that in this approach the effect of the $\mathbf{K}$ matrix cannot be included as it makes the objective non-concave (explained below) and $\mathbf{Q}_{\mathrm{CR}}$ is restricted to being a diagonal power allocation matrix. These limitations are discussed below. With these changes, **P1** can be rewritten as the

new problem **P2**:

$$\begin{aligned}\mathbf{P2:}\ \underset{\mathbf{S}_1,\mathbf{S}_2,\mathbf{Q}_{\mathrm{CR}}(\text{diagonal})}{\text{maximize}} \quad & \log_2 \det\big(\mathbf{I}_{M_{CR}} + \mathbf{S}_1\mathbf{H}_{\mathrm{CR}}\mathbf{S}_2\mathbf{Q}_{\mathrm{CR}}\mathbf{S}_2^{\dagger}\mathbf{H}_{\mathrm{CR}}^{\dagger}\mathbf{S}_1^{\dagger}\big) \\ \text{subject to} \quad & 0 \leq (\mathbf{S}_i)_{jj} \leq 1,\ j = 1,\ldots,M_{CR} \text{ if } i = 1 \\ & \text{and } j = 1,\ldots,N_{CR} \text{ if } i = 2 \\ & \mathrm{Tr}(\mathbf{Q}_{\mathrm{CR}}) \leq P_{CR}, \mathrm{Tr}(\mathbf{S}_1) = m_{cr}, \mathrm{Tr}(\mathbf{S}_2) = n_{cr} \\ & \mathrm{Tr}(\mathbf{H}_{\mathrm{INT}}\mathbf{Q}_{\mathrm{CR}}\mathbf{H}_{\mathrm{INT}}^{\dagger}) \leq \Omega, \quad \mathbf{Q}_{\mathrm{CR}} \succeq \mathbf{0}\end{aligned}$$

We note that the optimization problem **P2** is still not convex (as the objective function is not concave). We now seek a convex approximation (CA) to enable a solution to this problem. It can be shown that with two of the three variables known, the cost function is concave in the third one and this renders the problem convex in this variable. For example, with $\mathbf{S}_1$ and $\mathbf{Q}_{\mathrm{CR}}$ known the cost function is concave in $\mathbf{S}_2$ where we rely on a diagonal $\mathbf{Q}_{\mathrm{CR}}$ so that $\mathbf{S_2}\mathbf{Q}_{\mathrm{CR}}\mathbf{S_2}^{\dagger} = \mathbf{U}_{\mathrm{CR}}\mathbf{S_2}\mathbf{U}_{\mathrm{CR}}$, where $\mathbf{U}_{\mathrm{CR}} = (\mathbf{Q}_{\mathrm{CR}})^{1/2}$ and the objective function becomes $\log_2 \det\big(\mathbf{I}_{M_{CR}} + \mathbf{S}_1\mathbf{H}_{\mathrm{CR}}\mathbf{U}_{\mathrm{CR}}\mathbf{S_2}\mathbf{U}_{\mathrm{CR}}\mathbf{H}_{\mathrm{CR}}^{\dagger}\mathbf{S}_1^{\dagger}\big)$. Similarly, with $\mathbf{S}_2$ and $\mathbf{Q}_{\mathrm{CR}}$ known, the determinant in the objective function can be written as a concave function in $\mathbf{S}_1$, $\det(\mathbf{I}_{N_{CR}} + \mathbf{S}_2^{\dagger}\mathbf{H}_{\mathrm{CR}}^{\dagger}\mathbf{S}_1\mathbf{H}_{\mathrm{CR}}\mathbf{S}_2)$, which yields a convex problem in $\mathbf{S}_1$. Note that the problem cannot be made convex in $\mathbf{S}_1$ if $\mathbf{K}$ is also included in the argument of the cost function. Furthermore, the physical geometry of the system can prevent the PUs' signals from interfering with the CR RX. Finally, the log-determinant in **P1** already provides a convex problem in $\mathbf{Q}_{\mathrm{CR}}$. Thus to solve **P2**, we initialize $\mathbf{S}_1$ and $\mathbf{Q}_{\mathrm{CR}}$ and optimize over $\mathbf{S}_2$. After obtaining $\mathbf{S}_2$, we optimize over $\mathbf{S}_1$ and then, with $\mathbf{S}_2$ and $\mathbf{S}_1$ known, we obtain the optimized value of $\mathbf{Q}_{\mathrm{CR}}$. This procedure is repeated until the achieved rate stabilizes. The indices of the receive and transmit antennas to be selected are then obtained by choosing the largest m_{cr} and n_{cr} diagonal entries of $\mathbf{S}_1$ and $\mathbf{S}_2$, respectively. After rounding the possibly fractional diagonal entries of $\mathbf{S}_1$ and $\mathbf{S}_2$ to binary (0 or 1) values, we again optimize over $\mathbf{Q}_{\mathrm{CR}}$. This optimization involves the original interference constraint of **P1** over the selected CR transmit antennas.

A comment on the convergence of the proposed iterative algorithm is in order. Using a similar approach to [96], we argue that during the $(k+1)$st iteration

we calculate $\mathbf{S}_2^{k+1} = \text{argmax}_{\mathbf{S}_2}\mathbf{P2}(\mathbf{S}_1^k, \mathbf{Q}_{\text{CR}}^k, \mathbf{S}_2)$ and obtain data rate a. Then we calculate $\mathbf{S}_1^{k+1} = \text{argmax}_{\mathbf{S}_1}\mathbf{P2}(\mathbf{S}_1, \mathbf{Q}_{\text{CR}}^k, \mathbf{S}_2^{k+1})$ giving rate b. Finally, we evaluate $\mathbf{Q}_{\text{CR}}^{k+1} = \text{argmax}_{\mathbf{Q}_{\text{CR}}}\mathbf{P2}(\mathbf{S}_1^{k+1}, \mathbf{Q}_{\text{CR}}, \mathbf{S}_2^{k+1})$ and the corresponding data rate c. Since $a \leq b \leq c$ forms a monotonically increasing sequence which is bounded above (due to input power constraints) we conclude that the sequence of data rates converges to a limit. Our simulations indicate that iterating 6 times for the SU case (and $8-10$ times for the MU case) is almost always sufficient to attain a value of **P2** that is almost identical to the brute force optimum solution. Since the problem is not convex in nature, the maximum CR rates obtained from **P2** may not be globally optimum. However, our results suggest that the values obtained are robust and are globally optimal (arbitrarily close) most of the time for the parameters and scenarios discussed in Sec. 6.4.

6.2.3 Heuristic

From the above discussion it is evident that apart from being cumbersome, the CA approach suffers from various drawbacks. For example, complexity depends on the efficiency of the convex optimizer and the number of iterations needed to reach the optimal point. Also, the approach cannot be used with a full $\mathbf{Q}_{\text{CR}}$ matrix or in the presence of interference. To overcome these problems, we propose a heuristic involving norm-based transmit and receive antenna selection [90, 91, 92]. Norm based selection for i.i.d. channels with no interference constraints is straightforward and involves selecting the rows and columns of the channel matrix with the largest norms. In our situation the interference constraint prescribes different allowable powers for each transmit antenna and the interference plus noise covariance matrix results in different correlation values for different receive antenna selections. Hence, selection at both TX and RX is more complex and any approach must handle these difficulties. At the RX end we proceed by selecting the rows of $\mathbf{K}^{-1/2}\mathbf{H}_{\text{CR}}$ with the highest norm. This approximates the effect of $\bar{\mathbf{K}}$ without the need to cycle through the possible RX antenna selections. At the TX end the total transmit

power is limited to P_{CR} with no constraints on each antenna. In the heuristic it is simpler to assume that the maximum available transmit power from any CR TX antenna is bounded by P_{CR}. The idea behind the per-antenna power constraint is that antenna A is likely to be more effective than antenna B if, when they are both allocated maximum power, antenna A has a higher norm under interference constraints. The power inflation intrinsic to this approach is not a problem since we are only ranking antennas at this stage. After selection the correct power allocation is performed via the $\mathbf{Q}_{\mathrm{CR}}$ matrix. The algorithm described below deals with the MU case, and assumes that $\omega_1 = \ldots = \omega_{M_{PU}} = \omega$ for all M_{PU} single antenna PUs. The heuristic is given by:

1. Calculate $P_j = \min\left\{P_{CR}, \min_i\left\{\frac{\omega}{|(\mathbf{H}_{\mathrm{INT}})_{ij}|^2}\right\}\right\}$, where $j = 1, 2, \ldots, N_{CR}$, $i = 1, 2, \ldots, M_{PU}$.

2. Evaluate $\widetilde{\mathbf{H}} = \mathbf{K}^{-1/2}\mathbf{H}_{\mathrm{CR}}\mathrm{diag}([\sqrt{P_1}, \ldots, \sqrt{P_{N_{CR}}}], 0)$.

3. Find the column norms of $\widetilde{\mathbf{H}}$, i.e., $||\widetilde{\mathbf{H}}(:, j)||_2^2$, $j = 1, 2, \ldots, N_{CR}$.

4. Obtain the matrix $\widetilde{\mathbf{H}}_{\mathrm{COL}}$ by keeping the n_{cr} columns with the highest norms and setting the remaining $N_{CR} - n_{cr}$ columns of $\widetilde{\mathbf{H}}$ equal to zero. This gives $\mathbf{S}_2$.

5. Determine the top m_{cr} rows of $\widetilde{\mathbf{H}}_{\mathrm{COL}}$ on the basis of the row norms, $||\widetilde{\mathbf{H}}_{\mathrm{COL}}(k, :)||_2^2$, $k = 1, 2, \ldots, M_{CR}$. This gives $\mathbf{S}_1$.

6. With the final selection, $\mathbf{S}_1$ and $\mathbf{S}_2$, optimize the achievable rate over $\mathbf{Q}_{\mathrm{CR}}$ subject to $\mathrm{Diag}(\mathbf{H}_{\mathrm{INT}}\mathbf{S}_2\mathbf{Q}_{\mathrm{CR}}\mathbf{S}_2^{\dagger}\mathbf{H}_{\mathrm{INT}}^{\dagger}) \leq (\omega, \ldots, \omega)$ and the total transmit power constraint.

It is worth noting that the above heuristic can be optimized with a full $\mathbf{Q}_{\mathrm{CR}}$ matrix and is not restricted to a diagonal form as in the CA approach. To extend the heuristic to the SU case or the multiple multi-antenna PU case, only steps 1) and 6) need to be altered. To arrive at the most general scenario of multiple multi-antenna

PUs, we see that P_j in 1) should be changed to

$$P_j = \min\left\{P_{CR}, \min_i\left\{\frac{\Omega_i}{||(\mathbf{H}_{\text{INT},i}(:,j))||_2^2}\right\}\right\}, \quad j = 1, 2, \ldots, N_{CR},\ i = 1, 2, \ldots, M_{PU}, \tag{6.7}$$

where $\mathbf{H}_{\text{INT},i}(:,j)$ represents the jth column of the channel matrix to the ith PU RX. Similarly, as indicated in Sec. III, the interference constraints in step 6) should be modified to $\text{Tr}(\mathbf{H}_{\text{INT},i}\mathbf{S}_2\mathbf{Q}_{\text{CR}}\mathbf{S}_2^\dagger\mathbf{H}_{\text{INT},i}^\dagger) \leq \Omega_i$. The heuristic is an extension of the simple norm-based criteria [90, 91, 92] with interference constraints added. We stress that the per antenna power-constraint is not real but is used to avoid iteration over the antenna power allocation. This makes the heuristic able to select antennas based solely on row and column norms which is much faster to compute and the excellent results shown in Sec. 6.4 justify the use of this *ad hoc* approach.

6.2.4 A Note on Complexity

In order to compare the computational benefits of the CA and the heuristic approaches, we will investigate the worst case complexity of the three techniques. Roughly speaking, the worst case complexity (i.e., the number of iterations) of a generic convex optimization problem to obtain an ϵ accurate solution using interior point methods is $\mathcal{O}(\sqrt{\eta}\ln\epsilon^{-1})$, where η represents a measure of the problem size [47]. Since the brute force ES requires $\binom{N_{CR}}{n_{cr}} \times \binom{M_{CR}}{m_{cr}} \in \mathcal{O}(N_{CR}^{n_{cr}} M_{CR}^{m_{cr}}) \triangleq \kappa_1$ optimizations over $\mathbf{Q}_{\text{CR}}$, we can characterize its complexity as $\mathcal{O}(\kappa_1 \times \sqrt{\eta}\ln\epsilon^{-1})$. We mention that $\binom{n}{r} = \frac{n!}{(n-r)!k!}$. It must be emphasized here that κ_1 determines η (either in the form of greater dimensions of the MIMO CR system or the subset of antennas to be chosen), thereby, resulting in a drastic increase in the computational complexity of the ES approach. Compared with this, if we assume that in the worst case the CA approach needs n iterations to achieve stable CR rates, we can conclude that its worst case complexity is $\mathcal{O}(n \times \sqrt{\eta_{max}}\ln\epsilon^{-1})$, where η_{max} corresponds to the greatest size measure in the alternating sequence of optimization problems of the CA approach. It is clear that, unlike the ES case, n *does not* affect the problem size and hence, there is a big improvement in the worst case complexity. Finally,

in the heuristic, if we assume that all operations in step-1 to step-5 take constant time (this assumption is reasonable as these operations do not involve any iterative calculation), the worst case complexity is only $\mathcal{O}(\sqrt{\eta_0}\ln\epsilon^{-1})$, where η_0 is approximately the same as η of the ES method. Clearly, this suggests a huge improvement over previous cases. To give an idea of the number of iterations required, selecting the best $(4,4)$ system from an $(8,8)$ system requires 4900 optimizations over $\mathbf{Q}_{\mathrm{CR}}$ for the ES method, whereas the heuristic only requires 1.

6.3 Performance Analysis

A general performance analysis of the MIMO CR system with antenna selection is highly complex, and thus, we concentrate on specific cases for which analytical results are possible. In particular, we first derive the CDF of the SNR with single link (or SISO) selection via an exhaustive search in the presence of M_{PU} PUs. In this section we neglect the interference which may be caused by the PU TXs at the CR RX. Later, we explore the possibilities of extending the analysis to include the effect of multiple PUs that follow a spatial Poisson distribution.

6.3.1 CDF of CR-CR Link with Single Antenna Selection in the Presence of Multiple Single Antenna PUs

Throughout this section for notational ease, we use h_{ij} and $\tilde{h}_{ij}$ to denote the entries of $\mathbf{H}_{\mathrm{CR}}$ and $\mathbf{H}_{\mathrm{INT}}$, respectively. Using the system model in Sec. 6.1 it follows that all $|h_{ij}|^2$ are exponentially distributed with unit mean and the $|\tilde{h}_{ij}|^2$ are also exponentially distributed having means $1/\lambda_i, i = 1,\ldots,M_{PU}$. In addition to this, we suppose that the SNR from each of the CR TX antennas to the PU RXs is given by $\mathrm{SNR}_{PU_i} = 1/\lambda_i = \bar{\alpha}^i, i = 1 \ldots M_{PU}$. This assumption is not necessary and any model can be used for the SNR_{PU_i} values. However, this assumption requires no additional parameters and is reasonable in the sense that it models similar strengths for the channels between CR TX and PU RX and PU TX and CR RX, a type of

symmetry. With this setup, the power of the individual transmitting antennas is given by:

$$\begin{aligned} P_j &= \min\left\{P_{CR}, \frac{\omega}{\max\limits_i\{|\tilde{h}_{ij}|^2\}}\right\} \\ &= \min\left\{P_{CR}, \min_i\left\{\frac{\omega}{|\tilde{h}_{ij}|^2}\right\}\right\}, \qquad j = 1\ldots N_{CR}, i = 1\ldots M_{PU}, \end{aligned} \tag{6.8}$$

where, as before, P_{CR} represents the total power limit (now allocated to an individual antenna) and we have assumed that $\omega_1 = \omega_2 = \ldots = \omega$. By performing an exhaustive search for the best SISO link in the presence of M_{PU} single antenna PUs and with the power of the TX given in (6.8), we have $Y = \max_{i,j} P_j|h_{ij}|^2$ as the SNR of this link. Performance analysis of this optimum SISO selection follows from the CDF of Y defined by:

$$\begin{aligned} F_Y(y) &= P(\max_{i,j} P_j|h_{ij}|^2 \leq y) \\ &= \mathbb{E}[P(|h_{ij}|^2 \leq \frac{y}{P_j}\forall i,j|P_1,P_2,\ldots,P_{N_{CR}})] \\ &= \mathbb{E}\Big[\prod_{i,j}(1-e^{-y/P_j})\Big] \\ &= \prod_{j=1}^{N_{CR}}\mathbb{E}\big[(1-e^{-y/P_j})^{M_{CR}}\big] \\ &= \big[\mathbb{E}\big[(1-e^{-y/P_j})^{M_{CR}}\big]\big]^{N_{CR}} \\ &= \Bigg[\sum_{n=0}^{M_{CR}}\binom{M_{CR}}{n}(-1)^n\mathbb{E}\big[e^{-ny/P_j}\big]\Bigg]^{N_{CR}}, \end{aligned} \tag{6.9}$$

where $\binom{M_{CR}}{n} = \frac{M_{CR}!}{(M_{CR}-n)!n!}$. Before evaluating the inner expectation in the last equality above, let us determine the CDF and probability density function (PDF) of $Z = \max_i(|\tilde{h}_{ij}|^2)$. The CDF is given by:

$$F_Z(z) = P(Z \leq z) = P(|\tilde{h}_{ij}|^2 \leq z, \forall i) = \prod_{i=1}^{M_{PU}}(1-e^{-\lambda_i z}). \tag{6.10}$$

Thus, the PDF of Z is obtained as

$$f_Z(z) = dF_Z(z)/dz = \sum_{i=1}^{M_{PU}}\lambda_i e^{-\lambda_i z}\prod_{k\neq i}(1-e^{-\lambda_k z}). \tag{6.11}$$

We note from (6.8) that $P_j = P_{CR}$ when $Z < \omega/P_{CR}$ and $P_j = \omega/Z$ otherwise. Now consider the expectation in (6.9) as,

$$\begin{aligned}\mathbb{E}[e^{-ny/P_j}] &= \int_0^{\omega/P_{CR}} e^{\frac{-ny}{P_{CR}}} f_Z(z)dz + \int_{\omega/P_{CR}}^{\infty} e^{-nyz/\omega} f_Z(z)dz \\ &= e^{\frac{-ny}{P_{CR}}} F_Z\left(\frac{\omega}{P_{CR}}\right) + \sum_{i=1}^{M_{PU}} \lambda_i \int_{\omega/P_{CR}}^{\infty} e^{-(\lambda_i + \frac{ny}{\omega})z} \prod_{k\neq i}(1 - e^{-\lambda_k z})dz,\end{aligned} \tag{6.12}$$

where $F_Z(z)$ is given in (6.10). It is easy to see that the product term in (6.12) can be rewritten as,

$$\prod_{k\neq i}\left(1 - e^{-\lambda_k z}\right) = \sum_{r=0}^{M_{PU}-1} (-1)^r \sum_{\mathbf{s}(r)} \exp\left\{ -\left(\sum_{q=1}^{r} \lambda_{\mathbf{s}_q}\right) z \right\}. \tag{6.13}$$

where the summation over $\mathbf{s}(r)$ is over all $\binom{M_{PU}-1}{r}$ ways of selecting r integers from $1, 2, \ldots M_{PU}$ with each of the integers not equal to i. By defining $\Gamma_{\mathbf{s}(r)} \triangleq \sum_{q=1}^{r} \lambda_{\mathbf{s}_q}$, the integral in (6.12) is simplified to

$$\begin{aligned}\mathbb{E}[e^{-ny/P_j}] &= e^{\frac{-ny}{P_{CR}}} F_Z\left(\frac{\omega}{P_{CR}}\right) + \sum_{i=1}^{M_{PU}} \lambda_i \sum_{r=0}^{M_{PU}-1} (-1)^r \sum_{\Gamma_{\mathbf{s}(r)}} \int_{\omega/P_{CR}}^{\infty} e^{-\left(\lambda_i + \frac{ny}{\omega} + \Gamma_{\mathbf{s}(r)}\right) z} dz \\ &= e^{\frac{-ny}{P_{CR}}} F_Z\left(\frac{\omega}{P_{CR}}\right) + \sum_{i=1}^{M_{PU}} \lambda_i \sum_{r=0}^{M_{PU}-1} (-1)^r \sum_{\Gamma_{\mathbf{s}(r)}} \frac{e^{-\left(\lambda_i + \frac{ny}{\omega} + \Gamma_{\mathbf{s}(r)}\right)\omega/P_{CR}}}{\lambda_i + \frac{ny}{\omega} + \Gamma_{\mathbf{s}(r)}}.\end{aligned} \tag{6.14}$$

Substituting (6.14) in (6.9), the final expression for $F_Y(y)$ is given by:

$$\begin{aligned}F_Y(y) = \Bigg[\Bigg\{ \sum_{n=0}^{M_{CR}} \binom{M_{CR}}{n} (-1)^n \Bigg\{ e^{\frac{-ny}{P_{CR}}} F_Z\left(\frac{\omega}{P_{CR}}\right) \\ + \sum_{i=1}^{M_{PU}} \lambda_i \sum_{r=0}^{M_{PU}-1} (-1)^r \sum_{\Gamma_{\mathbf{s}(r)}} \frac{e^{-\left(\lambda_i + \frac{ny}{\omega} + \Gamma_{\mathbf{s}(r)}\right)\omega/P_{CR}}}{\lambda_i + \frac{ny}{\omega} + \Gamma_{\mathbf{s}(r)}} \Bigg\} \Bigg]^{N_{CR}}.\end{aligned} \tag{6.15}$$

Hence, (6.15) provides a closed form SNR CDF for the optimal SISO link selected from the MIMO CR with PU power constraints. This also gives the exact CDF for the optimal SISO capacity. Ergodic capacities are more difficult to compute and are discussed below.

6.3.2 Ergodic Capacities

The evaluation of ergodic capacity even for the case of single antenna selection with PU power constraints is very cumbersome involving products of several numerical integrals. Thus, we leave this and the general case as open problems. However, some insights and useful benchmarks can be obtained from various special cases of interest obtained from (6.15).

SISO System with No PU

Since there is no PU, the single CR antenna uses maximum power, P_{CR}, and the ergodic capacity is

$$\mathbb{E}(C) = \mathbb{E}[\log_2(1 + P_{CR}|h_{11}|^2)], \tag{6.16}$$

where h_{11} is the channel coefficient of the link assuming $\mathcal{CN}(0, 1)$. Hence, from [97], we have

$$\mathbb{E}(C) = \frac{1}{\ln 2} \exp(1/P_{CR}) E_1(1/P_{CR}), \tag{6.17}$$

where $E_1(x) = \int_1^\infty t^{-1} e^{-xt} dt$ represents the standard exponential integral.

SISO System with a Single PU

The CDF of the SNR of a SISO system in the presence of a single PU can be deduced from (6.15) by substituting $M_{CR} = N_{CR} = M_{PU} = 1$. This gives:

$$F_Y(y) = 1 - \exp\left(\frac{-y}{P_{CR}}\right) + \frac{y}{y + \omega\lambda_1} \exp\left(-\frac{y + \omega\lambda_1}{P_{CR}}\right), \qquad y \geq 0 \tag{6.18}$$

where λ_1 is the reciprocal of the mean of the channel response to the sole PU RX. As expected, the presence of a PU incurs a net loss in the CDF of SNR given by the third term in (6.18). Note that the third term disappears as $\lambda_1 \to \infty$ which is the case of no PU. Hence, the outage probability, $\mathbb{P}(Y \leq y)$ is increased by $y(y + \omega\lambda_1)^{-1} \exp(-(y + \omega\lambda_1)/P_{CR})$ in the presence of a PU. The ergodic capacity

in this case is given by,

$$\mathbb{E}(C) \overset{(a)}{=} \frac{1}{\ln 2}\Bigg\{\int_0^{\infty}\Bigg(\frac{e^{\left(-\frac{y}{P_{CR}}\right)}}{1+y} - \frac{ye^{\left(\frac{-y+\omega\lambda_1}{P_{CR}}\right)}}{(y+\omega\lambda_1)(1+y)}\Bigg)dy\Bigg\}$$
$$= \frac{1}{\ln 2}\Bigg\{e^{\left(\frac{1}{P_{CR}}\right)}E_1\left(\frac{1}{P_{CR}}\right) - Ae^{\left(\frac{-\omega\lambda_1+1}{P_{CR}}\right)}E_1\left(\frac{1}{P_{CR}}\right) - BE_1\left(\frac{\omega\lambda_1}{P_{CR}}\right)\Bigg\}, \quad (6.19)$$

where A and B are coefficients obtained by performing a partial fraction expansion of $y/(y+\omega\lambda_1)(1+y)$ in (a) with $A = 1/(1-\omega\lambda_1)$ and $B = -\omega\lambda_1/(1-\omega\lambda_1)$. Comparing (6.19) and (6.17) we observe that capacity is reduced by $\frac{1}{\ln 2}\big\{Ae^{\left(\frac{-\omega\lambda_1+1}{P_{CR}}\right)}E_1\big(\frac{1}{P_{CR}}\big)+ BE_1\big(\frac{\omega\lambda_1}{P_{CR}}\big)\big\}$ in the presence of a PU. The rate and the capacity losses depend on P_{CR} and $\omega\lambda_1$ and for fixed transmit power the losses are decreasing functions of $\omega\lambda_1$.

MIMO Single Link Selection with No PU

As a special case of (6.15), using $M_{PU} = 0$, it is easy to verify that for a MIMO link with no PU RXs to protect, the CDF of the direct link SNR is given by,

$$F_Y(y) = (1 - \exp(-y/P_{CR}))^{M_{CR}N_{CR}}. \quad (6.20)$$

Differentiating (6.20) gives the corresponding PDF as:

$$f_Y(y) = \frac{M_{CR}N_{CR}}{P_{CR}}(1 - e^{\left(\frac{-y}{P_{CR}}\right)})^{M_{CR}N_{CR}-1}e^{\left(\frac{-y}{P_{CR}}\right)}$$
$$= \frac{M_{CR}N_{CR}}{P_{CR}}\sum_{q=0}^{M_{CR}N_{CR}-1}\binom{M_{CR}N_{CR}-1}{q}(-1)^q e^{\left(\frac{-y(q+1)}{P_{CR}}\right)}. \quad (6.21)$$

With the PDF given in (6.21), the computation of ergodic capacity requires the integral,

$$\int_0^{\infty}\ln(1+y)e^{\left(\frac{-(q+1)y}{P_{CR}}\right)}dy = \frac{P_{CR}}{(1+q)}\int_0^{\infty}\frac{e^{\frac{-(q+1)y}{P_{CR}}}}{1+y}dy = \frac{P_{CR}}{(1+q)}E_1\left(\frac{(q+1)}{P_{CR}}\right)e^{\frac{(q+1)}{P_{CR}}}. \quad (6.22)$$

Thus, the final expression for ergodic capacity in this case is,

$$\mathbb{E}(C) = \frac{M_{CR}N_{CR}}{P_{CR}\ln 2}\sum_{q=0}^{M_{CR}N_{CR}-1}\binom{M_{CR}N_{CR}-1}{q}(-1)^q\frac{e^{((q+1)/P_{CR})}}{(q+1)/P_{CR}}E_1\left(\frac{(q+1)}{P_{CR}}\right), \quad (6.23)$$

which provides an upper bound on system performance in the presence of PUs. We note that throughout $E_1(.)$ represents the exponential integral defined after (6.17). Following a similar approach for the ergodic capacity in the MIMO single link selection case even in the presence of a single PU is very involved. Thus, we leave this and the general scenario as an open problem for future research.

6.3.3 Extension to More Realistic Scenarios

In Secs. 6.3.1 and 6.3.2 we analyzed single link selection in the context of a CR link of unit power and multiple interference paths of strength $\bar{\alpha}^i, i = 1, 2, \ldots, M_{PU}$. In this section we consider more realistic models for both the CR link and the CR-PU interference links. In particular, we consider shadowing, path loss effects and a random number of PUs. This allows us to investigate whether the broad trends and conclusions generated from the simple models remain valid for more realistic system models. Due to the extra complexity, we resort to a simulation study.

Using similar models to those utilized in Chapters 3 and 5, we consider a CR TX located at the origin. The corresponding CR RX is uniformly located in an annulus centered on the origin with inner radius, R_0, and outer radius r_{cr}. The inner radius is created to avoid the CR link becoming too short which creates problems with the inverse power relationship between link strength and distance [10]. The received power of the CR-CR link is modeled in the classical way as

$$P = A10^{X/10} r^{-\gamma}, \tag{6.24}$$

where A is a constant whose value can be determined using the methods discussed in Chapters 3 and 5, $X \sim \mathcal{N}(0, \sigma^2)$ provides the lognormal shadowing with standard deviation σ (dB), r is the link distance and γ is the path loss exponent. The link also experiences i.i.d. Rayleigh fading so that the channel gain between transmit antenna, j, and receive antenna, i, is given by $\sqrt{P}h_{ij}$ where $h_{ij} \sim \mathcal{CN}(0, 1)$. Assuming the noise power at the receive antennas as unity, P becomes the link SNR.

For the PUs, we assume a Poisson field of receivers [98] with intensity, θ, located in an annulus centered on the origin of inner radius, R_0, and outer radius, $R > r_{cr}$.

Hence, the number of PU RXs, N, is a Poisson variable with $\mathbb{E}(N) = \theta\pi(R^2 - R_0^2)$ and the RXs are uniformly located in the annulus. For the interference created by the CR at the PU RXs we use the same model as (6.24) so that the instantaneous interference-to-noise ratio (INR) at RX i due to transmit antenna antenna j is

$$P|\tilde{h}_{ij}|^2 = A10^{X_i/10} r_i^{-\gamma} |\tilde{h}_{ij}|^2, \tag{6.25}$$

where we have assumed unit noise power at the PU RXs. With models (6.24) and (6.25) defined, the scaling parameter A is proportional to the maximum transmit power. Hence, any power back off by the CR TX to satisfy interference constraints can be achieved by multiplying A by a factor $f_j \in [0, 1]$ for antenna j. With this notation, the single link selection problem becomes

$$P_j = f_j P, \tag{6.26}$$

where $f_j = \min_i\{1, \omega/P|\tilde{h}_{ij}|^2\}$ and the resulting link selection has SNR given by $Y = \max_{i,j} P_j|h_{ij}|^2$. Simulation results based on this approach are given in Sec. 6.4.

6.4 Results

6.4.1 MIMO Selection

In this section we explain the simulation results based on the ES, CA and the heuristic proposed in Sec. 6.2. However, before we describe the results, we introduce the parameter β which controls the interference threshold (Ω for the SU case and ω_j, $j = 1, \ldots, M_{PU}$ for the MU case) at the PU RX. β is chosen so that the allowable interference at the PU is a fraction of the PU SNR, i.e., Ω or $\omega_j = \beta \mathrm{SNR}_{\mathrm{PU}}$ at the PU RX(s). To compare the different approaches we use the measures of ergodic rates and the CDF of the achievable rates. The CDF curves and each point on the ergodic rate graphs are determined by averaging over the results obtained from 500 i.i.d. channel realizations. For the SU case we consider a single MIMO PU RX equipped with 3 antennas and for the MU case we take three PUs each having a single

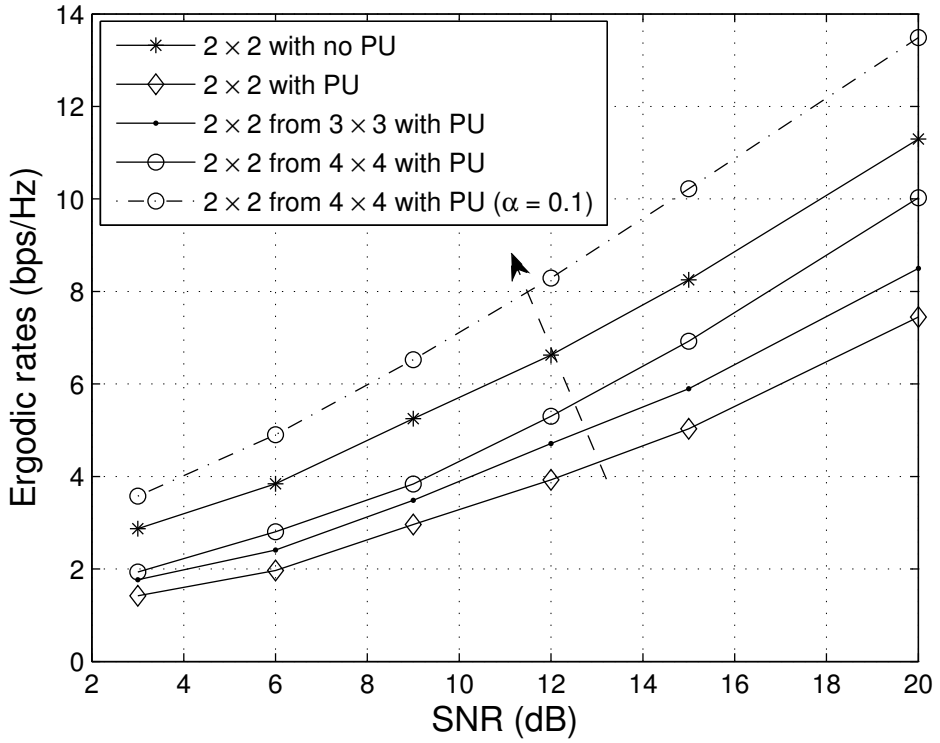

Figure 6.2: Ergodic rates vs SNR for different system sizes. These curves are based on the CA approach for the SU case. For all curves (except the one indicated in the figure) we take $\bar{\alpha} = 0.5$ and $\beta = 0.1$.

antenna (Fig. 6.1). The results shown focus on the rate gains offered by selection, the effects of diagonal $\mathbf{Q}_{\mathrm{CR}}$ (important in the CA approach) and a comparison of the techniques.

In Fig. 6.2 we demonstrate that (n_{cr}, m_{cr}) antenna selection from larger (N_{CR}, M_{CR}) systems can enhance the ergodic rates to reach and go beyond the benchmark performance of an (n_{cr}, m_{cr}) system without any PU interference constraints. These graphs are based on the SU case and are obtained using the CA approach for diagonal $\mathbf{Q}_{\mathrm{CR}}$. In particular, we see that if we select the best $(2, 2)$ antenna subsystem (according to **P2**) from $(3, 3)$ and then from $(4, 4)$ MIMO channel matrices, we are able to close the gap between the ergodic curves for these systems and the results for the benchmark $(2, 2)$ MIMO system without any PU. These results are for $\bar{\alpha} = 0.5$ and $\beta = 0.1$. Further, if the strength of the CR-PU interference channel is lowered

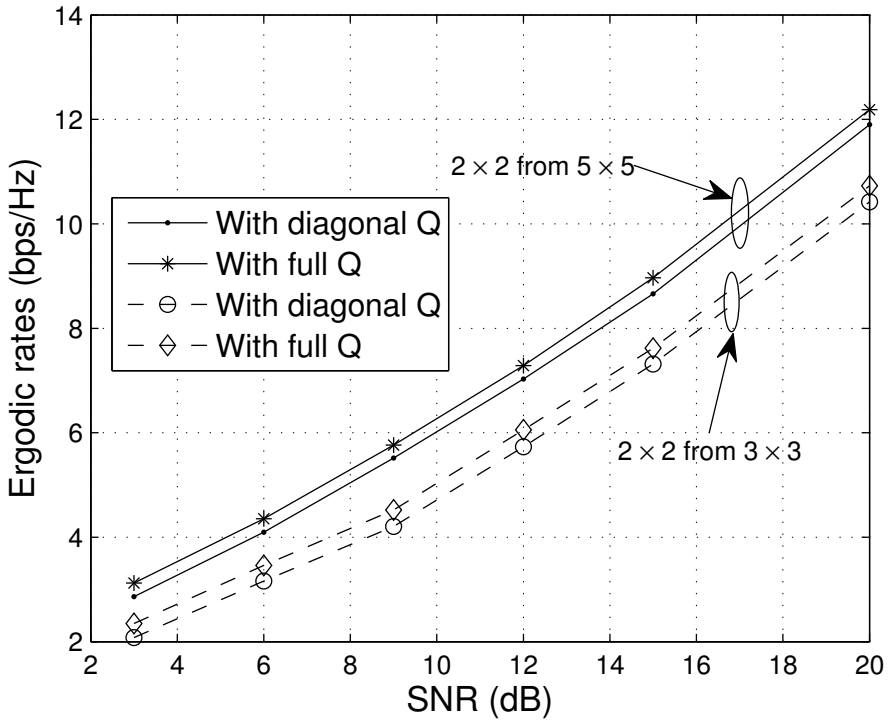

Figure 6.3: Ergodic rates vs SNR for different (with 3 single antenna PU RXs) system sizes and in the presence of a PU TX with 3 antennas. $\bar{\alpha} = 0.5$ for both from CR TX to PU RXs and PU TX to CR RX. We take $\beta = 0.35$. Antenna selection is performed using the heuristic and both diagonal and full $\mathbf{Q}_{\mathrm{CR}}$ (for the sake of brevity we have represented it as Q in the legend of the figure) matrices are considered.

with respect to the CR-CR channel by decreasing $\bar{\alpha}$ from 0.5 to 0.1 (which is plausible for environments with shorter range CRs), the ergodic rate curve for a $(2, 2)$ system obtained from a $(4, 4)$ system goes beyond that of a $(2, 2)$ system without any PU operating in its vicinity. This clearly indicates that even after performing antenna selection subject to the interference constraints, there are still enough degrees of freedom left for the CR to attain a substantial gain in terms of its maximum achievable rates.

In Fig. 6.3 we consider the effects of a diagonal input covariance matrix and incorporate interference from the PU TX. We plot the ergodic rate curves based on the heuristic for two different systems and make a comparison between a diagonal

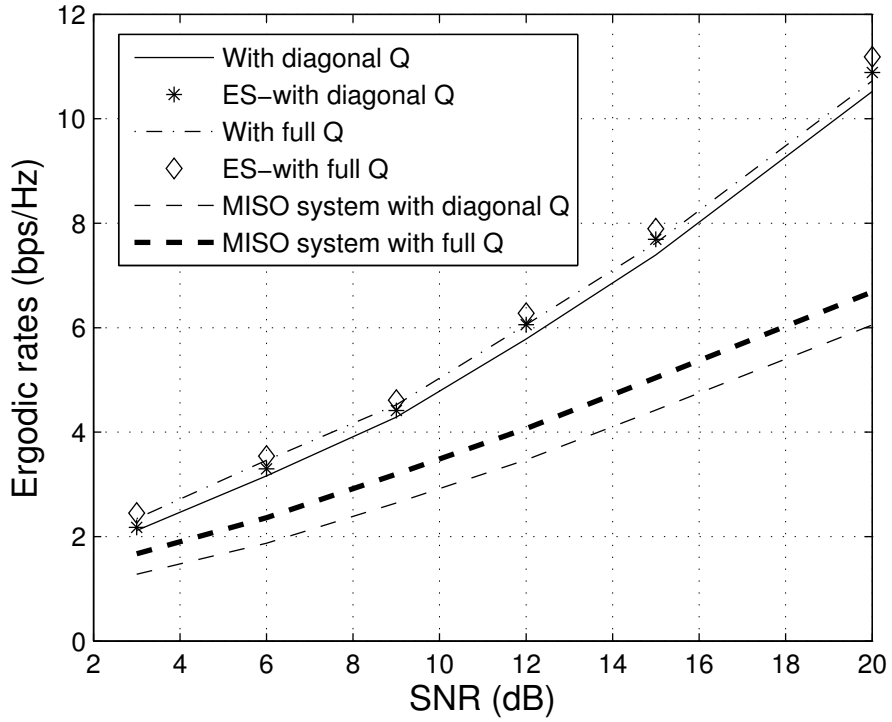

Figure 6.4: Ergodic rates vs SNR for different systems. The top two curves compare the performance of diagonal and full $\mathbf{Q}_{\mathrm{CR}}$ matrices with exhaustive search for a 2×2 system from a 3×3 system. The bottom 2 plots present ergodic rate performance of the best 1×2 system from a 1×5 system for diagonal and full $\mathbf{Q}_{\mathrm{CR}}$ matrices. For the sake of brevity we have represented $\mathbf{Q}_{\mathrm{CR}}$ as Q in the legend of the figure.

and a full $\mathbf{Q}_{\mathrm{CR}}$ matrix in the presence of an interfering PU TX. For reasons of symmetry and to avoid any further parameters we assume that the signal strength from the PU TX to the CR RX is also given by the parameter $\bar{\alpha}$. Hence, each element of $\mathbf{H}_{\mathrm{PC}}$ has power equal to $\bar{\alpha}$. For these results we consider a CR device with three single antenna PU RXs in its vicinity and a PU TX equipped with 3 antennas interfering at the CR RX. As expected there is a small loss of rate for both systems when $\mathbf{Q}_{\mathrm{CR}}$ is restricted to diagonal form. However, the rate loss for the larger system is slightly less than that of the smaller one.

In order to perform a comparison of the heuristic with the ES approach, in Fig. 6.4 we plot ergodic rates versus SNR with full and diagonal $\mathbf{Q}_{\mathrm{CR}}$ matrices. We take the same parameters as in Fig. 6.3 and assume CR operation in the presence of 3 PU RXs and a PU TX with 3 antennas interfering with the CR RX. It is observed

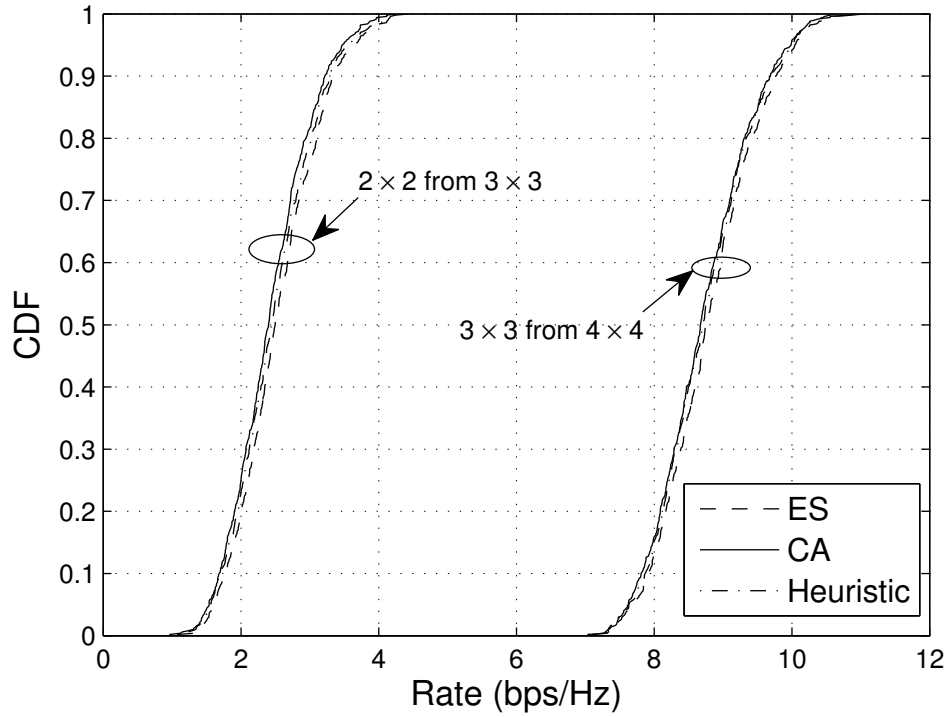

Figure 6.5: CDFs of rates achieved for various selection methods for two different systems at SNR = 8 dB for the MU case with 3 single antenna PUs.

that the difference between the two approaches is minimal. However, as we move towards higher SNR values the gap between the ES and the heuristics ergodic rates becomes more noticeable. In addition to this, we also compare ergodic rates of the best 1×2 multiple-input single-output (MISO) system chosen from a bigger 1×5 MISO system with full and diagonal $\mathbf{Q}_{\mathrm{CR}}$ matrices. It is important to note here that the difference between ergodic rates tends to become larger than that observed in Fig. 6.3. This can be attributed to the fact that in order to perform beamforming task, the $\mathbf{Q}_{\mathrm{CR}}$ matrices are not full rank and hence owing to the inter-dependence of columns of $\mathbf{Q}_{\mathrm{CR}}$ the difference is magnified.

In the absence of PU-CR interference all 3 techniques can be used and their performance is compared in Fig. 6.5 via CDFs of the achievable rates. The three techniques follow a hierarchy of complexity from the full solution in the ES through the relaxed iterative optimization in CA to the simple heuristic. Hence, it is notable that all 3 methods are remarkably similar and that even with its massively reduced

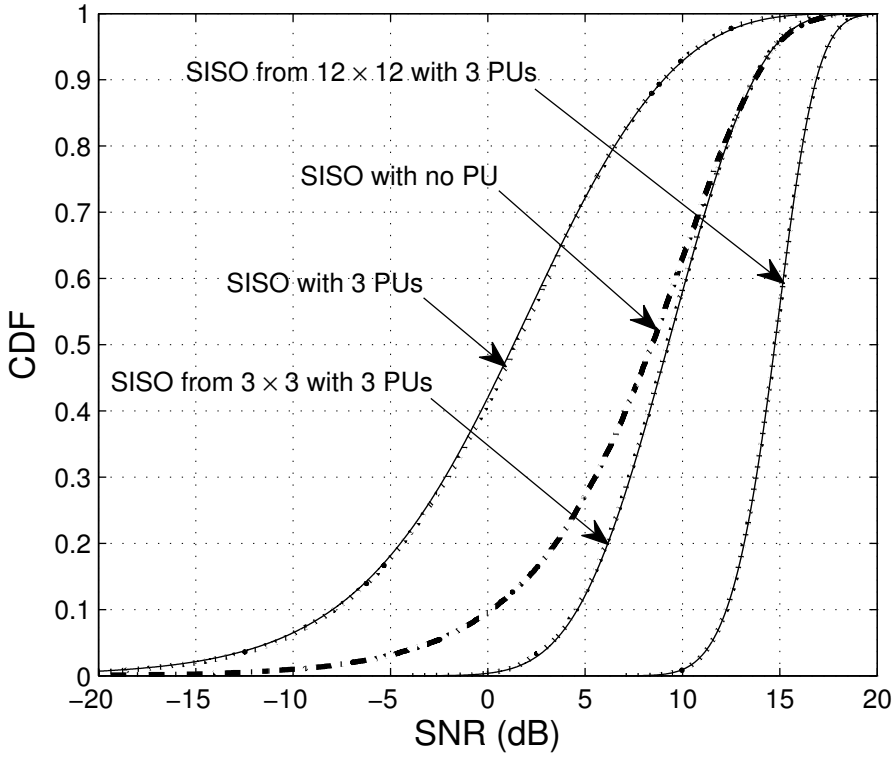

Figure 6.6: CDFs of SISO link obtained from a MIMO system. $\bar{\alpha} = 0.2, \beta = 0.03$ and CR system SNR is 10 dB. Analytical results are shown using solid lines while simulations use dotted lines. In addition to verifying analysis the curves show the gains harnessed by choosing the best SISO link from a given MIMO system.

complexity the heuristic is very similar to the CA approach and only a little behind the ES. Although the relative performance needs to be investigated in more detail over a wider range of parameters and scenarios, this is an excellent indication that near optimal results may be achieved with a very simple selection heuristic.

6.4.2 SISO Selection

Figure 6.6 presents SNR CDFs due to selection with varying numbers of CR antennas in the presence of 3 PUs. The other system parameters are $\bar{\alpha} = 0.2, \beta = 0.03$ and SNR = 10 dB. The performance of a SISO CR link in the absence of a PU is also shown as a benchmark. As the CR system grows from $(1, 1)$ to $(3, 3)$ to $(12, 12)$ we see corresponding increases of 8 dB and 5 dB in the median SNR. Hence, the first 2 antennas added provide an 8 dB increase while the subsequent 9 antennas

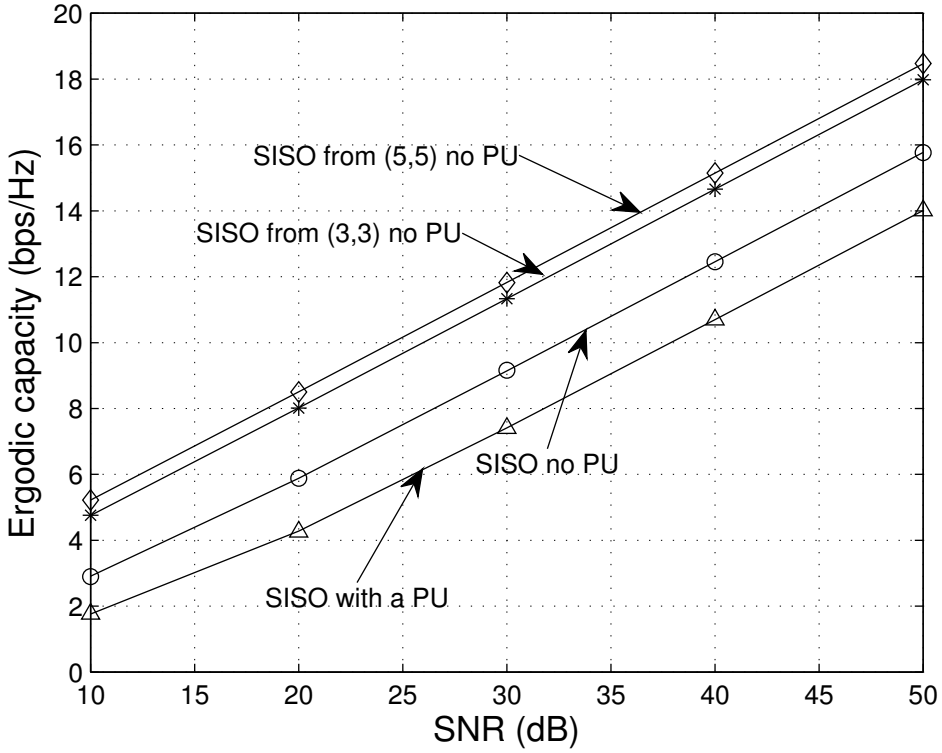

Figure 6.7: Ergodic capacity vs. SNR for SISO links obtained from different MIMO configurations. $\bar{\alpha} = 0.5$ and $\beta = 0.1$. Analytical results are shown using solid lines while special markers are used to show simulated results. In addition to verifying analysis, the bottom two curves quantify loss in rates even in the presence of a single PU.

provide only 5 dB. Clearly, these are rapidly diminishing returns due to the addition of extra antennas. Note that the baseline performance of the SISO CR with no PU can be achieved via SISO selection from a $(3, 3)$ system. Hence, selection can be used to recover the losses due to PU presence. In this simulation, however, there are only 3 PUs with relatively weak CR-PU paths ($\bar{\alpha} = 0.2$). Hence, it is not too difficult to counter their effects.

Figure 6.7 shows the ergodic capacity results of Sec. 6.3.2. The loss due to a single PU is shown (see (6.19)) and the diminishing returns due to the CR dimension grows are also seen. Note that even a single PU inflicts a heavy loss on capacity, especially at low SNR.

Before describing the results of more realistic scenarios in detail, we mention that unless otherwise stated, the default parameters taken are $\sigma = 8$ dB, $\gamma = 3.5$,

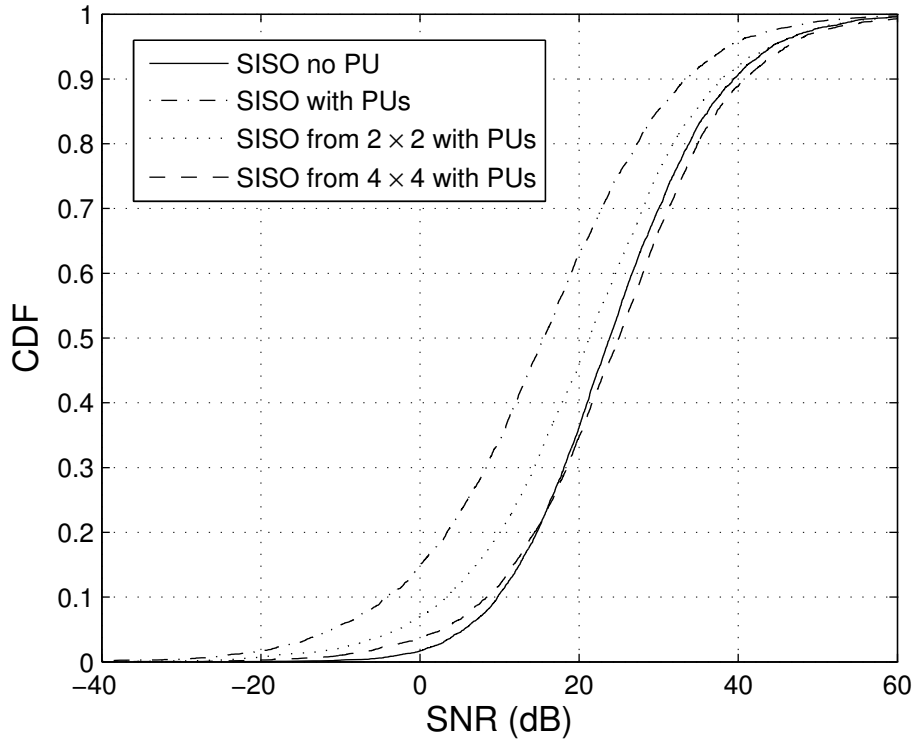

Figure 6.8: CDF plots of best SISO link from a given MIMO system in the presence of PUs following homogenous Poisson point process. The parameters taken are $\sigma = 8$ dB, $\gamma = 3.5, \theta = 35$ PU nodes per sq. km., $\omega = 0.3$ dB and $r_{cr} = 20$ m.

$r = 1000$ m and $r_{cr} = 20$ m. Figures 6.8 and 6.9 explore the impact of the more complex channel models of Sec. 6.3.3. Note that the broad trends and conclusions drawn from Fig. 6.8 are the same as those observed in the analysis given in Fig. 6.6. In particular, selection gains decrease as the CR dimension grows and the SISO baseline can be outperformed with a moderate number of antennas (4 in Fig. 6.8 and 3 in Fig. 6.6). However, as in Fig. 6.6, such results are found in a sparse PU environment. In Fig. 6.8, 35 PUs per km^2 are used and the CR link is short at 20 m. Figure 6.9 explores the effect of different system parameters. A comparison of the curves in Fig. 6.9 shows that performance is increased as γ increases, θ decreases and σ decreases. Decreasing θ results in fewer power constraints and so a performance increase is obvious. Increasing γ (and as high as 6.5) and decreasing σ tends to reduce the occurrence of large interference values at the PU RXs. Hence, this also increases performance.

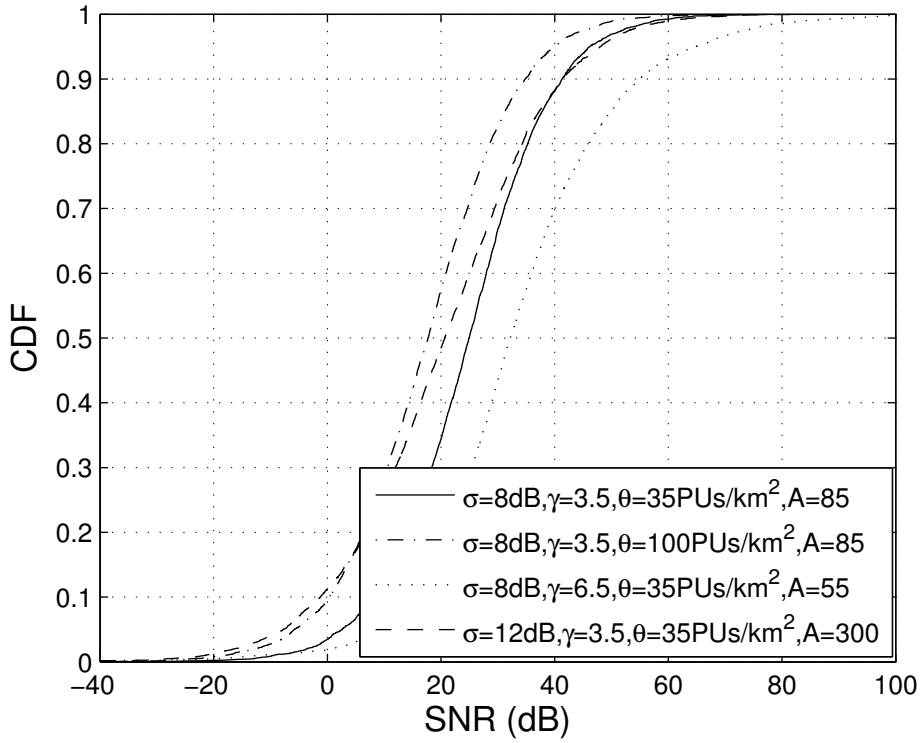

Figure 6.9: Effect of various parameters on the CDF plots of best SISO link from a given MIMO system in the presence of PUs following homogenous Poisson point process. Best SISO link is chosen from a 4×4 system with $\omega = 0.3$ and $r_{cr} = 20$ m.

Lastly, we consider Table-6.1. In this table we consider the dimension required for a square CR MIMO link so that optimal SISO selection outperforms the equivalent SISO link in the absence of any PUs. By outperforming, we mean that the median SNR is exceeded. Hence, Table-6.1 gives the size of the array required so that selection completely removes the losses due to the presence of the PUs. Clearly, the required dimension grows with θ and reduces with ω. The scale of the system dimensions is of interest. Selection by itself can only remove the losses due to the PUs in sparse PU environments or when weak interference constraints are present. This is to be expected as the selection process is being worked very hard. Hence, in sparse PU environments selection may be possible as a stand-alone technique. In denser environments, selection may be a potential solution in conjunction with other techniques such as scheduling or the use of other bands.

Table 6.1: MIMO system dimensions for different θ and ω under default parameters

θ (nodes km^{-2})	ω	MIMO system needed
35	0.25	4×4
35	0.5	3×3
35	1.0	2×2
50	0.25	6×6
50	0.5	4×4
50	1.0	2×2
80	0.25	15×15
80	0.5	7×7
80	1.0	4×4

6.5 Summary

In this chapter we have used the idea of antenna selection to jointly satisfy interference constraints at the PU RXs while improving the achievable rates of the CR device. We have presented three schemes in order of decreasing complexity to solve this problem. The optimal search approach is the most computationally intensive while the CA approach solves the problem by iteratively optimizing a series of small convex programs. We then present a norm-based separate transmit receive antenna selection technique. This approach results in huge complexity reductions and produces very accurate results. It is notable that this simple technique performs almost indistinguishably from the CA approach which is a well established optimization approach to approximating the full solution. In addition, we have included a performance analysis based on the SNR of the best link of the MIMO CR device. Furthermore, results have also been extended to more realistic scenarios based on Monte Carlo simulations. Broadly speaking, our results suggest that antenna selection for CR systems is a powerful technique in sparse PU environments with the potential for obtaining greater gains if we employ MIMO rather than SISO link selection. For denser PU environments, antenna selection can provide a partial solution for CR operation.

Chapter 7

Optimal SINR Balancing in the Downlink of Cognitive Radio Networks with Imperfect Channel State Information

The downlink of CR networks has received much attention from the research community [86, 99, 100]. The problem of balancing the SINR, i.e., maximizing the worst SINR of a CR device in the downlink of a CR network operating in the vicinity of multiple PUs, was solved in [99] using the uplink-downlink duality concept. The work of [99], based on perfect channel knowledge, was recently extended in [100] to the case of imperfect channel estimates at the CR BS. This extension assumed that errors in the channel state information (CSI) are bounded by ellipsoids. Based on this channel matrix uncertainty model, the problem was formulated as a quasi-convex optimization program using the $\mathcal{S}$-procedure [101]. To be precise, in the case of channel uncertainty, the authors first derived an equivalent problem that involved rank-1 constraints on the cone of PSD matrices modeling the beamforming vectors. These constraints rendered the problem non-convex. Later, the problem was solved by relaxing the rank-1 constraints and using the *bisection search* [36] algorithm. The

approach is based on the original classical work of [102]. By assuming an ellipsoidal CSI uncertainty model, [100] formulated a quasi-convex optimization problem after dropping rank-1 constraints.

Relaxing such rank constraints results in an upper bound to the optimal solution. However, under certain conditions (e.g., by showing that the optimum cost of the original problem is equal to that of the Lagrange dual of its relaxed version [102]) we can obtain the optimal solution, one with rank-1 constraints satisfied. In addition to this, there are many optimization problems in communications, for example [103, 104, 105] to name just a few, that can be formulated as semidefinite programs (SDPs) [36] with rank constraints. As a result of these nonconvex rank constraints, various relaxations and approximations are usually adopted. Different techniques have also been developed to obtain *approximate* rank-1 solutions [105, 104] from the optimized, but relaxed, variables. In [86], the problem of constraining the rank of separable SDPs was studied in the context of power optimization in the downlink of CR networks with perfect channel estimates available at the BS. By elegantly fine tuning the results of [106], SDP relaxation of three classes of optimal beamforming problem was shown to always possess rank-1 solutions in [86].

In this chapter, we study the problem of SINR balancing in the downlink of CR networks with imperfect CSI at the CR BS without relaxing rank constraints. Our main contributions include: a) showing a successful incorporation of the recently developed *convex iteration* [107] technique in the problem's solution; b) developing a low complexity algorithm to solve the problem; and c) extending previous results to include PU interference and to maximizing minimum data rates.

In this chapter we use $[i : l]$ to represent the i-th to l-th elements of a row vector and diag($\mathbf{N}$) returns the principal diagonal of a square matrix $\mathbf{N}$.

7.1 System Model

Let us consider a CR BS having N_{CR} antennas serving C single antenna cognitive devices. It is assumed that the cognitive broadcast channel is operating in the

vicinity of K single antenna PU RXs. Suppose $\mathbf{s} \in \mathbb{C}^C$ represents the column vector of data symbols meant for the C different CR RXs such that the symbol for the ith RX is $s_i \sim \mathcal{CN}(0,1)$[1], $i = 1, \ldots, C$. The CR BS transmits a vector, $\mathbf{x} \in \mathbb{C}^{N_{CR}}$, obtained by a linear precoding of $\mathbf{s}$, i.e.,

$$\mathbf{x} = \sum_{j=1}^{C} \mathbf{p}_j s_j = \mathbf{P}\mathbf{s}, \tag{7.1}$$

where $\mathbf{P} \in \mathbb{C}^{N_{CR} \times C}$ is the precoding matrix and $\mathbf{p}_j$ represents its jth column. With the above model we have $\mathbb{E}[\mathbf{s}\mathbf{s}^\dagger] = \mathbf{I}$. Thus, assuming that the total available power is P_{total}, the constraint on the transmit power becomes $\mathbb{E}[\|\mathbf{x}\|^2] = \sum_{j=1}^{C} \|\mathbf{p}_j\|^2 = \mathrm{Tr}(\mathbf{P}^\dagger\mathbf{P}) \leq P_{total}$. The BS then transmits the vector $\mathbf{x}$ over a quasi-static flat-fading channel. The received signal, y_i, at the ith CR user is given by:

$$y_i = \mathbf{h}_i\mathbf{x} + n_i = \mathbf{h}_i\mathbf{p}_i s_i + \sum_{\substack{j=1 \\ j \neq i}}^{C} \mathbf{h}_i\mathbf{p}_j s_j + n_i, \tag{7.2}$$

where $\mathbf{h}_i \in \mathbb{C}^{1 \times N_{CR}}$ is the downlink channel vector for the ith user and $n_i \sim \mathcal{CN}(0, \sigma_i^2)$. The effect of PU interference on the CR RXs will be later incorporated in Sec. 7.2.2. In a similar way

$$z_m = \mathbf{h}_{\mathrm{int}_m}\mathbf{x} + v_m = \sum_{n=1}^{C} \mathbf{h}_{\mathrm{int}_m}\mathbf{p}_n s_n + v_m, \tag{7.3}$$

is the signal received at the mth PU RX where $\mathbf{h}_{\mathrm{int}_m} \in \mathbb{C}^{1 \times N_{CR}}$ and $v_m \sim \mathcal{CN}(0, \sigma_m^2)$ are the channel and noise at the mth PU RX, respectively.

Channel Uncertainty: In practice the CR BS is not able to obtain perfect CSI for both the CR-CR and CR-PU channels. This is partly due to the *centralized* nature of the proposed scheme detailed below, which makes it very difficult for the CR BS to acquire near perfect instantaneous CSI. For example, the centralized processor would require CSI from all terminals simultaneously. Since all mobile stations suffer from different conditions including those of the channel, terrain etc., it is highly

[1]Note that for our purposes the elements of $\mathbf{s}$ could follow any distribution as long as they are i.i.d. with zero mean and unit variance. However, we have used a complex normal distribution for this purpose since it is the entropy maximizing distribution.

difficult to acquire perfect CSI from all users at the BS. Thus, we model the CSI error for the CR-CR channel $\mathbf{h}_i$ as:

$$\mathbf{h}_i = \hat{\mathbf{h}}_i + \mathbf{e}_i, \tag{7.4}$$

where $\hat{\mathbf{h}}_i$ is the estimated channel for user i at the CR BS and $\mathbf{e}_i \in \mathcal{H}_i(\delta_i)$ where

$$\mathcal{H}_i(\delta_i) = \{\mathbf{a}_i : \|\mathbf{a}_i\| \leq \delta_i\}. \tag{7.5}$$

The process of determining CSI from the CR BS to the PU RXs is unclear and depends on the particular system considered. Ideally, there is no cooperation between the PUs and the CR BS, however, various levels of cooperation and CSI transfer are considered in the literature [6]. Here, we do not consider any particular procedures to acquire CSI (as it is beyond the scope of the current work), and model it in a standard way as an imperfectly acquired CSI estimate. Thus, the channels for the CR-PU links are modeled as

$$\mathbf{h}_{\text{int}_m} = \hat{\mathbf{h}}_{\text{int}_m} + \mathbf{e}_{\text{int}_m}, \tag{7.6}$$

where $\hat{\mathbf{h}}_{\text{int}_m}$ is the estimated channel for the mth PU at the CR BS and $\mathbf{e}_{\text{int}_m} \in \mathcal{H}_{\text{int}_m}(\delta_{\text{int}_m})$ where

$$\mathcal{H}_{\text{int}_m}(\delta_{\text{int}_m}) = \{\mathbf{b}_m : \|\mathbf{b}_m\| \leq \delta_{\text{int}_m}\}. \tag{7.7}$$

The ball uncertainty models described above are common models used to characterize errors caused by processes such as quantization and estimation [108].

7.2 Analytical Framework

With the system model elaborated in Sec. 7.1, it is easy to see that the total signal power received at the ith CR RX, $P_i \triangleq \mathbb{E}[|y_i|^2]$, is given by:

$$P_i = \mathbf{h}_i \mathbf{p}_i \mathbf{p}_i^\dagger \mathbf{h}_i^\dagger + \sum_{\substack{j=1 \\ j \neq i}}^{C} \mathbf{h}_i \mathbf{p}_j \mathbf{p}_j^\dagger \mathbf{h}_i^\dagger + \sigma_i^2, \tag{7.8}$$

where the first term on the right hand side of (7.8) is the power of the desired signal while the second term represents the inter-user interference. Thus, for user i, the SINR is defined by:

$$\text{SINR}_i = \frac{(\hat{\mathbf{h}}_i + \mathbf{e}_i)\mathbf{p}_i\mathbf{p}_i^\dagger(\hat{\mathbf{h}}_i + \mathbf{e}_i)^\dagger}{\sum_{\substack{j=1 \\ j\neq i}}^{C}(\hat{\mathbf{h}}_i + \mathbf{e}_i)\mathbf{p}_j\mathbf{p}_j^\dagger(\hat{\mathbf{h}}_i + \mathbf{e}_i)^\dagger + \sigma_i^2}, \qquad i = 1, \ldots, C. \tag{7.9}$$

Similarly, the interference power received at the mth PU, IP_m, is:

$$\text{IP}_m = \sum_{n=1}^{C}(\hat{\mathbf{h}}_{\text{int}_m} + \mathbf{e}_{\text{int}_m})\mathbf{p}_n\mathbf{p}_n^\dagger(\hat{\mathbf{h}}_{\text{int}_m} + \mathbf{e}_{\text{int}_m})^\dagger, \qquad m = 1, \ldots K. \tag{7.10}$$

7.2.1 Problem Formulation

We aim to balance the SINR of the users in the CR system subject to transmit power constraints while simultaneously maintaining interference power at the PU RXs below a certain acceptable threshold. These problems, in the context of ordinary broadcast channels, are generally categorized as max-min fair SINR problems [108, 109]. Thus, the main problem is:

$$\begin{aligned} \mathcal{P}_1: \underset{t,\mathbf{P}}{\text{maximize}} \quad & t \\ \text{subject to} \quad & \text{SINR}_i \geq t,\ i = 1, \ldots, C,\ \forall \mathbf{e}_i \in \mathcal{H}_i(\delta_i) \\ & \text{IP}_m \leq \zeta_m,\ \forall \mathbf{e}_{\text{int}_m} \in \mathcal{H}_{\text{int}_m}(\delta_{\text{int}_m}),\ \sum_{n=1}^{C}\text{Tr}(\mathbf{p}_i\mathbf{p}_i^\dagger) \leq P_{total} \end{aligned}$$

where ζ_m is the maximum tolerable interference level for the mth PU RX. Later we normalize this with respect to noise spectral density.

7.2.2 Approximate Solution of $\mathcal{P}_1$

Recently, $\mathcal{P}_1$ has been solved in [100] by using the powerful $\mathcal{S}$-procedure [101]. Their result for the case of spherical channel uncertainty can be written as:

Lemma 1 ([100]). *With the substitution, $\mathbf{W}_i = \mathbf{p}_i\mathbf{p}_i^\dagger$, problem $\mathcal{P}_1$ can be equivalently*

rewritten as:

$$\mathcal{P}_2 : \underset{\tau_i,\lambda_m,t,\mathbf{W}_i}{\textit{maximize}} \quad t$$

$$\textit{subject to} \quad \begin{bmatrix} \hat{\mathbf{h}}_i\mathbf{Q}_i\hat{\mathbf{h}}_i^{\dagger} - t\sigma^2 - \tau_i\delta_i^2 & \hat{\mathbf{h}}_i\mathbf{Q}_i \\ (\hat{\mathbf{h}}_i\mathbf{Q}_i)^{\dagger} & \mathbf{Q}_i + \tau_i\mathbf{I} \end{bmatrix} \succeq 0,\ \tau_i \geq 0\,, i = 1, 2, \ldots, C$$

$$\begin{bmatrix} -\hat{\mathbf{h}}_{int_m}\mathbf{S}\hat{\mathbf{h}}_{int_m}^{\dagger} + \zeta_m - \lambda_m\delta_{int_m}^2 & -\hat{\mathbf{h}}_{int_m}\mathbf{S} \\ (-\hat{\mathbf{h}}_{int_m}\mathbf{S})^{\dagger} & -\mathbf{S} + \lambda_m\mathbf{I} \end{bmatrix} \succeq 0,\ \lambda_m \geq 0\,, m = 1, 2, \ldots, K$$

$$Tr(\mathbf{S}) \leq P_{total}, \mathbf{W}_i \succeq 0, rank(\mathbf{W}_i) = 1, \forall i.$$

where $\mathbf{Q}_i = \mathbf{W}_i - t\sum_{\substack{j=1 \\ j\neq i}}^{C} \mathbf{W}_j$ *and* $\mathbf{S} = \sum_{i=1}^{C} \mathbf{W}_i$.

While it is not always possible to extend results such as those presented above to the more complex model of ellipsoids representing channel uncertainty, it is relatively easy to accomplish this task in the particular scenario of $\mathcal{P}_2$ [100]. $\mathcal{P}_2$ can be efficiently solved using a bisection search [108, 36, 110] after formulating it as a quasi-convex optimization problem by dropping rank constraints. In [100], the authors modify the basic bisection search by storing those iterations that returned rank-1 solutions and later, if the final beamforming solution is not optimal, they use that rank-1 solution with the largest SINR.

Now we extend *Lemma 1* to incorporate the effect of interference due to PU signals at the CR RXs. For this we assume that there are I single antenna PU TXs each interfering with the single antenna CR RXs. Note that it is not necessary to take $I = K$, since the I interfering PU TXs need not correspond to the K receivers. Let $\mathbf{h}_{pi} \in \mathbb{C}^{1\times I}$ be the channel vector containing the interfering signals due to I PU TXs at the ith CR RX.

Corollary 1. *Assuming that* $\mathbf{h}_{pi} = \hat{\mathbf{h}}_{pi} + \mathbf{e}_{pi}$*, where* $\hat{\mathbf{h}}_{pi}$ *is the available estimate of the composite PU interference channel and* $\mathbf{e}_{pi}$ *lies in the same region as specified in (7.5),* $\mathcal{P}_2$ *remains the same except its ith SINR constraint is changed to:*

$$\begin{bmatrix} \hat{\mathbf{h}}_i\mathbf{Q}_i\hat{\mathbf{h}}_i^{\dagger} - t(\hat{\mathbf{h}}_{pi}\hat{\mathbf{h}}_{pi}^{\dagger} + \sigma^2) - \tau_i\delta_i^2 & \hat{\mathbf{h}}_i\mathbf{Q}_i - t\hat{\mathbf{h}}_{pi} \\ (\hat{\mathbf{h}}_i\mathbf{Q}_i - t\hat{\mathbf{h}}_{pi})^{\dagger} & \mathbf{Q}_i - (t - \tau_i)\mathbf{I} \end{bmatrix} \succeq 0 \tag{7.11}$$

Proof. With interfering PU devices, SINR_i is given by:

$$\text{SINR}_i = \frac{\mathbf{h}_i \mathbf{p}_i \mathbf{p}_i^\dagger \mathbf{h}_i^\dagger}{\sum_{\substack{j=1 \\ j \neq i}}^{C} \mathbf{h}_i \mathbf{p}_j \mathbf{p}_j^\dagger \mathbf{h}_i^\dagger + \mathbf{h}_{pi} \mathbf{h}_{pi}^\dagger + \sigma_i^2}, \; i = 1, \ldots, C. \tag{7.12}$$

Using (7.12) it is easy to see that the constraint, $\text{SINR}_i \geq t$, can be rewritten as:

$$\text{SINR}_i = (\hat{\mathbf{h}}_i + \mathbf{e}_{pi}) \mathbf{Q}_i (\hat{\mathbf{h}}_i + \mathbf{e}_{pi})^\dagger - t\{\sigma_i^2 + (\hat{\mathbf{h}}_{pi} + \mathbf{e}_{pi})(\hat{\mathbf{h}}_{pi} + \mathbf{e}_{pi})^\dagger\} \geq 0, \forall \mathbf{e}_{pi} \in \mathcal{H}_i(\delta_i) \tag{7.13}$$

Now invoking the $\mathcal{S}$-procedure [101] on (7.13) results in (7.11). □

Remark 1. *Balanced rates in the network can easily be solved by transforming the SINR obtained from* $\mathcal{P}_2$ *to the corresponding spectral efficiency using* $\log_2(1+SINR)$ *bps/Hz. Further, individual powers of antennas can be constrained by introducing* $diag(\mathbf{S}) \leq \mathbf{p}_{ind}$ *in* $\mathcal{P}_2$*. Elements of* $\mathbf{p}_{ind}$ *represent individual transmit power constraints for the individual antennas and the inequality is to be interpreted element wise.*

7.3 Proposed Solution

As is evident from the above discussion, the known solution to the problem at hand is approximate due to the rank-1 constraints. There are many problems in communications, for example [103, 105, 104], that involve rank constraints on the unknown matrix variables and these are often solved based on some approximating technique like the one presented in [105]. We stress here that, in our case, we cannot apply the randomization techniques in [105] owing to the complex robust constraints [100]. For an overview of issues involved in extracting rank-1 solutions from the approximate answers, the reader is referred to [111]. Before describing the details of our solution, let us first explore the structural aspects of the proposed technique. Rank is a quasiconcave function on the cone of PSD matrices. It has been proposed in [112, 113] to approximate the rank function by its best convex lower bound (also known as the *convex envelope*) in the context of rank minimization problems. Such a

bound is conveniently represented by the scaled trace of PSD matrices. We note this bound represents an approximation. The original problem can then be judiciously replaced with an iterative method in which the rank constraints are incorporated as trace constraints. Motivated by this, [107] devised a technique to solve rank-constrained optimization problems. Since problem $\mathcal{P}_2$ also falls in the category of rank constrained SDPs with the rank of each precoding matrix constrained to be 1, it is natural to consider the application of this technique in solving this problem. Hence, our solution utilizes the *convex iteration* algorithm [107] approach to solve rank constrained SDPs. Suppose we have an SDP in the variable $\mathbf{F}$ and we are to solve the corresponding semidefinite feasibility problem

$$\begin{aligned} \mathcal{FP}: \text{ find} \quad & \mathbf{F} \\ \text{subject to} \quad & \mathbf{F} \in \mathcal{C}, \mathbf{F} \succeq 0, \text{rank}(\mathbf{F}) \leq n, \end{aligned}$$

where $\mathbf{F} \in \mathbb{S}^N$, $\mathbb{S}^N$ is the set of $N \times N$ Hermitian matrices and $\mathcal{C}$ is a convex set assumed to contain PSD matrices with rank-n or less. Then, $\mathbf{F}$ can be determined by iteratively solving the following two convex problems:

$$\begin{aligned} \mathcal{FP}_1: \underset{\mathbf{F}}{\text{minimize}} \quad & \text{Tr}(\mathbf{FD}) \\ \text{subject to} \quad & \mathbf{F} \in \mathcal{C}, \mathbf{F} \succeq 0 \end{aligned}$$

where $\mathbf{D} \in \mathbb{S}^N$ is the *direction vector* (we call it a vector since it is conveniently represented in a $\mathbb{R}^{N(N+1)/2}$ space) obtained by solving the following SDP,

$$\begin{aligned} \mathcal{FP}_2: \underset{\mathbf{D}}{\text{minimize}} \quad & \text{Tr}(\mathbf{F}^\star\mathbf{D}) \\ \text{subject to} \quad & \mathbf{0} \preceq \mathbf{D} \preceq \mathbf{I}, \text{Tr}(\mathbf{D}) = N - n \end{aligned}$$

where $\mathbf{F}^\star$ is an optimal solution to $\mathcal{FP}_1$ for some given iterate $\mathbf{D}$. It is stated in [107] that we cannot interpret direction as a projection method. Instead, it represents a hyperplane-normal moving opposite to the direction describing the minimization of an affine trace function [107]. We continue iterating between $\mathcal{FP}_1$ and $\mathcal{FP}_2$ until $\text{Tr}(\mathbf{F}^\star\mathbf{D}^\star)$ attains a vanishingly small value or we have determined $\mathbf{F}^\star$ with required rank constraint, where $\mathbf{D}^\star$ is the optimal direction vector. After convergence is

achieved, the final pair $(\mathbf{D}^\star, \mathbf{F}^\star)$ provides an $\mathbf{F}^\star$ with $\text{rank}(\mathbf{F}^\star) \leq n$, if it existed in $\mathcal{C}$. We stress that iteratively solving $\mathcal{FP}_1$ and $\mathcal{FP}_2$ gives an *equivalent representation* [36] of the original problem $\mathcal{FP}$ instead of a *relaxation*. Hence, a solution of rank-n or less will be obtained if it exists in $\mathcal{C}$.

Both $\mathcal{FP}_1$ and $\mathcal{FP}_2$ are SDPs that require numerical solution. In fact, by replacing a single SDP given in $\mathcal{F}$ by two SDPs, we have increased the complexity of the problem. However, the optimization matrices are Hermitian (and thus possess real eigenvalues that can be arranged in, say, nonincreasing order) and problem $\mathcal{FP}_2$ can be solved analytically. Therefore, we present the following proposition.

Proposition 1. *The problem $\mathcal{FP}_2$ admits an analytical solution. Define the singular value decomposition (SVD) $\mathbf{F}^\star = \mathbf{U}\mathbf{\Sigma}\mathbf{O}^\dagger$, where $\mathbf{U}$, $\mathbf{O}$ are unitary matrices and $\mathbf{\Sigma}$ is a diagonal matrix with singular values on its diagonal. Then, the value of $\mathbf{D}^\star$ which gives the optimum solution of $\mathcal{FP}_2$ is $\mathbf{D}^\star = \mathbf{V}^\star\mathbf{V}^{\star\dagger}$, where $\mathbf{V}^\star = \mathbf{U}(:, [n+1 : N])$ and $[n+1 : N]$ indicates the indices of the columns of $\mathbf{U}$. Suppose $\theta(\mathbf{F}^\star) \in \mathbb{R}^N$ are the eigenvalues of $\mathbf{F}^\star$ arranged in nonincreasing order, then for $0 \leq n \leq N-1$, the optimum value of $\mathcal{FP}_2$ is $\sum_{j=n+1}^{N} \theta(\mathbf{F}^\star)_j$.*

Proof. See [114, Sec. 4.1] and [42, Sec. 4.3.18]. □

7.3.1 Incorporation of "Convex Iteration" in $\mathcal{P}_2$

As mentioned above, the relaxed version of $\mathcal{P}_2$ can be efficiently solved by performing a bisection search. Such a search involves solving a convex semidefinite feasibility program for a particular value of t and then, depending on whether or not the program is feasible for that t, the search interval for the next step is updated accordingly [36]. In contrast, we execute the *convex iteration* described above, together with the bisection search. This avoids the need for any relaxation. This modified procedure is detailed in **Algorithm 1**. Comments are indicated by the symbol '$\triangleright$', while the symbol '$\star$' represents the optimum value. The Boolean condition `true` for the inner while loop indicates that the loop keeps on executing until we break out of it. k

Algorithm 1 SINR balancing with rank-1 precoders

1: `Input:` SINRmax, SINRmin, $\hat{\mathbf{h}}_i, \hat{\mathbf{h}}_{\mathrm{int}_m}, \hat{\mathbf{h}}_{pi}, \delta_i, \delta_{\mathrm{int}_m}, \sigma, P_{total}$
2: `Output:` t_0(max-min SINR), $\mathbf{p}_i^\star$
3: $\mathcal{H}_W \leftarrow \emptyset, \mathcal{H}_t \leftarrow \emptyset, k \leftarrow 0$ ▷ Initialization
4: **while** (SINRmax − SINRmin) > thresh.1 **do**
5: $k \leftarrow k + 1$
6: $t \leftarrow (\mathrm{SINRmax} + \mathrm{SINRmin})/2$
7: $\mathbf{D}_i \leftarrow \mathbf{0}$ ▷ Initialize direction vectors
8: **while** `true` **do**
9: minimize $\sum_i \mathrm{Tr}(\mathbf{W}_i\mathbf{D}_i)$ ▷ 1st cvx
10: subject to SINR_i constraints
11: IP_m constraints
12: $\mathrm{Tr}(\sum_i \mathbf{W}_i) \leq P_{total}$
13: **if** above program infeasible **then**
14: break the second **while** (line 8)
15: **end if**
16: $\mathbf{D}_i \leftarrow \arg\min_{\substack{\mathbf{0}\preceq\mathbf{D}_i\preceq\mathbf{I} \\ \mathrm{Tr}(\mathbf{D}_i)\leftarrow N_{CR}-1}} \mathrm{Tr}(\mathbf{W}_i^\star\mathbf{D}_i)$ ▷ 2nd cvx
17: **if** $\sum_i \mathrm{rank}(\mathbf{W}_i^\star)$ **equals** C **then**
18: break the second **while** (line 8) ▷ Rank-1 obtained with some tolerance
19: **end if**
20: **if** $\mathrm{Tr}(\mathbf{W_i^\star D_i^\star}) \leq$ thresh.2 **then**
21: break the second **while** (line 8) ▷ No rank-1 precoder available
22: **end if**
23: **end while**
24: **if** program solved **then** ▷ Bisection is performed
25: SINRmin $\leftarrow t$
26: **else**
27: SINRmax $\leftarrow t$ ▷ The program is infeasible
28: **end if**
29: $\mathcal{H}_W \leftarrow \mathcal{H}_W \cup \{\mathbf{W}_i^{(k)}\}, \mathcal{H}_t \leftarrow \mathcal{H}_t \cup \{t^{(k)}\}$
30: **end while**
31: We obtain t_0 and $\mathbf{W}_i^\star$ having unit rank.
32: To recover $\mathbf{p}_i$ obtain eigenvalue decompositions (EVDs) $\mathbf{W}_i^\star = \mathbf{T}_i\mathbf{E}_i\mathbf{T}_i^\dagger$, where $\mathbf{T}_i$ are unitary and $\mathbf{E}_i$ contains the eigenvalues of $\mathbf{W}_i$ on its diagonal. Then, $\mathbf{p}_i^\star = \mathbf{T}_i\mathbf{E}_i^{1/2}$.

denotes the iteration index and $\mathbf{W}^{(k)}, t^{(k)}$ represent the values of $\mathbf{W}$ and t in the kth iteration, respectively. The sets $\mathcal{H}_W$ and $\mathcal{H}_t$ are used to collect the values of $\mathbf{W}$ and t, respectively, for each iteration. For implementation purposes, the set $\mathcal{H}_W$ can be updated with special matrices (for example, zero matrices) when the problem is found to be infeasible. Furthermore, in **Algorithm 1**, SINRmax and SINRmin represent the upper and lower limits on the SINR of the system and we iterate the bisection search until the difference between these limits is less than or equal to some threshold, 'thresh.1'. To solve the rank constrained problem exactly, we replace the convex feasibility problem for some iterate, t, with the equivalent convex iteration. This is shown in lines 9-12 of **Algorithm 1**. Similarly, the second convex program giving the optimal direction vectors is included in line 16 of the algorithm. Note that we terminate the convex iteration when either we have obtained all precoders of desired rank (line 17) or once we have determined that the value of the objective has become sufficiently small i.e., smaller than some threshold, 'thresh.2' (line 20) to deduce that no such rank matrices are available. We remark that the precoding matrices and the corresponding t_0 can be obtained from $\mathcal{H}_W$ and $\mathcal{H}_t$ respectively, by observing the last entries of these sets for which the problem was found to be feasible. **Algorithm 1** does not contain any procedure for handling stalls as these were not observed in the simulations.

7.3.2 Computational Issues With the "Convex Iteration" Approach

The first issue is related to the convergence of the convex iteration approach. The process of iteratively solving cvx-1 and cvx-2 (see comments in lines 9 and 16 of **Algorithm 1**), or for that matter $\mathcal{FP}_1$ and $\mathcal{FP}_2$, always converges [107]. This occurs because iterating between cvx-1 and cvx-2 results in a nonincreasing sequence of objective values that is bounded below in $\mathbb{R}$ and is thus convergent. However, such a convergence is *local* and the issue of *global* convergence remains open [107].

The second possible problem is concerned with the *stalling* of the algorithm at a

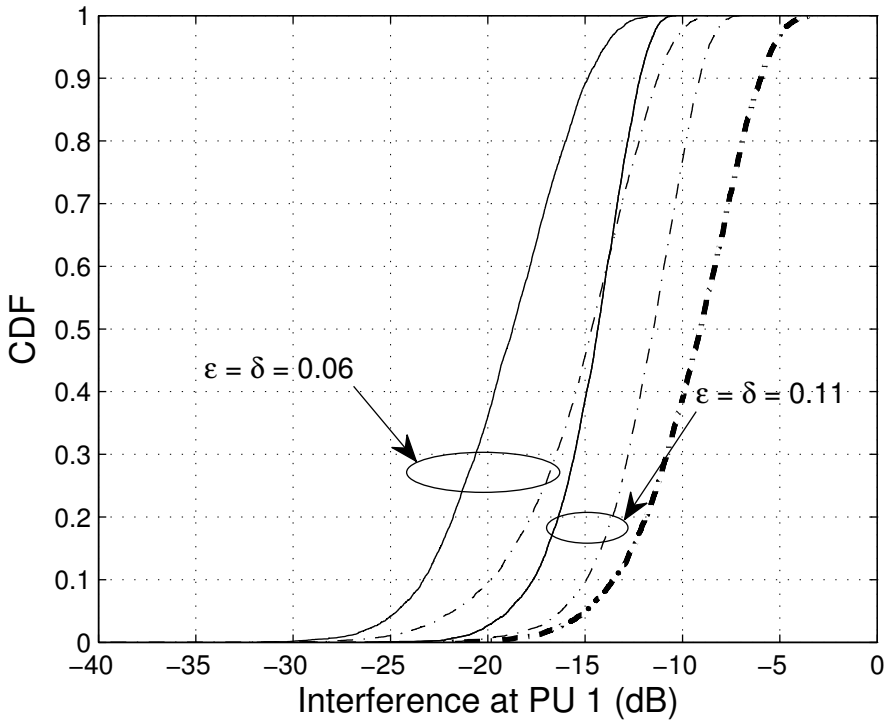

Figure 7.1: A comparison of the interference seen at the first PU RX. Solid lines show the CDF obtained using **Algorithm 1**, dotted-dashed curves show the interference CDF obtained using [99, **Algorithm 1**] and the bold dotted-dashed curve shows non-robust case.

local minimum of the multimodal objective function. Such problems were seen while solving cardinality constrained problems in [107]. A possible remedy to stalling could be maneuvering the direction vectors on the occurrence of such stalls. However, no such problems were observed in our implementation of **Algorithm 1**.

Finally, initializing $\mathbf{D}_i$ to $\mathbf{0}$ usually produces the minimum number of iterations while using *Proposition 1.*

7.4 Results

In order to validate the proposed scheme, numerical simulations are performed. To conduct these simulations it is assumed that the CR BS is equipped with a uniform linear array having $N_{CR} = 5$ elements spaced half a wavelength apart. Further, the BS serves 3 CR devices located at angles $\theta_1 = 20°, \theta_2 = 45°$ and $\theta_3 = 60°$ with

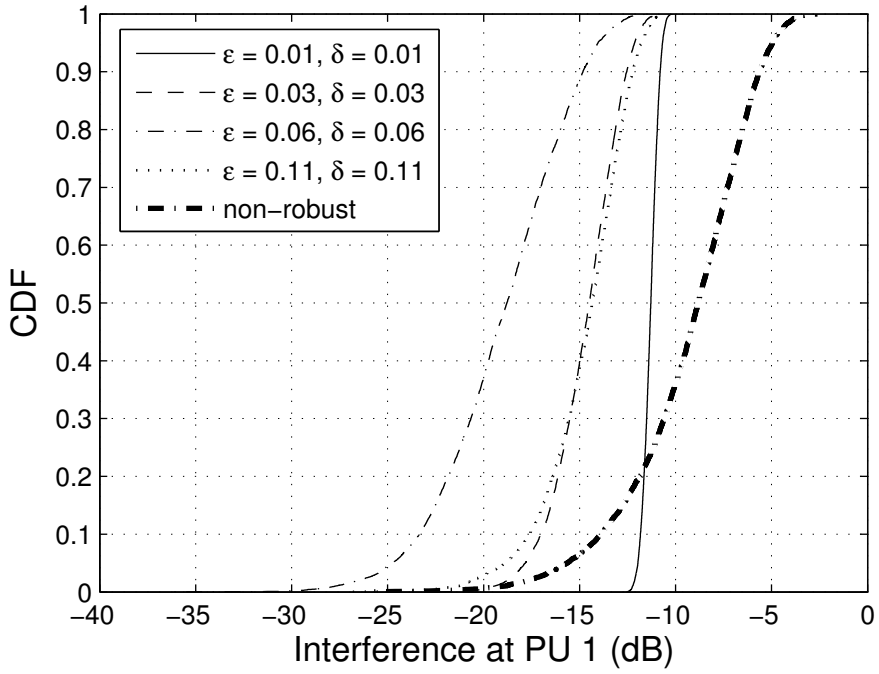

Figure 7.2: CDF of the interference due to the CR BS at the first PU for different values of ϵ, δ.

respect to antenna broadside, respectively. Similarly, 2 PU devices are assumed to be located along the directions of $\phi_1 = 40°$ and $\phi_2 = 75°$ respectively. At the CR receivers the noise is taken as $\mathcal{CN}(0, 1)$. Unless otherwise stated, it is assumed that $\zeta_m = \zeta = -10$ dB. With these assumptions, the channels from the BS to the CR and PU RXs, for $k = 1 \ldots N_{CR}$, are respectively given by the following simple model [115]:

$$(\hat{\mathbf{h}}_i)_k = e^{\frac{j2\pi d}{\lambda}(k-1)\cos(\theta_i)},\ i = 1, 2, 3,\ (\hat{\mathbf{h}}_{\mathrm{int}_m})_k = e^{\frac{j2\pi d}{\lambda}(k-1)\cos(\phi_m)},\ m = 1, 2. \quad (7.14)$$

where d and λ represent antenna separation and wavelength (we have taken $d/\lambda = 0.5$) respectively and $j = \sqrt{-1}$. For each true channel realization (estimated channel with error), the corresponding CSI error vector is normally distributed, truncated to lie within a sphere of radius $\delta_i = \delta,\ \forall i$ and $\delta_{\mathrm{int}_m} = \epsilon,\ \forall m$ for the CR and PU channels, respectively. Furthermore, to demonstrate the effect of interference from the PU TXs on the CR RXs, we assume there are 5 single antenna PU TXs and each entry of $\hat{\mathbf{h}}_p$ is $\mathcal{CN}(0, 1)$. The entries of the corresponding error vector are again normally distributed, truncated to a sphere of radius δ. While implementing **Al-**

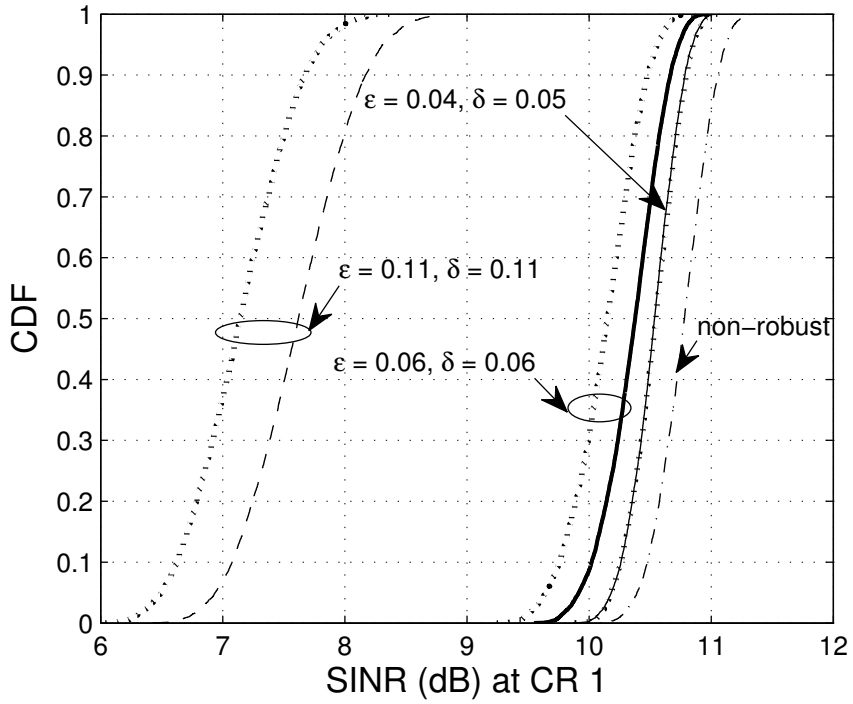

Figure 7.3: CDF of SINR at the first CR RX for different values of ϵ, δ without interference from the PU TXs. Bold dotted curves represent the SINR CDF using [99, **Algorithm 1**].

gorithm 1 'thresh.1' and 'thresh.2' are taken as 0.05 and `1e-10`, respectively. In addition to this, it is assumed that SINRmin = 0 dB, SINRmax = 13.01 dB and the average total transmit signal-to-noise ratio (SNR) is $P_{total}/N_0 = 13.97$ dB. We note that these values are arbitrary. To make a comparison, results for the non-robust case have also been plotted. In the non-robust case, the beamformers are obtained based on the estimated channels by ignoring the uncertainty regions. The optimization problems (SDPs) are solved using `cvx` [46]. First of all we compare the ranks of the beamforming matrices obtained using the proposed method and the ranks of the beamforming matrices obtained using the algorithm presented in [100]. To do so, we implement [100, Eqs. (16a) and (16b)] in [100, **Algorithm 1**] and note that the solution in the final iteration is usually the closest to rank-1 as shown in Table-I of [100]. To evaluate the rank we use the `[u,s,v] = svd(.)` function of MATLAB. The rank is calculated using `sum(diag(s)>max(diag(s))*tolerance)`,

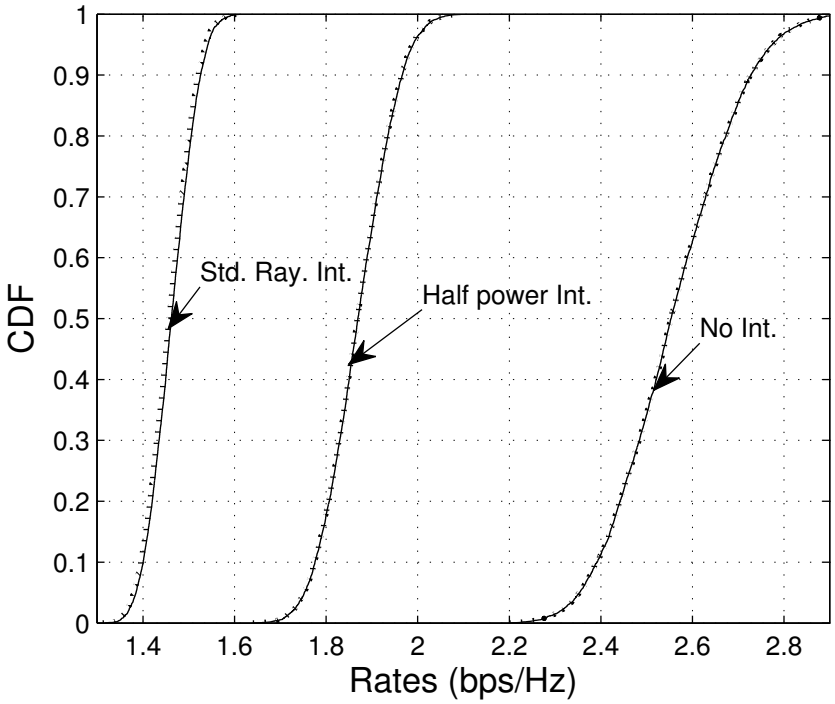

Figure 7.4: Effect of licensed user (PU) interference on the rates of the first CR device for $\epsilon = 0.11$ and $\delta = 0.11$. The interfering PU signals are Rayleigh faded. Bold dotted curves represent the CDF of rates using [99, **Algorithm 1**].

where `tolerance` is taken as `1e-08`. The precision of the software `cvx` [46] is kept at its default value. With these settings, it is observed that **Algorithm 1** in [100] returns full rank matrices with a probability that is extremely close to 1 in the final iteration for all values of ϵ and δ considered. In contrast, unit rank beamforming matrices are obtained using the proposed method. As another comparison of the beamformers obtained using **Algorithm 1** and [100, **Algorithm 1**], we plot the CDF curves for the interference observed at the first PU RX (see Fig. 7.1). The beamformers, in both cases, are obtained using eigenvectors corresponding to the largest eigenvalues of the $\mathbf{W}_i$ matrices. Since non-unit rank precoding matrices prevent exact extraction of beamformers, the approach in [100, **Algorithm 1**] results in larger interference at the PU RX. Figure 7.1 also shows that this problem can cause the interference to cross the threshold in the case of [100, **Algorithm 1**]. Hence, the rank of the matrices obtained during the last iteration of [100, **Algo-**

rithm 1] is not exactly 1 and the solution *may not* be robust enough for all error vector realizations inside the spherical ball. It is worth mentioning that in these simulations the inner while loop in **Algorithm 1** took only 1-3 iterations in each of the bisection procedure runs $\left(\text{which are}\lceil\log_2((\frac{\text{SINRmax}-\text{SINRmin}}{\text{thresh.1}}))\rceil\text{in number}\right)$ to determine the desired precoding matrices. In addition to this, the complexity of each convex iteration run is dominated by the complexity of the SDP (which is well known to be polynomial time [36]) involved in determining the precoding matrices. Hence, we can observe that the complexity of the proposed approach is roughly the same as that of [100].

In a second experiment, the CDF of interference at the first PU RX is obtained for different values of ϵ and δ (see Fig. 7.2). The CDF is taken over the distribution of possible channels which lie in the ball uncertainty regions for the given channel estimates. Results for the case of a non-robust design are also plotted. It is clear from Fig. 7.2 that, as expected, the non-robust design performs the worst. In fact, it exceeds the interference threshold (-10 dB) around 64% of the time. Furthermore, the interference in Fig. 7.2 shows an interesting trend. For small values of ϵ, δ the CR TX is able to direct a sharp null in its beam pattern towards each PU RX as the channel is precisely known. As ϵ, δ are increased, at first the CDFs spread out since the range of possible channels in the uncertainty ball increases and most of these channels lie in a deep null. As ϵ, δ are increased further the channel knowledge decreases and the TX has to use a broad null which is less deep to cater for a wide range of possible channels. Hence, the beam pattern flattens out in the direction of the uncertainty region and the interference values become less variable. This is shown in Fig. 7.2 where the spread of the CDF increases from $\epsilon = \delta = 0.01$ to $\epsilon = \delta = 0.06$ but then decreases for $\epsilon = \delta = 0.11$. This observation has another implication. For small ϵ, δ the sharp nulls mean that the interference constraint can be attained by beamforming and then full transmit power can be used to boost the CR-CR SINR. However, for larger ϵ, δ values the beam pattern does not have sharp nulls and power back-off may be required. For example, in Fig. 7.2 full transmit power was used for $\epsilon = \delta \in \{0.01, 0.03, 0.06\}$ but a 20% back off was required for

$\epsilon = \delta = 0.11$.

In Fig. 7.3 the CDF for the SINR at CR RX 1 for different values of ϵ, δ is plotted. As in Fig. 7.2, the CDF is over the possible channels in the uncertainty region. It is seen that, as expected, higher ϵ, δ result in a decrease in the mean SINR as decreased channel knowledge limits the ability of the TX to direct strong beams towards the CR RXs while simultaneously directing nulls towards the PU RXs. The non-robust design provides higher SINR, however, as seen in Fig. 7.2, such non-robust beamformers perform poorly in terms of maintaining interference below the threshold at the PU RXs. For example, in this case the interference at PU RX 1 exceeded its threshold 64% of time. We also provide a comparison with the results obtained using [100, **Algorithm 1**]. With our thresh.1 = 0.05, the SINR of the proposed approach tends to be higher. This difference is magnified especially for larger radii of spherical balls representing the channel uncertainty. A comparison with [100, **Algorithm 1**] also was performed using thresh.1 = .00001 and it was observed that the two SINRs can be approximately the same, albeit at the cost of greater leakage interference to the PU RXs in [100, **Algorithm 1**]. The greater interference at PU RXs in [100, **Algorithm 1**] is again due to the unavailability of exact rank-1 matrices, thus, prohibiting accurate extraction of beamformers from the matrix precoders. This clearly shows the superiority of the proposed approach.

Finally, in Fig. 7.4 we explore the effect of interference due to the presence of PU TXs. We assume there are 5 single antenna TXs and that the interfering channels experience Rayleigh fading. In the "Std. Ray. Int." case the interfering signals are unit power and the powers are halved in the "Half power Int." case. Hence, the values of $P_{total}/(I + N_0)$ are 6.2 dB, 8.5 dB and 13.97 dB for the 3 curves in Fig. 7.4 where I represents the total interference power. We have taken $\epsilon = 0.11, \delta = 0.11$ in Fig. 7.4. It is seen that standard Rayleigh interference results in the worst performance. If the power of each of the interfering signals is halved, the mean rate of CR 1 increases from 1.46 bps/Hz to 1.87 bps/Hz. However, as is evident from Fig. 7.4, the best performance (mean rate of 2.5 bps/Hz) is obtained in the absence of any such interference. With the proposed algorithm performing

slightly better than [100, **Algorithm 1**] in the standard Rayleigh interference case (leftmost curve), it is seen that the performance of both algorithms is almost the same in terms of rate in the remaining two scenarios. Thus, in addition to validating the analysis in (7.11), this clearly shows that ignoring interference from the licensed users can drastically over estimate the quality-of-service expected to be provided by CR devices. [100, **Algorithm 1**].

7.5 Summary

We have studied the the problem of balancing SINR in the downlink of a multiple input single output CR network. The beamformers obtained also satisfy interference constraints at the PU RXs and total transmit power constraints at the CR BS. The optimal beamforming problem is tackled by exactly solving a SDP, to within a certain acceptable tolerance, without relaxing the rank-1 constraints. A low complexity algorithm implementing the proposed approach has been presented. Furthermore, the results are extended to include the effect of interference from PU TXs and numerical simulations have been presented that show the effectiveness of the proposed procedure.

Chapter 8

Conclusions and Future Work

We conclude the thesis by providing the main conclusions that can be drawn from the earlier chapters. We also point out some open problems and research directions for future work.

8.1 Conclusions

CRs are being considered as a remedy to the perceived RF-spectrum scarcity. The inefficient usage of spectrum and the ever increasing demand of wireless devices has been the main reason for the tremendous research interest in CR technology.

After presenting an overview of some fundamentals of wireless communications and convex optimization techniques, Chapter 3 explores the information theoretic limits of a CR system operating in overlay mode. With a realistic interference channel incorporating both shadowing and fast fading, we show that the so called low interference regime constitutes the dominant mode of operation. This conclusion is especially true in the case when the CR coverage radius is small in comparison to that of the PU coverage area. However, as these coverage radii become comparable, the low and high interference regimes may occur with roughly equal probability. In addition to this, we have presented a simplified expression for a key parameter, α, that dictates the amount of power the CR dedicates to relaying PU message. Furthermore, we have concluded this chapter by presenting the effect of various

system parameters on the statistics of α.

The statistics of the strength of interfering signals in CR networks will play a very significant role in the design of future CR networks. Similarly, the fluctuation rates of signals from interfering CR devices and their impact on PU performance will decide the fate of CR networks. In Chapter 4, we have studied the interference statistics from various different perspectives. In particular, we model the interference due to a single CR in a closed form. Then we have shown that the sum interference due to multiple CRs does not admit an approximation with a two and three parameter lognormal density. In the second half of the chapter, we study second order statistics of interference in CR networks. In particular, we have shown that the LCR of cumulative interference in Rayleigh and Rician environments can be well approximated by equating the random processes representing total interference with a gamma and a noncentral χ^2 variables. Based on the LCR and AED results we conclude that a CR allocation process should give priority to several small CR interferers rather than one dominant one.

The CRs should access the spectrum in such a way that, in addition to satisfying interference constraints, they should also maintain QoS operation. Exploiting REM forms one such feasible option which is likely to deliver the desired goals. In Chapter 5 we study and compare various CR allocation schemes. To begin with, we compare the PEZ technique with a REM approach that requires signal strength data at all points in space. By performing a comparison on the basis of the admissible number of CRs or the percentage of CRs allowed to operate, we observe that the REM method is beneficial compared to PEZ only if the CRs are allocated in an intelligent manner. For example, a first-come-first-served basis can perform worse than the PEZ approach, thus failing to exploit the benefits of the huge amount of REM information available at its disposal. We also compare the two schemes in different environmental conditions. Later, we explore the effect of discretizing the REM information. We have shown using a coarse REM can have a huge negative impact in terms of the CRs significantly underestimating the interference at the PU device.

Up to this point in the thesis, we concentrate on single antenna CR devices. Multiple antennas on communicating terminals are well known to ensure high date rates and reliability. In the case of CR networks, they can provide an additional benefit in helping maintain the PU interference constraints. Chapter 6 aims to exploit this potential while simultaneously ensuring reduced complexity hardware by employing antenna selection at the CR TX and RX. We aim at choosing the best subset of transmit and receive antennas that can maximize the achievable data rates and satisfy the interference tolerance limits at the PU RXs as well. We present three schemes in order of decreasing complexity to accomplish this goal. Surprisingly, it is observed that the least complex of these schemes, namely, the one that involves choosing separate TX and RX antennas on the basis of norms of signal strengths, performs nearly the same as the exhaustive search approach. In addition to this, we have also presented some preliminary performance analysis of the exhaustive search method used to find the best SISO link in the system. We also extend these investigations to real world environments via simulation. We conclude that antenna selection based underlay CR systems can be a plausible option in sparse PU environments. Serving mobile terminals on the basis of SINR without consideration of fairness can effect the QoS expected from delay constrained users. In the case of CR networks, this effect can become increasingly pronounced keeping in view the stringent interference constraints to be met at the PU RXs. In Chapter 7 we devise an algorithm aimed at balancing SINR among CR users with various PU RXs in the proximity and imperfect CSI available at the base-station. The initial non-convex problem is relaxed to a quasi-convex problem by dropping rank constraints. It is then solved exactly by using a newly developed convex iteration technique. The benefits of the proposed technique are asserted via simulations.

8.2 Future Research Directions

The thesis has presented a broad range of research in different areas of CR networks. Although the bulk of CR research is still being carried out in the academic research

environment, there is, in general, a great interest in realizing CR networks in the future. At present, TV bands have proved to be the most attractive option in terms of exploiting cognitive capabilities [5], but very recent results show that researchers are exploring the potential of CRs implementation over a wide range of spectrum [116]. In what follows, we present a brief outline of future research options in the field of CR networks in general and in the context of topics considered in the thesis in particular. We emphasize that the suggestions given below do not, in any case, form an exhaustive list.

With reference to the information theoretic study of CR networks, the thesis presented the idealistic situation where all nodes perfectly know the CSI in the overlay model. Of course, this is not going to happen in reality. Hence, investigating the results under different models expressing imperfect CSI needs to be carried out. If a dedicated bandwidth limited feedback channel is used, then this study could further be extended to the case of exploring limited feedback consequences on the system performance. On top of this, the considered overlay model is very basic and only consists of a pair of CR and PU transceivers. It would be useful to expand this simple network to the multiple user case. Such a model can then be used for different research developments.

Statistical modeling of the interference at a PU due to all interfering CRs is still a wide open area to conduct research in. We think that, instead of trying to exactly obtain an expression for, say, the CDF of the random variable representing such interference, it will be much better to try and fit a simple distribution. Such a fit can be very fruitful in terms of designing CR networks. On top of this, there does not seem to be literature available where the problem of finding the distribution of SINR in lognormally faded CR environment is considered. It may very well turn out that a distribution showing a poor fit in the case of cumulative interference only may result in a better fit over a wide range of system parameter values when the SINR is considered. Similarly, the case of LCR evaluation need to be extended to the SINR metric. Furthermore, various different combinations of fading may be considered while developing expressions for the LCR performance measure.

CR scheduling schemes exploiting REM information need to be explored in more depth. In addition to the critical issue of what information should constitute a REM, the issue of imperfect/coarse REM should be investigated in more depth. The results presented in the thesis rely on various idealistic assumptions and thus correspond to upper bounds on exact values. Similarly, comparisons need to be obtained between the REM based techniques and the conventional overlay and underlay methodologies.

As mentioned previously, MIMO CRs form a very hot area of research. With only few investigations available, the MIMO techniques need more development for CR purposes. For example, the formulation of antenna selection based CRs assumes perfect CSI at all nodes. This assumption should be relaxed to imperfect CSI modeled using various different strategies. It may very well turn out that the proposed techniques are no longer as efficient as they are in the case of imperfect CSI. Similarly, the analysis presented should also be extended to the case of a MIMO link selected out of the given system. With regard to the SINR balancing, the approach presented is highly centralized and the scenarios needed to transform it to a distributed implementation should be investigated.

Appendix A

Distribution of the Ratio r_{cc}/r_{cp}

The variable r_{cc} represents the distance of the CR link where the receiver is uniformly located in an annulus of dimension $[R_0, R_c]$ around the transmitter. Similarly, r_{cp} describes the the distance of the CR transmitter to the PU receiver where the CR transmitter is uniformly located in an annulus of dimension $[R_0, R_p]$ around the PU receiver. To evaluate the distribution of r_{cc}/r_{cp} in the case where $R_p > R_c$, we proceed with

$$\begin{aligned} P(r_{cc} < xr_{cp}) &= \mathbb{E}_{r_{cp}}[P(r_{cc} < xr_{cp}|r_{cp})] \\ &= \int_{\alpha}^{\beta} \frac{2r_{cp}(x^2 r_{cp}^2 - R_0^2)}{(R_c^2 - R_0^2)(R_p^2 - R_0^2)}\, dr_{cp} \\ &= \frac{0.5x^2(\beta^4 - \alpha^4) - R_0^2(\beta^2 - \alpha^2)}{(R_c^2 - R_0^2)(R_p^2 - R_0^2)}, \end{aligned} \tag{A.1}$$

where we have used the facts that the PDF of the variable r_{cp} is given by $2r_{cp}/(R_p^2 - R_0^2)$ and that $P(r_{cc} < xr_{cp}) = (x^2 r_{cp}^2 - R_0^2)/(R_c^2 - R_0^2)$. A little inspection reveals that the random variable r_{cp} takes on the values $\alpha < x \leq \beta$ corresponding to the three different ranges of x as below:

- for $R_0/R_p < x < R_c/R_p$, r_{cp} ranges from $\alpha = R_0/x$ to $\beta = R_p$,
- for $R_c/R_p < x < 1$, r_{cp} has a range from $\alpha = R_0/x$ to $\beta = R_c/x$, and
- for $1 < x < R_c/R_0$, r_{cp} spans a range from $\alpha = R_0$ to $\beta = R_c/x$.

Hence, using the above ranges of x and r_{cp} in (C.1), some mathematical manipulations lead to (3.7). For the opposite case where $R_p < R_c$ the same approach leads to the result

$$P\left(\frac{r_{cc}}{r_{cp}} < x\right) = d_{i0}x^{-2} + d_{i1} + d_{i2}x^2, \quad x \in T_i \tag{A.2}$$

for $i = 1, 2, 3, 4, 5$. The regions in (A.2) are defined by $T_1 = \{x|x \leq R_0/R_p\}, T_2 = \{x|R_0/R_p < x \leq 1\}, T_3 = \{x|1 < x \leq R_c/R_p\}, T_4 = \{x|R_c/R_p < x \leq R_c/R_0\}$ and $T_5 = \{x|x > R_c/R_0\}$. With $\Delta = (R_c^2 - R_0^2)(R_p^2 - R_0^2)$, the constants in (A.2) are given by $d_{10} = d_{11} = d_{12} = 0$, $d_{21} = 0.5R_0^4/\Delta$, $d_{22} = -R_0^2R_p^2/\Delta$, $d_{23} = 0.5R_p^4/\Delta$, $d_{31} = 0$, $d_{32} = (R_0^4 - R_0^2R_p^2)/\Delta$, $d_{33} = 0.5(R_p^4 - R_0^4)/\Delta$, $d_{41} = (0.5R_c^4 - R_0^2R_c^2)/\Delta - R_c^2/(R_p^2 - R_0^2)$, $d_{42} = R_0^4/\Delta + R_p^2/(R_p^2 - R_0^2)$, $d_{43} = -0.5R_0^4/\Delta$, $d_{51} = 0$, $d_{52} = 1$ and $d_{53} = 0$.

Appendix B

Evaluation of (3.25) for Rayleigh Fading

When there is Rayleigh fading in all links of the CR interference channel, the distribution and density functions given in (3.25) are those of a standard unit mean exponential random variable. Thus, with this substitution in (3.25) we get

$$\begin{aligned}
&P\left(UW < \zeta x | U < \frac{V}{d}\right) \\
&= \frac{\int_0^\infty (1-e^{-\zeta xd/v})(1-e^{-v/d})e^{-v}dv + \int_0^\infty (1-e^{-\zeta x/w})e^{-w}e^{-\zeta xd/w}dw}{\int_0^\infty (1-e^{-v/d})e^{-v}dv} \\
&= 1 + \frac{\int_0^\infty e^{-\zeta xd/v - v(1+1/d)}dv - \int_0^\infty e^{-w-\zeta/w(x+xd)}dw}{1-d/(1+d)} \\
&= 1 + (d+1)\left[\int_0^\infty e^{-\zeta xd/v - v(1+d)/d}dv - \int_0^\infty e^{-w-\zeta x(1+d)/w}dw\right] \\
&\overset{(a)}{=} 1 + (d+1)\left[\int_0^\infty e^{-\zeta xd/v - v(1+d)/d}dv - (1+d)/d\int_0^\infty e^{-v(1+d)/d - \zeta xd/v}dv\right] \\
&= 1 - (d+1)/d\int_0^\infty e^{-\zeta xd/v - v(1+d)/d}dv \\
&\overset{(b)}{=} 1 - \int_0^\infty e^{-\zeta x(1+d)/t - t}dt. \qquad \text{(B.1)}
\end{aligned}$$

where in both (a) and (b) above we have used the substitutions $w = v(1+d)/d$ and $t = v(1+d)/d$ respectively. Now using $\zeta = 4/\mu_s\mu_t$ and evaluating the integral in the last equality using a standard result in [117] we arrive at (3.26).

Appendix C

Evaluation of Moments of Cumulative Interference Under Rician Conditions

Let Y denote the random variable defined by (4.31). The first three moments of Y are [60]

$$\mathbb{E}[Y] = \frac{(\lambda + v)}{\tilde{\alpha}},\ \mathbb{E}[Y^2] = \frac{((\lambda + v)^2 + 2(\lambda + v) + 2\lambda)}{\tilde{\alpha}^2} \tag{C.1}$$

$$\mathbb{E}[Y^3] = \frac{(\lambda + v)^3 + 6(\lambda + v)^2 + 6\lambda(\lambda + v) + 8(\lambda + v) + 16\lambda}{\tilde{\alpha}^3}. \tag{C.2}$$

Similarly, suppose m_1, m_2 and m_3 denote the moments of $I_{Ric}(t)$ in (4.30) about the origin. Expanding $I_{Ric}(t)$, $I^2_{Ric}(t)$ and $I^3_{Ric}(t)$ into multiple sums and taking expectation using standard results in [60] leads to

$$m_1 = \sum_{i=1}^{N} I_i, \quad m_2 = \left(\sum_{i=1}^{N} I_i\right)^2 + \sum_{i=1}^{N} I_i^2 \left(1 - \left(\frac{K}{K+1}\right)^2\right) \tag{C.3}$$

$$\begin{aligned} m_3 = &\left(\sum_{i=1}^{N} I_i\right)^3 + 3\sum_{i=1}^{N}\sum_{k\neq i, k=1}^{N} I_i^2 I_k \left(1 - \left(\frac{K}{K+1}\right)^2\right) \\ &+ \sum_{i=1}^{N} I_i^3 \left(5 - 9\left(\frac{K}{K+1}\right)^2 + 4\left(\frac{K}{K+1}\right)^3\right). \end{aligned} \tag{C.4}$$

Now applying the method of moments, we solve $m_k = \mathbb{E}[Y^k]$ for $k = 1, 2, 3$ and obtain the following:

$$\lambda = 0.5\tilde{\alpha}(\tilde{\alpha}m_2 - \tilde{\alpha}m_1^2 - 2m_1), \quad v = \tilde{\alpha}m_1 - \lambda, \tag{C.5}$$

where $\tilde{\alpha}$ is the solution to the following quadratic equation

$$-2\tilde{\alpha}^2 m_1^3 - \tilde{\alpha}^2 m_3 + 3\tilde{\alpha}^2 m_1 m_2 + 8\tilde{\alpha}m_2 - 8\tilde{\alpha}m_1^2 - 8m_1 = 0. \tag{C.6}$$

Appendix D

Equivalence of the LCR of a Noncentral-χ^2 Random Variable with Non-Integer Degrees of Freedom

In [77] a noncentral χ^2 process, denoted r, is considered. The only part of the derivation in [77] that requires integer dof is the proof that the conditional distribution of $\dot{r}$ given r is Gaussian with variance $Var(\dot{r}|r) = 4\tilde{\sigma}^2 r$ where $\tilde{\sigma}^2$ is a variance parameter. In this Appendix we show that this is true for a general noncentral χ^2 process. The LCR of a stationary gamma process was first derived by Barakat [76] in an optics context building on previous results in [118]. This analysis is based on the representation [76]

$$\Omega = \int_{A_r} |E(x)|^2 dx \tag{D.1}$$

where A_r is the region of integration (an aperture in [76]), $E(x)$ is a circular complex zero-mean Gaussian process and Ω is the resulting gamma variable. If $E(x)$ is allowed to have a constant non-zero mean then for certain A_r, the resulting Ω has a scaled noncentral χ^2 distribution with arbitrary degrees of freedom (not

necessarily integer). For this noncentral case let $E(x) = E_1(x) + jE_2(x)$ and

$$\Omega = \int_{A_r} E_1^2(x) + E_2^2(x)dx, \tag{D.2}$$

where $E_1(x)$ and $E_2(x)$ are both non-zero mean Gaussian processes. The derivative of Ω is therefore

$$\dot{\Omega} = \int_{A_r} [2E_1(x)\dot{E}_1(x) + 2E_2(x)\dot{E}_2(x)]dx. \tag{D.3}$$

Now it is well known [119, 77, 75, 74, 78] that $\dot{E}_1(x)$, $\dot{E}_2(x)$ are zero-mean Gaussian variables which are independent of $E_1(x)$, $E_2(x)$ and each other. Let the distribution of both derivatives be denoted by $\mathcal{N}(0, \sigma^2)$. Hence, conditioned on $E_1(x)$ and $E_2(x)$ over $x \in A_r$, the derivative, $\dot{\Omega}$, is also zero mean Gaussian. The variance of $\dot{\Omega}$ conditioned on $\{E_1(x), E_2(x)|x \in A_r\}$ is given by

$$\begin{aligned}
&\mathbb{E}\left[\int_{A_r}\int_{A_r}(2E_1(x)\dot{E}_1(x) + 2E_2(x)\dot{E}_2(x))(2E_1(y)\dot{E}_1(y) + 2E_2(y)\dot{E}_2(y))dxdy\right] \\
&= \mathbb{E}\left[\int_{A_r}\left(4E_1^2(x)\dot{E}_1^2(x) + 4E_2^2(x)\dot{E}_2^2(x)\right)dx\right]
\end{aligned} \tag{D.4}$$

since $\dot{E}_i(x)$ is independent of $\dot{E}_i(y)$ for $x \neq y$. Also, since $\mathbb{E}[\dot{E}_i^2(x)] = \sigma^2$, the conditional variance is

$$4\sigma^2 \int_{A_r} [E_1^2(x) + E_2^2(x)]dx = 4\sigma^2\Omega \tag{D.5}$$

Hence, $\dot{\Omega}$ has the representation $\dot{\Omega} = 2\sigma\Omega^{1/2}Z$ where $Z \sim \mathcal{N}(0, 1)$ and $\dot{\Omega}$ has the conditional density

$$f_{\dot{\Omega}|\Omega} = \frac{\exp(\frac{-x^2}{8\sigma^2\Omega})}{\sqrt{8\pi\sigma^2\Omega}}. \tag{D.6}$$

Since $\dot{\Omega} \sim \mathcal{N}(0, 4\sigma^2\Omega)$, conditional on Ω, the proof is complete.

Bibliography

[1] "Spectrum Policy Task Force Report (ET Docket-135)," Federal Communications Comsssion, Tech. Rep., 2002, http://hraunfoss.fcc.gov/edocs_public/attachmatch/DOC-228542A1.pdf.

[2] M. A. McHenry, "NSF Spectrum Occupancy Measurements Project Summary," Shared Spectrum Company, Tech. Rep., 2005.

[3] A. F. Molisch, L. J. Greenstein, and M. Shafi, "Propagation issues for cognitive radio," *Proceedings of the IEEE*, vol. 97, no. 5, pp. 787–804, May 2009.

[4] J. Mitola, "Cognitive radio: An integrated agent architecture for software defined radio," Ph.D. dissertation, Royal Inst. Technol. (KTH), Stockholm, Sweden, 2000.

[5] "In the matter of unlicensed operation in the TV broadcast bands: Second report and order and memorandum opinion and order," Federal Communications Comsssion, Tech. Rep. 08-260, Tech. Rep., Nov. 2008, http://hraunfoss.fcc.gov/edocs public/attachmatch/FCC-08-260A1.pdf.

[6] A. Goldsmith, S. A. Jafar, I. Maric, and S. Srinivasa, "Breaking spectrum gridlock with cognitive radios: An information theoretic perspective," *Proceedings of the IEEE*, vol. 97, no. 5, pp. 894–914, May 2009.

[7] S. Srinivasa and S. A. Jafar, "The throughput potential of cognitive radio: A theoretical perspective," *IEEE Communications Magazine*, vol. 45, no. 5, pp. 73–79, May 2007.

[8] S. Haykin, D. J. Thomson, and J. H. Reed, "Spectrum sensing for cognitive radio," *Proceedings of the IEEE*, vol. 97, no. 5, pp. 849 –877, May 2009.

[9] G. L. Stuber, *Principles of Mobile Communication*, 2nd ed. Boston: Kluwer Academic, 2001.

[10] A. J. Goldsmith, *Wireless Communications*. New York: Cambridge University Press, 2006.

[11] E. Biglieri, *Coding for Wireless Channels*. New York: Springer, 2005.

[12] R. H. Clarke, "A statistical theory of mobile radio reception," *Bell Syst. Tech. J.*, pp. 957–1000, Jul-Aug 1968.

[13] J. W. C. Jakes, *Microwave Mobile Communications*. New York: Wiley, 1974.

[14] A. Papoulis and S. U. Pillai, *Probability, Random Variables and Stochastic Processes*, 4th ed. New York: McGraw Hill, 2002.

[15] M. K. Simon and M. S. Alouini, *Digital Communication over Fading Channels*, 2nd ed. New Jersey: Wiley-IEEE, 2004.

[16] M. Gudmundson, "Correlation model for shadow fading in mobile radio systems," *IEE Electronics Letters*, vol. 27, no. 23, pp. 2145–2146, 1991.

[17] P. Agrawal and N. Patwari, "Correlated link shadow fading in multi-hop wireless networks," *IEEE Trans. Wirel. Comm.*, vol. 8, no. 8, pp. 4024–4036, Aug. 2009.

[18] G. J. Foschini and M. J. Gans, "On limits of wireless communications in a fading environment when using multiple antennas," *Springer Wireless Personal Commun.*, vol. 6, no. 3, pp. 311–335, 1998.

[19] E. Telatar, "Capacity of multi-antenna Gaussian channels," *Europ. Trans. Telecommun.*, vol. 10, no. 6, pp. 585–595, 1999.

[20] D. Tse and P. Viswanath, *Fundamentals of Wireless Communication*. Cambridge University Press, 2005.

[21] T. M. Cover and J. A. Thomas, *Elements of Information Theory*, 2nd ed. New York: Wiley, 2006.

[22] C.-N. Chuah, D. N. C. Tse, J. M. Kahn, and R. A. Valenzuela, "Capacity scaling in MIMO wireless systems under correlated fading," *IEEE Trans. Inf. Theory*, vol. 48, no. 3, pp. 637–650, Mar. 2002.

[23] K. Yu and B. Ottersten, "Models for MIMO propagation channels: a review," *Wiely Journal on Wireless Communications and Mobile Computing*, vol. 2, no. 7, pp. 653–666, Nov. 2002.

[24] P. Almers, E. Bonek, A. Burr, N. Czink, M. Debbah, V. D.-Esposti, H. Hofstetter, P. Kyosti, D. Laurenson, G. Matz, A. F. Molisch, C. Oestges, and H. Ozcelik, "Survey of channel and radio propagation models for wireless MIMO systems," *EURASIP Journal on Wireless Communications and Networking*, vol. 2007, no. 1, pp. 1–19, Nov. 2007.

[25] D. Gesbert, H. Bolcskei, D. A. Gore, and A. J. Paulraj, "Outdoor MIMO wireless channels: models and performance prediction," *IEEE Trans. Commun.*, vol. 50, no. 12, pp. 1926–1934, Dec. 2002.

[26] P. J. Smith, S. Roy, and M. Shafi, "Capacity of MIMO systems with semicorrelated flat fading," *IEEE Trans. Inf. Theory*, vol. 49, no. 10, pp. 2781–2788, Oct. 2003.

[27] M. Chiani, M. Z. Win, and A. Zanella, "On the capacity of spatially correlated MIMO Rayleigh-fading channels," *IEEE Trans. Inf. Theory*, vol. 49, no. 10, pp. 2363–2371, Oct. 2003.

[28] A. Narula, M. J. Lopez, M. D. Trott, and G. W. Wornell, "Efficient use of side information in multiple-antenna data transmission over fading channels," *IEEE J. Sel. Areas Commun.*, vol. 16, no. 8, pp. 1423–1436, Oct. 1998.

[29] E. Jorswieck and H. Boche, "Channel capacity and capacity-range of beamforming in MIMO wireless systems under correlated fading with covariance feedback," *IEEE Trans. Wireless Commun.*, vol. 3, no. 5, pp. 1543–1553, Sep. 2004.

[30] S. A. Jafar and A. J. Goldsmith, "Transmitter optimization and optimality of beamforming for multiple antenna systems," *IEEE Trans. Wireless Commun.*, vol. 3, no. 4, pp. 1164–1175, Jul. 2004.

[31] A. J. Goldsmith, S. A. Jafar, N. Jindal, and S. Vishwanath, "Capacity limits of MIMO channels," *IEEE J. Sel. Areas Commun.*, vol. 21, no. 5, pp. 684–702, June 2003.

[32] E. Biglieri, R. Calderbank, T. Constantinides, A. Goldsmith, A. Paulraj, and H. V. Poor, *MIMO Wireless Communications*. Cambridge University Press, 2006.

[33] P. J. Smith and M. Shafi, "On a Gaussian approximation to the capacity of wireless MIMO systems," in *Proc. ICC*, May 2002, pp. 406–410.

[34] M. Patzold, *Mobile Fading Channels*. West Sussex: Wiley, 2002.

[35] R. T. Rockfellar, *Convex Analysis*. New Jersey: Princeton University Press, 1996.

[36] S. Boyd and L. Vandenberghe, *Convex Optimization*. Cambridge University Press, 2004.

[37] D. P. Bertsekas, *Convex Optimization Theory*. Nashua: Athena Scientific, 2009.

[38] G. B. Dantzig, "Notes on linear programming," *The RAND Corporation, Research Memorendum*, October 1954.

[39] G. B. Dantzig and M. N. Thapa, *Linear Programming: Theory and Extensions*. New York: Springer, 2003.

[40] M. S. Lobo, L. Vandenberghe, S. Boyd, and H. Lebret, "Applications of second-order cone programming," *Linear Algebra and its Applications*, vol. 284, no. 1-3, pp. 1993–228, Nov. 1998.

[41] S. Boyd, L. E. Ghoui, E. Feron, and V. Balakrishnan, *Linear Matrix Inequalities in System and Control Theory.* Philadelphia: SIAM, 1994.

[42] R. A. Horn and C. R. Johnson, *Matrix Analysis.* Cambridge University Press, 1985.

[43] L. Vandenberghe and S. P. Boyd, "Semidefinite programming," *SIAM Review*, vol. 38, no. 1, pp. 49–95, Mar. 1996.

[44] M. Chiang, C. W. Tan, D. P. Palomar, D. O'Neill, and D. Julian, "Power control by geometric programming," *IEEE Trans. Wireless Commun.*, vol. 6, no. 7, pp. 2640–2651, July 2007.

[45] S. Boyd, S.-J. Kim, L. Vandenberghe, and A. Hassibi, "A tutorial on geometric programming," *Optimization and Engineering*, vol. 8, no. 1, pp. 67–127, Apr. 2007.

[46] M. Grant and S. Boyd, "CVX: Matlab software for disciplined convex programming, version 1.21," http://cvxr.com/cvx, 2010.

[47] Y. Nesterov and A. Nemirovskii, *Interior Point Polynomial Algorithms in Convex Programming.* Philadelphia: SIAM, 1994.

[48] A. Ghasemi and E. S. Sousa, "Spectrum sensing in cognitive radio networks: requirements, challenges and design trade-offs [cognitive radio communications]," *IEEE Communications Magazine*, vol. 46, no. 4, pp. 32–39, April 2008.

[49] R. Tandra, S. M. Mishra, and A. Sahai, "What is a spectrum hole and what does it take to recognize one?" *Proceedings of the IEEE special issue on Cognitive Radio*, vol. 97, no. 5, pp. 824–848, May 2009.

[50] A. Ghasemi and E. S. Sousa, "Fundamental limits of spectrum-sharing in fading environments," *IEEE Transactions on Wireless Communications*, vol. 6, no. 2, pp. 649–658, Feb. 2007.

[51] N. Devroye, P. Mitran, and V. Tarokh, "Achievable rates in cognitive radio channels," *IEEE Transactions on Information Theory*, vol. 52, no. 5, pp. 1813–1827, May 2006.

[52] I. Maric, A. Goldsmith, G. Kramer, and S. Shamai, "On the capacity of interference channels with one cooperating transmitter," *European Transactions on Telecommunications*, vol. 19, pp. 405–420, Apr. 2008.

[53] A. Jovicic and P. Viswanath, "Cognitive radio: An information-theoretic perspective," *IEEE Transactions on Information Theory*, vol. 55, no. 9, pp. 3945–3958, Sept. 2009.

[54] J. Jiang and Y. Xin, "A new achievable rate region for the cognitive radio channel," in *Proc. IEEE International Conference on Communications*, May 2008, pp. 1055–1059.

[55] W. Wu, S. Vishwanath, and A. Arapostathis, "Capacity of a class of cognitive radio channels: Interference channels with degraded message sets," *IEEE Transactions on Information Theory*, vol. 53, no. 11, pp. 4391–4399, Nov. 2007.

[56] G. Kramer, "Review of rate regions for interference channels," in *Proc. International Zurich Seminar on Communications*, 2006, pp. 162–165.

[57] M. Costa, "Writing on dirty paper (corresp.)," *IEEE Transactions on Information Theory*, vol. 29, no. 3, pp. 439–441, May 1983.

[58] M. Vu, N. Devroye, and V. Tarokh, "On the primary exclusive region of cognitive networks," *IEEE Transactions on Wireless Communications*, vol. 8, no. 7, pp. 3380–3385, July 2009.

[59] H. A. Suraweera, J. Gao, P. J. Smith, M. Shafi, and M. Faulkner, "Channel capacity limits of cognitive radio in asymmetric fading environments," in *Proc. IEEE International Conference on Communications*, May 2008, pp. 4048–4053.

[60] N. L. Johnson, S. Kutz, and N. Balakrishnan, *Continuous Univariate Distributions, vol. 2*, 2nd ed. New York: Wiley, 1995.

[61] A. Ghasemi and E. S. Sousa, "Interference aggregation in spectrum-sensing cognitive wireless networks," *IEEE Journal of Selected Topics in Signal Processing*, vol. 2, pp. 41–56, Feb. 2008.

[62] X. Hong, C.-X. Wang, and J. Thompson, "Interference modeling of cognitive radio networks," in *Proc. IEEE Vehcular Technology Conference (VTC) Spring*, 2008, pp. 1851–1855.

[63] A. Ghasemi and E. S. Sousa, "Fundamental limits of spectrum-sharing in fading environments," *IEEE Transactions on Wireless Communications*, vol. 6, no. 2, pp. 649–658, Feb. 2007.

[64] M. F. Hanif, M. Shafi, P. J. Smith, and P. Dmochowski, "Interference and deployment issues for cognitive radio systems in shadowing environments," in *Proc. IEEE International Conference on Communications*, June 2009, pp. 1–6.

[65] M. F. Hanif, P. J. Smith, and M. Shafi, "Performance of cognitive radio systems with imperfect radio environment map information," in *IEEE Australian Communications Theory Workshop (2009)*, Feb. 2009, pp. 61–66.

[66] L. F. Fenton, "The sum of lognormal probability distributions in scatter transmission systems," *IRE Trans. Commun. Syst*, vol. CS-8, pp. 57–67, 1960.

[67] S. Schwartz and Y. Yeh, "On the distribution function and moments of power sums with lognormal components," *Bell Syst. Tech. Journal*, vol. 61, pp. 1441–1462, 1982.

[68] A. Abu-Dayya and N. C. Beaulieu, "Outage probabilities in the presence of correlated lognormal interferers," *IEEE Trans. Veh. Technol.*, vol. 43, pp. 164–173, Feb. 1994.

[69] N. C. Beaulieu, A. Abu-Dayya, and P. McLance, "Estimating the distribution of a sum of independent lognormal random variables," *IEEE Trans. Commun.*, vol. 43, pp. 2869–2873, Dec. 1995.

[70] N. C. Beaulieu and Q. Xie, "An optimal lognormal approximation to lognormal sum distributions," *IEEE Trans. Veh. Technol.*, vol. 53, pp. 479–489, Mar. 2004.

[71] N. B. Mehta, J. Wu, A. F. Molisch, and J. Zhang, "Approximating a sum of random variables with a lognormal," *IEEE Transactions on Wireless Communications*, vol. 6, no. 7, pp. 2690–2699, July 2007.

[72] Z. Liu, J. Almhana, and R. McGorman, "Approximating lognormal sum distributions with power lognormal distributions," *IEEE Transactions on Vehicular Technology*, vol. 57, no. 4, pp. 2611–2617, July 2008.

[73] J. F. C. Kingman, *Poisson Processes*. New York: Oxford Univ. Press, 1993.

[74] X. Dong and N. C. Beaulieu, "Average level crossing rate and average fade duration of low-order maximal ratio diversity with unbalanced channels," *IEEE Communications Letters*, vol. 6, no. 4, pp. 135–137, July 2002.

[75] P. Ivanis, D. Drajic, and B. Vucetic, "The second order statistics of maximal ratio combining with unbalanced branches," *IEEE Communications Letters*, vol. 12, no. 7, pp. 508–510, July 2008.

[76] R. Barakat, "Level-crossing statistics of aperture-integrated isotropic speckle," *J. Opt. Soc. Amer.*, vol. 5, pp. 1244–1247, 1988.

[77] N. C. Beaulieu and X. Dong, "Level crossing rate and average fade duration of MRC and EGC diversity in Ricean fading," *IEEE Trans. on Communications*, vol. 51, pp. 722–726, May 2003.

[78] M. Patzold, U. Killat, and F. Laue, "An extended Suzuki model for land mobile satellite channels and its statistical properties," *IEEE Transactions on Vehicular Technology*, vol. 47, no. 2, pp. 617–630, May 1998.

[79] H.-Y. Kim, M. J. Gribbin, K. E. Muller, and D. J. Taylor, "Analytic, computational, and approximate forms for ratios of noncentral and central Gaussian quadratic forms," *Journal of Computational and Graphical Statistics*, vol. 15, pp. 443–459, June 2006.

[80] R. A. Silverman, "The fluctuation rate of the chi process," *IRE Trans. Inform. Theory*, vol. 4, no. 1, pp. 30–34, Mar. 1958.

[81] N. L. Johnson and S. Kotz, *Continuous Univariate Distributions, vol. 2*, 1st ed. New York: John Wiley & Sons, 1973.

[82] Y. Zhao, D. Raymond, C. da Silva, J. H. Reed, and S. F. Midkiff, "Performance evaluation of radio environment map-enabled cognitive spectrum-sharing networks," in *Proc. IEEE Military Communications Conference (MILCOM)*, Oct. 2007, pp. 1–7.

[83] Y. Zhao, L. Morales, J. Gaeddert, K. K. Bae, J.-S. Um, and J. H. Reed, "Applying radio environment maps to cognitive wireless regional area networks," in *Proc. IEEE International Symposium on New Frontiers in Dynamic Spectrum Access Networks (DySPAN)*, April 2007, pp. 115–118.

[84] H. Stark and J. W. Woods, *Probability and Random Processes with Applications to Signal Processing*. Prentice Hall, 2001.

[85] A. M. Viterbi and A. J. Viterbi, "Erlang capacity of a power controlled CDMA system," *IEEE J. Select. Areas Communications*, vol. 11, no. 6, pp. 892–900, Aug. 1993.

[86] G. Scutari, D. Palomar, and S. Barbarossa, "Cognitive MIMO radio," *IEEE Signal Process. Mag.*, vol. 25, no. 6, pp. 46–59, Nov. 2008.

[87] R. Zhang and Y. C. Liang, "Exploiting multi-antennas for opportunistic spectrum sharing in cognitive radio networks," *IEEE J. Select. Topics Signal Process.*, vol. 2, no. 1, pp. 88–102, Feb. 2008.

[88] L. Zhang, Y. Xin, and Y. C. Liang, "Weighted sum rate optimization for cognitive radio MIMO broadcast channels," in *Proc. ICC*, May 2008, pp. 3679–3683.

[89] S. Sridharan and S. Vishwanath, "On the capacity of a class of MIMO cognitive radios," *IEEE J. Selec. Topics Signal Process.*, vol. 2, no. 1, pp. 103–117, Feb. 2008.

[90] A. F. Molisch and M. Z. Win, "MIMO systems with antenna selection," *IEEE Microwave Mag.*, vol. 5, no. 1, pp. 46–56, Mar. 2004.

[91] S. Sanayei and A. Nosratinia, "Antenna selection in MIMO systems," *IEEE Commun. Mag.*, vol. 42, no. 10, pp. 68–73, Oct. 2004.

[92] P. J. Smith, T. W. King, L. M. Garth, and M. Dohler, "A power scaling analysis of norm-based antenna selection techniques," *IEEE Trans. Wireless Commun.*, vol. 7, no. 8, pp. 3140–3149, 2008.

[93] J. Zhou, J. Thompson, and I. Krikidis, "Multiple antennas selection for linear precoding MISO cognitive radio," in *Proc. WCNC*, Apr. 2009, pp. 1–6.

[94] H. Gao, P. J. Smith, and M. V. Clark, "Theoretical reliability of MMSE linear diversity combining in Rayleigh-fading additive interference channels," *IEEE Trans. Commun.*, vol. 46, no. 5, pp. 666–672, May 1998.

[95] A. Dua, K. Medepalli, and A. J. Paulraj, "Receive antenna selection in MIMO systems using convex optimization," *IEEE Trans. Wireless Commun.*, vol. 5, no. 9, pp. 2353–2357, Sep. 2006.

[96] P. Ubaidulla and A. Chockalingam, "Non-linear transceiver designs with imperfect CSIT using convex optimization," in *Proc. WCNC*, Apr. 2009, pp. 1–6.

[97] C. G. Gunther, "Comment on "estimate of channel capacity in Rayleigh fading environment"," *IEEE Trans. Veh. Tech.*, vol. 45, no. 2, pp. 401–403, May 1996.

[98] E. S. Sousa, "Performance of a spread spectrum packet radio network link in a Poisson field of interferers," *IEEE Trans. Inf. Tech.*, vol. 38, no. 6, pp. 1743–1754, Nov. 1992.

[99] L. Zhang, R. Zhang, Y. C. Liang, Y. Xin, and H. V. Poor, "On Gaussian MIMO BC-MAC duality with multiple transmit covariance constraints," *preprint*. [Online]. Available: http://www.citebase.org/abstract?id=oai:arXiv.org:0809.4101

[100] G. Zheng, K. K. Wong, and B. Ottersten, "Robust cognitive beamforming with bounded channel uncertainties," *IEEE Transactions on Signal Processing*, pp. 4871–4881, Dec. 2009.

[101] A. Beck and Y. Eldar, "Strong duality in nonconvex quadratic optimization with two quadratic constraints," *SIAM J. Opt.*, vol. 17, no. 3, pp. 844–860, 2006.

[102] M. Bengtsson and B. Ottersten, "Optimal downlink beamforming using semidefinite optimization," in *Proc. the 37th Annual Allerton Conf. Commun., Control and Comput.*, Illinois, USA, Sep. 1999, pp. 987–996.

[103] O. Filiz and A. Yener, "Rank constrained temporal-spatial matrix filters for CDMA systems," *IEEE Transactions on Wireless Communications*, vol. 3, no. 6, pp. 1974–1979, Nov. 2004.

[104] A. Wiesel, Y. C. Eldar, and S. Shamai, "Semidefinite relaxation for detection of 16-QAM signaling in MIMO channels," *IEEE Signal Processing Letters*, vol. 12, no. 9, pp. 653–656, Sep. 2005.

[105] W. K. Ma, T. N. Davidson, K. M. Wong, Z. Q. Luo, and P. C. Ching, "Quasi-maximum-likelihood multiuser detection using semi-definite relaxation with application to synchronous CDMA," *IEEE Transactions on Signal Processing*, vol. 50, no. 4, pp. 912–922, April 2002.

[106] G. Pataki, "On the rank of extreme matrices in semidefinite programs and the multiplicity of optimal eigenvalues," *Mathematics of Operations Research*, vol. 23, no. 2, pp. 339–358, 1998.

[107] J. Dattorro, *Convex Optimization & Euclidean Distance Geometry*. Meboo Publishing USA, 2009.

[108] M. Botros and T. N. Davidson, "Convex conic formulations of robust downlink precoder designs with quality of service constraints," *IEEE Journal of Selected Topics in Signal Processing*, vol. 1, no. 4, pp. 714–724, Dec. 2007.

[109] M. Schubert and H. Boche, "Solution of the multiuser downlink beamforming problem with individual SINR constraints," *IEEE Transactions on Vehicular Technology*, vol. 53, no. 1, pp. 18–28, Jan. 2004.

[110] A. Wiesel, Y. C. Eldar, and S. Shamai, "Linear precoding via conic optimization for fixed MIMO receivers," *IEEE Transactions on Signal Processing*, vol. 54, no. 1, pp. 161–176, Jan. 2006.

[111] Z.-Q. Luo, W.-K. Ma, A. M.-C. Suo, Y. Ye, and S. Zhang, "Semidefinite relaxation of quadratic optimization problems," *IEEE Signal Processing Magazine*, vol. 27, no. 3, pp. 20–34, May 2010.

[112] M. Fazel, H. Hindi, and S. P. Boyd, "A rank minimization heuristic with application to minimum order system approximation," in *Proc. American Control Conference, American Automatic Control Council (AACC)*, June 2001, pp. 4734–4739.

[113] ——, "Rank minimization and applications in system theory," in *Proc. American Control Conference, American Automatic Control Council (AACC)*, June 2004.

[114] F. Alizadeh, "Interior point methods in semidefinite programming with applications to combinatorial optimization," *SIAM Journal on Optimization*, vol. 22, no. 1, pp. 13–51, Feb. 1995.

[115] A. Mutapcic, S. J. Kim, and S. Boyd, "A tractable method for robust downlink beamforming in wireless communications," in *Proc. Asilomar Conference on Signals, Systems, and Computers (ACSSC)*, Asilomar, CA, Nov. 2007, pp. 1224–1228.

[116] B. Razavi, "Cognitive radio design challenges and techniques," *IEEE Journal of Solid-State Circuits*, vol. 45, no. 8, pp. 1542–1553, Aug. 2010.

[117] I. S. Gradshteyn and I. M. Ryzhik, *Table of Integrals, Series, and Products*, 7th ed. California USA: Academic Press, 2007.

[118] R. Barakat, "Second-order statistics of integrated intensities and of detected photoelectrons," *J. Mod. Opt.*, vol. 34, pp. 91–102, 1987.

[119] S. O. Rice, "Statistical properties of a sine wave plus random noise," *Bell Syst. Tech. J.*, vol. 27, pp. 109–157, Jan. 1948.